Precise timing of the trypanosome cell division cycle

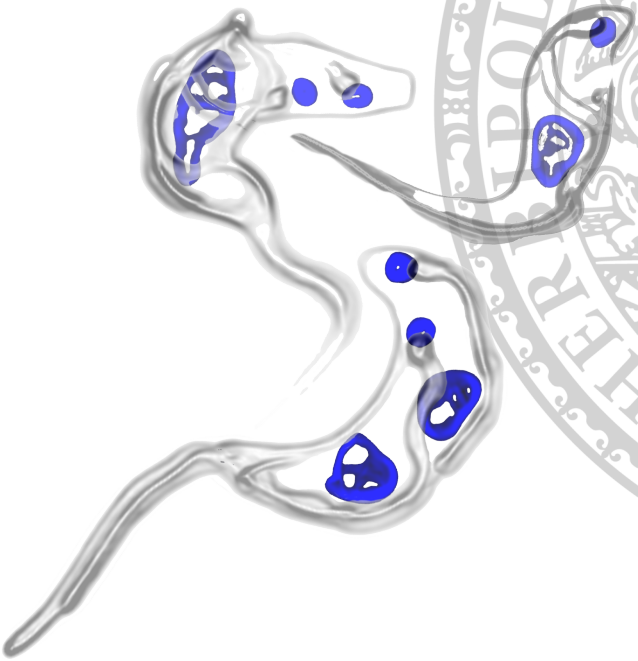

Dissertation zur Erlangung des
naturwissenschaftlichen Doktorgrades
der Julius-Maximilians-Universität Würzburg

vorgelegt von

Jamin Jung

geboren in Frankfurt am Main

Würzburg, 2015

Eingereicht am: 09. Juni 2015

Mitglieder der Promotionskommission:

Vorsitzender: Prof. Dr. Markus Engstler

1. Gutachter: Prof. Dr. Markus Engstler

2. Gutachter: Prof. Dr. Thomas Dandekar

Tag des Promotionskolloquiums: 03. Juli 2015

Doktorurkunde ausgehändigt am:

Diese Arbeit wurde betreut von: Prof. Dr. Markus Engstler

Die vorliegende Arbeit wurde gefördert von:

DFG EN 305/5-1 und SFB 630

Deutsche Forschungsgemeinschaft

SFB 630

"After climbing a great hill, one only finds that there are many more hills to climb."

Nelson Mandela

List of contents

List of figures

List of tables

1 Summary

Summary

African trypanosomes are the causative agents of fatal diseases in humans and livestock. Trypanosomes show a complex lifecycle and shuttle between the transmitting vector, the tsetse (*Glossina spec*.), and the mammalian host. As a result of this the parasite undergoes tremendous changes in morphology and metabolism to adapt to the different living environments. The two best-studied lifecycle stages are the procyclic forms (PCF) that live in the tsetse fly and the proliferative bloodstream form (BSF) that resides in the mammalian blood. The most conspicuous weapon that trypanosomes use to evade the host immune attack is a dense layer of a single protein type, the variant surface glycoprotein (VSG), which shields the entire cell surface. Immune evasion required high rates of surface membrane turnover and surface coat recycling.

Trypanosomes show highly polarised cell architecture with all major eukaryotic organelles (endoplasmic reticulum, Golgi apparatus, endosomal apparatus, lysosome, mitochondrion and peroxisome-like glycosomes) generally present in single copy. Furthermore, trypanosomes possess a single flagellum, which is important not only for cellular motility but also for cell division. How the duplication of all these cellular components is coordinated in order to progresss through the cell division cycle is poorly understood.

We used trypanosomes as a model organism due to the relative simplicity and the polarised nature of their cell architecture and determined the duplication of all their compartments. This was only possible due to a new synchronisation approach developed during this project.

In the first part of the thesis a precise temporal map of the cell division cycle of the BSF *T. brucei* cell division cycle was generated. By the use of well-described morphological markers (K/N status, new flagellum outgrowth and DNA synthesis) the position of individual cells was determined with high temporal resolution; this allowed us for the first time to synchronise a cell population *in silico* without affecting the naturally asynchronous growth.

In the second part of the thesis we used this tool to follow duplication events of the major organelles during progression through the cell division cycle. We precisely determined the time points of organelle duplication and found that it is ordered in trypanosomes. Furthermore we found that BSF *T. brucei* cells do not grow continuously, cell size start to increase rapidly, during a short period of time, late in the cell division cycle. We speculate that the initiation of cell volume increase is temporally separated from the formation of all secretory organelles in order to ensure maintenance of the protective coat, which must remain intact at all times in order for BSF trypanosomes to be able to evade the host immune response.

Zusammenfassung

Afrikanische Trypanosomen sind Erreger fataler Krankheiten sowohl bei Menschen also auch bei Nutztieren. Trypanosomen weisen einen komplexen Lebenszyklus auf und wechseln hierbei zwischen ihrem Überträger, der Tsetse Fliege (*Glossina spec*.) und ihrem Säugerwirt. Hieraus resultierend, erlebt der Parasit dramatische Veränderungen der Zellmorphologie und des Zellmetabolismus um sich an die jeweiligen Lebensräume anzupassen. Die zwei am besten untersuchten Lebensstadien sind die Prozyklische Form (PCF), welche in der Tsetse Fliege vorkommt und die Blutstrom Form, welche im Säugerwirt zirkuliert. BSF Trypanosomen leben extrazellulär im Säugerblut und sind hier kontinuierlich der Immunabwehr des Wirtes ausgesetzt. Durch einen dichten Proteinmantel eines einzigen Proteintyps, dem variablen Oberflächenglykoproteins (VSG) ummantelt der Parasit seine Zelloberfläche und schützt so invariable Proteine vor der Erkennung durch das Immunsystem. Um diesen VSG Mantel aufrecht zu erhalten werden enorm hohe Raten an Oberflächen-membran- und VSG- Recycling benötigt.
Trypanosomen weisen eine hoch polarisierte Zellarchitektur auf und die wichtigen Organellen (Endoplasmatisches Retikulum, Golgi Apparat, Endosomaler Apparat, Lysosome, Mitochondrium und Glykosomen) sind generell in einfacher Kopie vorhanden. Weiterhin besitzen Trypanosomen ein einzenes Flagellum welches sowohl für die Bewegung als auch die Zellteilung des Parasiten von großer Bedeutung ist. All diese Bestandteile müssen während des Zellzyklus verdoppelt werden um zwei lebensfähige Tochterzellen zu generieren. Über die Koordinierung und die Mechanismen der Organellenteilung ist kaum etwas bekannt. Wir nutzen den einfachen Zellaufbau und die polarisierte Zellarchitektur von Trypanosomen um die Verdopplung der zellulären Bestandteile zu untersuchen. Dies war jedoch nur durch einen neuen Synchronisierungsansatz möglich der im Rahmen dieser Arbeit entwickelt und etabliert wurde.
Im ersten Teil der Arbeit wurde eine zeitlich hoch aufgelöste Kartierung des Zellzyklus vorgenommen. Wir nutzen morphologisch gut beschriebene Marker um die Position einzelner Zellen im Zellzyklus zeitlich sehr genau zu bestimmen, somit kann eine *in silico* Synchronisierung durchgeführt werde ohne das natürliche Verhalten der Zellpopulation zu beeinflussen.
Im zweiten Teil der Arbeit wurde mittels dieser zeitlichen Zellzykluskarte der Teilungszeitpunkt aller wichtigen Organellen bestimmt. Hierbei fanden wir heraus, dass die Teilung der Zellorganellen in einer definierten Reihenfolge stattfindet. Weiterhin konnten wir zeigen, dass Trypanosomen nicht kontinuierlich wachsen, die Zelle wächst in einer relativ kurzen Phase, spät im Zellzyklus. Wir vermuten, dass die Teilung der sekretorischen Organellen und das Zellwachstums zeitlich voneinander getrennt sind um so den schützenden Proteinmantel, der für das überleben im Blut unabdingbar ist, aufrecht zu erhalten.

2 Introduction

2.0 Introduction

The cell surface of eukaryotes is a complex mixture of an indefinite number of proteins present in unknown quantities. Understanding how this cell surface homeostasis is controlled, maintained and fine-tuned is poorly understood. In principle, cells have to ensure that proteins are moved to the cell surface, during the process of secretion. Sorting of proteins for secretion is a crucial step for eukaryotes. Proteins destined for secretion run through several modification steps and controls within the endoplasmic reticulum and the Golgi apparatus. Then these proteins are packed into membrane vesicles and released by fusion with the cell membrane. Deciphering details of protein progression is difficult because most eukaryotes show redundant secretory pathways. There are multiple exocytic routes for protein delivery to the cell surface. Furthermore, the mechanism of organelle duplication and biogenesis of most cellular organelles remains unknown. A number of aspects of trypanosome biology appear to be more originally compared to current model eukaryotes like *Arabidopsis thaliana*, yeast, *Drosophila melanogaster*, *Caenorhabditis elegans*, the zebrafish *Danio rerio* or mice. Trypanosomes, which diverged earlier in eukaryotic evolution (Dacks et al., 2008), may provide a more native view on eukaryotic cell biology. In trypanosomes, the secretory organelles are present in single copy this seems to be the basic organelle configuration. This simplifies analysis of the biosynthetic and endocytic pathway and gives us hints how other eukaryotes developed and adapted during evolution. Furthermore, trypanosomes rely on efficient protein secretion to survive in the bloodstream of their mammalian host. The most conspicuous weapon that trypanosomes use to evade the host immune attack is a dense layer of a single protein type, the variant surface glycoprotein (VSG), which shields the entire cell surface. Maintaining the integrity of this VSG coat is essential for survival of the parasite in the mammalian bloodstream. During cell growth and duplication of the whole cellular compartments this protective VSG coat has to be maintained. This makes an effective cell division mechanism, in which VSG trafficking is never compromised, indispensable. For these reasons, the trypanosome is an ideal model for studying organelle duplication and membrane homeostasis.

Acquiring information on the temporal events in the *T. brucei* cell division cycle is difficult because a trypanosome population cannot be synchronised efficiently. Hydroxyurea (HU) induced cell-cycle arrest has been applied (Forsythe et al., 2009), but it is questionable whether a block-release approach for cell cycle synchronisation does not influence the analysis of cell cycle regulated events. Furthermore, it is questionable whether populations that are not synchronised in nature should be treated with harsh chemicals to enforce synchronised growth. The limitations in the temporal analysis of events can be bypassed by determining the exact cell cycle position of individual cells within an asynchronously growing culture.

2.1 *Trypanosoma brucei* as a model organism

2.2 Trypanosome cell architecture

Trypanosoma brucei features eminently polarised cell architecture. A network of highly ordered subpellicular microtubules underlies the entire pellicular cell membrane with the exception of the flagellar pocket (Angelopoulus, 1970). The cytoskeleton defines the cell shape, as the microtubules are connected to the plasma membrane (Hemphill et al., 1991), and grow in a semi-conservative manner (Sherwin and Gull, 1988) which maintains cytoskeleton integrity during the cell division cycle. The flagellar pocket marks the posterior side of the cell and accounts for 5% of the total cell membrane area and is the only place of endo- and exocytosis (Grünfelder et al., 2002). Trypanosomes possess a single flagellum that is maintained throughout the cell division cycle and is essential for survival of the parasite (Kohl et al., 2003; Broadhead et al., 2006). The single flagellum emerges from the flagellar pocket and is attached to the cell body by the flagellum attachment zone (FAZ) (Taylor and Godfrey, 1969). The FAZ consists of a FAZ filament and four specialized microtubules named the microtubule quartet (MtQ) (Sherwin and Gull, 1989). Theses specialized microtubules show inverted polarity compared to the rest of the microtubule corset (Robinson et al., 1995). The procyclic form (PCF), present in the tsetse fly midgut and the bloodstream form (BSF), the proliferating stage in the mammalian host are the best-studied forms of *T. brucei* and differ in morphological as well as physiological aspects.

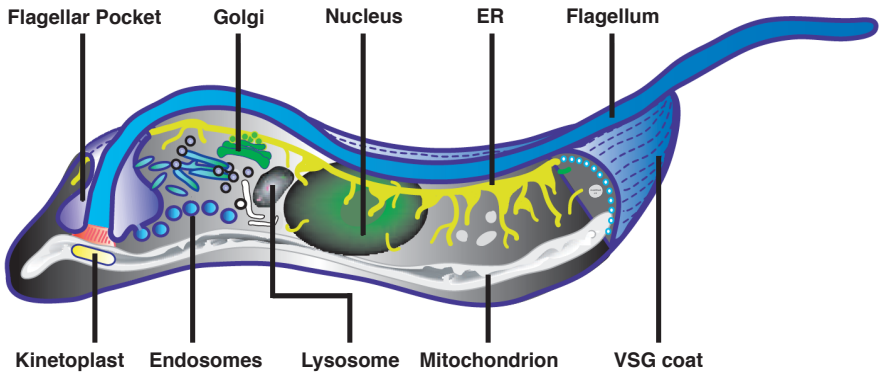

Figure 1. Schematic drawing of a bloodstream form trypanosome cell Trypanosomes are highly polarised cells. Most organelles are present in single copy and are located in the posterior between the kinetoplast and the nucleus. The ER and the mitochondrion span the whole cell. Modified from (Overath and Engstler, 2004)

The long slender bloodstream form of *T. brucei* is a spindle shaped cell of approximately 18 µm length and 3 µm width. The single flagellum is laterally attached to the cell body length with a free distal tip at the anterior cell pole. In PCF trypanosomes the flagellar pocket, the origin of the flagellum, is located further to the anterior end than in the bloodstream form (Robinson et al., 1995). In PCF trypanosomes the new growing flagellum is attached to the mature

flagellum by a structure called the flagellar connector (Moreira-Leite et al., 2001), this structure is not present in the bloodstream form. Recently Sue Vaughan and colleagues described an invagination in the cell plasma membrane of BSF trypanosomes, named the groove, that seems to have a similar function to the flagellar connector of PCFs (Hughes et al., 2013). The duplication of the kinetoplast, basal body and flagellum is well described and seems to be strictly controlled for PCF trypanosomes. First the basal body is duplicated, movement of the duplicated basal bodies then leads to segregation of the kinetoplasts (Robinson and Gull, 1991). The basal body further orchestrates cell morphology and is the nucleation site for the new flagellum (Lacomble et al., 2010). The increase in inter basal body distance as well as cell body length occur at a similar rate; it was suggested that these processes are controlled by similar mechanisms (Robinson et al., 1995).

2.3 The classic description of the cell division cycle

In principle, the cell division cycle describes the events that take place leading to duplication and division of a cell. In prokaryotes such as bacteria cells divide by binary fission, in eukaryotes the cell division cycle can be divided into different periods. During interphase, consisting of G1-, S- and G2-phase, cells grow and prepare for mitosis. In G1-phase cells increase in size, control mechanisms ensure that the DNA is ready for replication, followed by S-phase as the DNA gets replicated. During G2-phase the cell continues to grow, control mechanisms ensure that the cell is ready for mitosis, when cell growth stops and the nucleus divides. Cytokinesis divides the cytoplasm, organelles and cell membrane and in most eukaryotes occurs simultaneously with mitosis. This is why mitosis and cytokinesis are often used synonymously, but mitosis is diverse in eukaryotes (De Souza and Osmani, 2007). In animals the nuclear envelope breaks down during mitosis leading to an open mitosis whereas fungi show a closed mitosis (De Souza and Osmani, 2007). Trypanosomes show a closed mitosis. The events leading to cell division in trypanosomes have been describes for the procyclic form by Woodward and colleagues (Woodward and Gull, 1990). In trypanosomes mitosis and cytokinesis are uncoupled. Trypanosomes show a post mitosis phase for both the kinetoplast and the nucleus followed by cytokinesis (Woodward and Gull, 1990). Trypanosomes lack several classic cell division cycle checkpoints. To date no mitosis checkpoint has been identified. Incomplete mitosis and cytokinesis often lead to multinucleate cells with different numbers in kinetoplasts and nuclei (Ploubidou et al., 1999). Conversely defects in cytokinesis lead to multinucleated cells that further proceed through mitosis (Das et al., 1994; Sheader et al., 2005; Hu et al., 2012).

2.4 Cell cycle regulation

Trypanosomes show some differences in cell cycle regulation compared to other eukaryotes, as there are orthologoues of conserved eukaryotic cell cycle regulators, which have diverged in function or are absent in *Trypanosoma brucei* (Hammarton, 2007). In most eukaryotes cyclins (CYC) and cyclin-dependent kinases (Cdk) are key players in cell cycle regulation. Cyclins and Cdks work as heterodimeric protein kinases with cyclins acting as the regulatory subunit, increasing and decreasing in concentration during the cell cycle and CdKs working as the catalytic subunit associating with several different cyclins. Depending on the associated cyclin, these complexes can phosphorylate different proteins, required for activation of genes involved in cell cycle progression (Nigg, 1995). In trypanosomes several homologues of cyclins and cyclin-dependent kinases are present; termed cyclins and cdc2-related kinases, respectively (Mottram and Smith, 1995). 11 cyclins and 12 cdc2-related kinases (CRK) have been described in trypanosomes. CYC2 and CRK1 are involved in G1/S-phase transition (Tu et al., 2005; Gourguechon et al., 2007). G2/M-phase transition is controlled by CYC2, CRK3 and CYC6 in PCF *Trypanosoma brucei* (Van Hellemond et al., 2000; Hammarton et al., 2003; Gourguechon et al., 2007). Furthermore Wang and colleagues showed that cyclin 10 and 11 as well as CRKs 7 to 12 are not essential in PCFs (Gourguechon and Wang, 2009). Knockdown of CRK9 leads to accumulation of PCFs in G2/M showing one kinetoplast, one nucleus but two basal bodies. The two basal bodies do not separate in these cells, as inter basal body distance is reduced compared to control cells. Gourguechon and colleagues emphasize the importance of correct basal body segregation for progression through the cell division cycle (Gourguechon and Wang, 2009).

2.5 Cell cycle synchronisation

Cell cycle synchronisation is a process, by which cells at different stages of the cell division cycle are selected or brought to a transient halt at the same phase of the cell division cycle. This can be achieved by two different strategies, either by physical fractionation or by a chemical blocking approach. Cell synchronisation by physical fractionation is based on differences in physical properties of cells, such as cell size or their affinity to antibodies. Centrifugal separation can be used to sort cell populations by size whereas fluorescence-activated cell sorting (FACS) is used to distinguish between cells based on differences in size or fluorescence emission; here single cells pass through a light beam and are sorted based on their specific properties. Chemical blocking approaches are based on blocking a metabolic reaction e.g. DNA synthesis or organelle separation. Likewise, starvation can lead to accumulation of cells at G1-phase or cell synchrony is achieved by restoring nutritional supply. The ciliated protozoan, Tetrahymena was the first cell that showed synchronised division in suspension culture (Zeuthen, 1971), which led to the first insights into the existence of mechanisms that control the cell cycle. Common methods for mammalian cell cycle synchronisation are based on chemical blocking of DNA replication, synthesis or mitotic spindle formation due to treatment with colchicine or hydroxyurea (Taylor, 1965; Adams and Lindsay, 1967; Romsdahl, 1968). Cell cycle synchronisation of *T. brucei* is a major challenge since most synchronisation attempts failed either due to toxicity issues (Forsythe et al., 2009). Mitosis inhibition does not arrest trypanosomes, as mitosis seems to be uncoupled from cell division cycle progression, leading to anucleate cells termed zoids (Ploubidou et al., 1999). Chowdhury and colleagues were able to demonstrate a high degree of synchronisation of PCF *T. brucei* using hydroxyurea (Chowdhury et al., 2008) and Hammarton and colleagues adapted this hydroxyurea based approach for cell cycle synchronisation of bloodstream form *T. brucei* (Forsythe et al., 2009). Treating BSF T. brucei with 10 µg ml^{-1} for 6 hours led to enrichment of cells in S-phase. After hydroxyurea (HU) removal cells proceeded synchronously only through one round of the cell cycle. This synchronisation approach was rather inaccurate, since enrichment of cells in S-phase does not reflect a specific timepoint. This explains how synchronous cell growth was lost within a short period of time. All in all, sufficiently synchronised cell growth to study cell cycle events in BSF *T. brucei* is not achievable so far. Furthermore, it is questionable whether the behaviour of cells, forced to synchronised growth, reflects their behaviour in the natural population. Treatment with harsh chemicals such as hydroxyurea may interfere with fine-tuned, cell division cycle dependent mechanisms, even hours after removal.

2.6 Models for organelle biogenesis

Several different models for maintaining and duplicating organelles and cellular compartments have been discussed in the literature. One way an organelle can be built is by *de novo* biogenesis, where the blueprint needed to build a new organelle is stored in the genome and the cell can hence produce a new organelle independent of a pre-existing one. A second mechanism of organellogenesis is by growth and fission, here the old organelle grows and divides by fission to produce two organelles out of one. A further mechanism combines both principles. Here the basic infrastructure of the organelle is built *de novo* and then this premature new organelle maturates to develop to a functional organelle by importing enzymes and components from the pre-existing mature organelles. This means that the new organelle cannot develop into a functional organelle without a pre-existing one that serves as a template. Figure 2 illustrates the different models for organelle biogenesis (taken from Lowe and Barr, 2007).

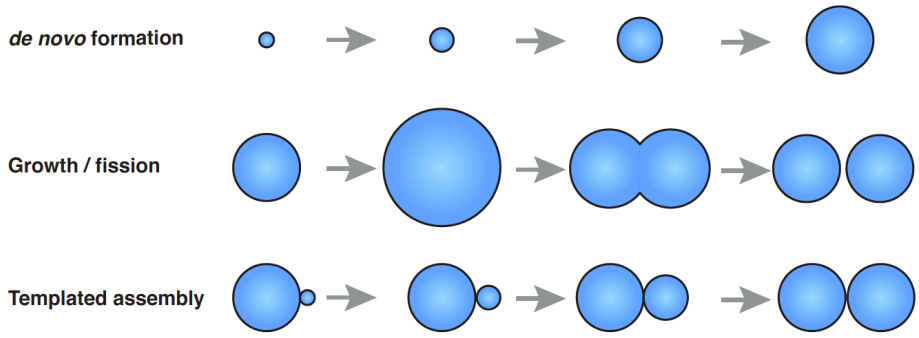

Figure 2. Schematic of organelle duplication models. Modified from (Lowe and Barr, 2007).

To maintain organelle inheritance cells must ensure, that each daughter contains at least one copy after cell division. Loew suggests that a single copy organelle has to be actively segregated to ensure that each cell retains one functional organelle. Active segregation has been described for the PCF *T. brucei* Golgi apparatus, here the single Golgi apparatus is always linked to the basal body, this link assigns each Golgi to a basal body after duplication and thus to the two daughter cells, respectively (He et al., 2004). Lowe suggests that for multi-copy organelles, stochastic partitioning seems to be efficient to maintain organelle inheritance. This mechanism is used for the mammalian endoplasmic reticulum, mitochondrion and Golgi apparatus, due to the fact that mammalian cells host a large number of dispersed organelles in the cytoplasm. Due to a cytokinetic mechanism, that divides the mother cell into two equally sized daughter cells the organelles are partitioned by chance. The same can be seen for the plasma membrane where stochastic partitioning devides the surface of the mother cell (Warren and Wickner, 1996). An ordered mechanism for multi copy organelles has been described for the *S. cerevisiae* mitochondrion, where the dividing organelle forms a filamentous network and the

tip invades into the bud. The inheritance of this organelle is regulated by spatial distribution and attachment of the organelles to cellular architecture structures and is further temporally linked to the cell division cycle (Warren and Wickner, 1996).

2.7 Eukaryotic organelles

The endoplasmic reticulum

The nucleus is a characteristic organelle for eukaryotes enclosed by two membranes, the inner and the outer nuclear membrane. The inner layer surrounds the nucleus and the outer layer is part of the endoplasmic reticulum (ER). The ER appears to be an extensive network of sheets and tubules, interconnected and spanning through the whole cell. By means of the structure one can distinguish between two types of ER, the rough and the smooth ER. The rough ER is studded with ribosomes and is located around the nuclear envelope, where the mRNA, for proteins destined for secretion is translated into the ER lumen and further processed. The smooth ER is free of ribosomes and functions in several metabolic processes such as lipid and steroid synthesis. Secretory proteins are translated into the ER lumen, where proteins are sorted, modified and further transported to the cytoplasm or the Golgi apparatus. Proteins that fulfil functions in the ER lumen are retained in the ER by a retention motif composed of the four amino acids KDEL (lysine, aspartic acid, glutamic acid, leucine) at the C-terminus of the protein (Pelham, 1989). This retention motif is conserved in eukaryotes but can differ between different species as in trypanosomes, where the ER retention signal is composed of the amino acids MDDL (methionine, aspartic acid, aspartic acid, leucine) (Bangs et al., 1993). Secretory proteins leave the ER in COPII vesicles, which transport the cargo to the *cis*-side of the Golgi apparatus (anterograde transport). The retrograde transport returns proteins of the molecular transport machinery, as well as incorrectly routed components via COP I vesicles from the *cis*-side of the Golgi apparatus back to the ER. In trypanosomes the transport of cargo between the ER and the Golgi occurs exclusively at the so-called endoplasmic reticulum exit-site (ERES). It is a characteristic feature of trypanosomes that parts of the smooth ER are attached to four specialized subpellicular microtubules, which mark the flagellum attachment zone (Vaughan et al., 2008).

The Golgi apparatus

The Golgi apparatus is a polarised organelle consisting of flattened cisternae. In the Golgi apparatus modifications, sorting and packaging of proteins for secretion takes place. Proteins that exit the ER enter the Golgi from the so-called *cis*-side and are processed moving towards the *trans*-side of the Golgi. How cargo is transported through the Golgi is debated. The two favoured hypotheses are the vesicular transport and the cisternal maturation model. The vesicular transport model describes the Golgi as a stable organelle with cisternae separated from each other in cis to trans direction, with membrane bound vesicles that shuttle cargo between different cisternae (Glick and Malhotra, 1998; Glick and Luini, 2011). In the cisternal maturation model, COPII vesicles from the ERES fuse and form the first *cis*-cisterna of the Golgi stack, which maturates and finally forms secretory vesicles (Glick, 2000; Glick and Luini, 2011). The function of the Golgi is highly conserved, whereas the structure and number vary from species to species. Mammalian cells can contain hundreds of Golgi in the perinuclear region (Mogelsvang et al., 2004) whereas in plant cells Golgi stacks are spread independently in the cytoplasm, each associated with an ERES (daSilva et al., 2004). In yeast we find a new situation, here the Golgi is not stacked but instead has dispersed cisternae and tubular networks (Lowe and Barr, 2007). In contrast to most eukaryotes, several protozoon parasites such as *Toxoplasma gondii*, *Leishmania* and trypanosomes possess only a single Golgi apparatus. The diversity in Golgi number and location in different eukaryotes has led to several proposed mechanisms for Golgi duplication. In mammalian as well as plant cells it has been suggested that the Golgi is duplicated by binary fission after elongation of the old Golgi structure (Langhans et al., 2007). In yeast the duplication of the Golgi apparatus is linked to the ER, as it is formed *de novo* at the ERES (Rossanese et al., 1999; Bevis et al., 2002; Losev et al., 2006). In the obligate intracellular parasite *Toxoplasma gondii* the Golgi is a single copy organelle that grows by extension and is split by medial fission (Pelletier et al., 2002). The PCF of *Trypanosoma brucei*, which also harbours a single Golgi apparatus, differs in the duplication mechanism, as the new Golgi apparatus is built *de novo,* but in addition receives material from the old Golgi apparatus (He et al., 2004).

The endosomal system

Endo- and exocytosis are fundamental processes in eukaryotes for the exchange of components with the environment. In most eukaryotes the endosomal system, subdivided into early, late and recycling endosomes, is the major sorting machinery. In mammalian cells and yeast endo- and exocytosis are performed via various mechanisms, with internalisation performed via clathrin-coated vesicles (CCV), non-coated vesicles, phagosomes, caveola and macropinosomes. In trypanosomes endocytosis is performed exclusively via clathrin coated vesicles

(Allen et al., 2003), whereas exocytosis is performed via Rab11 positive carriers (Grünfelder, 2003). A distinctive feature of trypanosomes is that both endo- and exocytosis take place at the flagellar pocket only, an invagination comprising approximately 5% of the cell surface area (Grünfelder et al., 2002; Engstler et al., 2004; Overath and Engstler, 2004). *Trypanosoma brucei* is an established model organism for endo- and exocytotic processes and is characterised by extremely high turnover rates compared to other organisms (Overath and Engstler, 2004).

The lysosome

Lysosomes are organelles, which contain a subset of enzymes and proteins for protein degradation and are responsible for the final degradation of endocytosed and recycled material. Lysosomes maintain cellular homeostasis due to their involvement in secretion and degradation, plasma membrane repair and energy metabolism related to health and diseases of cells (Appelqvist et al., 2013; Settembre et al., 2013). The lysosome maintains a highly acidic environment where various numbers of enzymes are only active at a pH of about 5 or less. It has been suggested, that lysosomal enzymes are synthesized in the ER and are released from the Golgi in vesicles maturating to final lysosomes by fusion with acidic vesicles derived from endosomes, but detailed mechanisms of lysosome biogenesis and duplication are still unknown. Immunofluorescence analysis has suggested that *Trypanosoma brucei* possesses a single lysosome and thus is well suited as a model organism to study lysosome biogenesis and inheritance.

Glycosomes

Glycosomes are specialised organelles found exclusively in kinetoplastida. They were first discovered in *Trypanosoma brucei* and classified to belong to the family of peroxisomes (Opperdoes and Borst, 1977). In contrast to other eukaryotes, trypanosomes compartmentalize glycolysis. This compartmentalization is essential, as mislocalisation of glycolytic enzymes into the cytosol of trypanosomes is lethal, causing the accumulation of hexose-phosphatase in the cytoplasm (Bakker et al., 1997; Blattner et al., 1998). The biogenesis of peroxisomes is not fully understood and different duplication models have been described in different organisms (Hettema and Motley, 2009). In dividing *S. cerevisiae* the number of peroxisomes doubles due to fission prior to every cell division and peroxisomes are distributed between mother and daughter cell (Hoepfner et al., 2001). In contrast to the situation in yeast, mammalian cells show both *de novo* formation and multiplication of peroxisomes by fission. It is not known whether peroxisomes can be made *de novo* in yeast (Kim et al., 2006). It is further thought that peroxisomes mature from pre-existing membrane vesicles as peroxins transport matrix proteins into the lumen of precursor peroxisomes (Purdue and Lazarow, 2001). Peroxisome mem-

brane assembly and maintenance requires three peroxins, Pex3, 16 and 19 (Distel et al., 1996). Peroxin 11 has a direct role in peroxisome division as knockdown leads to elongated and clustered peroxisomes (Li and Gould, 2002).

2.8 Organelle inheritance

Different organisms have evolved different strategies to maintain organelle number and size, as well as cell size. The inheritance strategy adopted by an organelle varies from organelle to organelle and cell type to cell type (Warren and Wickner, 1996). Despite these variations, organelle and membrane homeostasis has to be controlled and regulated during the cell division cycle to maintain the cellular infrastructure. Up to date there is little known on how cells fulfil these tasks and stay functional. Organelles that have their own DNA, i.e. chloroplasts and the mitochondrion are maintained over several generations in eukaryotes. It also seems obvious to maintain the endoplasmic reticulum, as these membranes cannot be synthesized *de novo*. In principle the mode for organelle inheritance depends on the number of organelles present. A single copy organelle has to be segregated actively prior to cell division in order to be maintained. For multi-copy organelles it was suggested, that stochastic partitioning mechanism could explain organelle inheritance (Lowe and Barr, 2007). Still how the size and number of organelles in a cell is controlled and maintained is not understood. To date, the only organisms were a controlled cell elongation is described is *Schizosaccharomyces pombe*. A spatial gradient of protein kinases is thought to coordinate cell size and elongation as well as mitotic entry into fission (Moseley et al., 2009). Still for most eukaryotes is is not known how cell size is controlled or maintained.

2.9 The VSG and antigenic variation

The surface of *Trypanosoma brucei* is covered with a monolayer of the variant surface glycoprotein (VSG), acting as a physical barrier to the host immune response (Cross, 1975). The genome of trypanosomes encodes for many different VSGs. Although the primary structure of different VSGs is highly divergent, the tertiary structure appears to be well conserved (Blum et al., 1993; Jones et al., 2008). VSGs are GPI anchored (Ferguson et al., 1988), which allows diffusion on the cell surface. VSGs diffuse within the cell membrane with an average velocity of approximately 0.02 – 0.03 $\mu m^2/s$ (Hartel, 2013). This high mobility could also play a role in VSG trafficking and recycling (Overath and Engstler, 2004). Trypanosomes express approximately 5 x 10^6 VSG dimers on their surface (Jackson et al., 1985). Due to recycling the VSG coat is exchanged every 12.5 minutes (Engstler et al., 2004). The VSG trafficking takes place exclusively at the flagellar pocket. It is a fascinating question how trypanosomes achieve these high rates of protein trafficking. The variability of the VSG surface coat is achieved by antigenic variation (Borst et al., 1996), this adaptability as well as the mobility and density of the VSG coat are essential for parasite survival. *T. brucei* expresses only a single VSG at any given time and the surface coat changes by stochastic switching to a new VSG (Turner and Barry, 1989; Barry and McCulloch, 2001). The host immune response identifies each VSG as an antigen and mounts an attack every time. A new subpopulation expressing a new distinct VSG will evade this immune response and will cause a new 'parasitic wave' (Ross and Thomson, 1910).

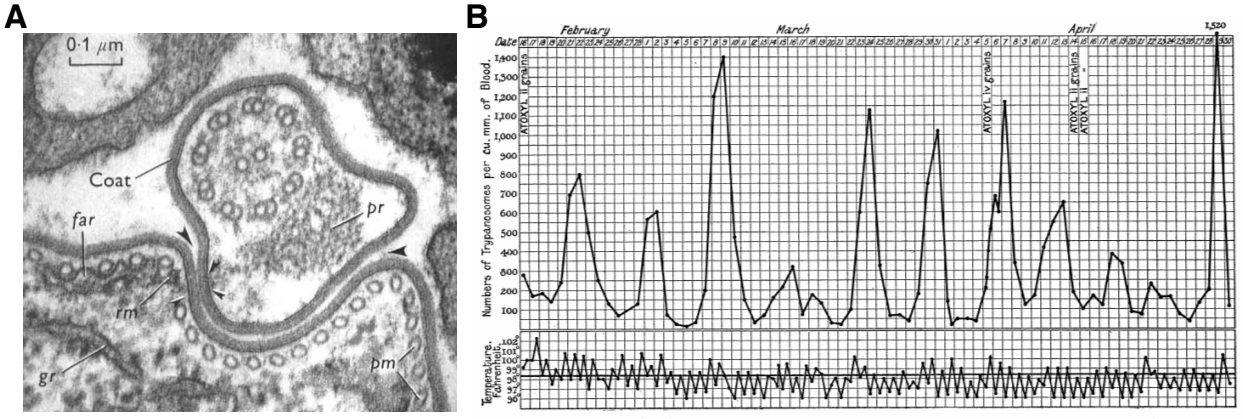

Figure 3. Basis for trypanosome pathogenicity. (A) Shows the VSG coat (Coat) in a transverse section taken from glutaraldehyde fixed *T. b. rhodesiense*. Scale bars = 0.1 μm. Taken from (Vickerman, 1969). (B) Shows the periodical progression of a *T. b. gambiense* infection. Taken from (Ross and Thomson, 1910).

2.10 VSG trafficking and recycling

In order to maintain the VSG surface coat trypanosomes have perfected protein trafficking and recycling. It has been shown that *T. brucei* performs endosomal membrane trafficking at a very high rate and a lower level of complexity than in mammalian cells (Overath and Engstler, 2004). First, endo- and exocytosis are restricted to the flagellar pocket. Second, endo- and exocytosis are performed by non-redundant pathways. Endocytosis occurs exclusively via a clathrin-dependent mechanism (Allen et al., 2003), while Rab11 positive vesicles are responsible for exocytosis (Grünfelder, 2003). Third, the endomembrane system is compactly located in the posterior part of the cell.

In the ER the VSGs undergo posttranslational modifications, like the addition of oligosaccharides and attachment of the GPI anchor. The modified VSG is transported via COPII vesicles to the *cis*-Golgi, where further modifications, such as glycosylation occur. How the VSG is finally transported to the flagellar pocket is still debated. At least three different routes are described for the VSGs delivery to the flagellar pocket. Besides direct transport via vesicle budding from the Golgi, VSGs can be transported to the flagellar pocket via clathrin coated vesicles (CCV) and late endosomes or non-clathrin coated vesicles, so called recycling endosomes (Grünfelder, 2003). To maintain the high surface coat density, the concentration of VSGs is increased between the different membrane compartments by 50-fold (Grünfelder et al., 2002). VSGs are internalized at the flagellar pocket via CCV, which move towards the nucleus, where the VSGs enter Rab5 positive early endosomes (EE). From early endosomes the VSG directly enters Rab11 positive recycling endosomes (RE) or Rab7 positive late endosomes (LE). To date it is not known how recycled membranes are delivered from LE to the lysosome. Afterwards the recycled VSGs are transported to the flagellar pocket via Rab11 positive recycling endosomes and Rab11 positive exocytic carriers.

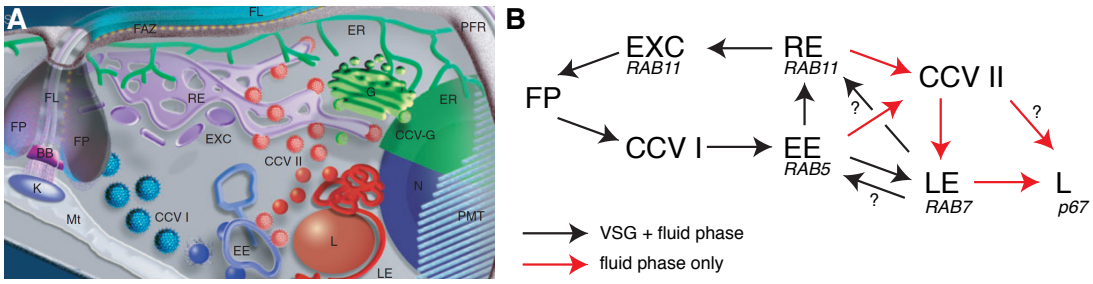

Figure 4. Illustration of the posterior part of the *Trypanosoma brucei* cell. (A) Shows structures present in the posterior part of a trypanosome. (B) Illustrates the passage of VSG and fluid phase cargo through endosomal structures. AX, axoneme; BB, basal body; CCV I, class I clathrin coated vesicles; CCV II, class II clathrin coated vesicles; EE, early endosomes; ER, endoplasmic reticulum; EXC, exocytic carrier; FAZ, flagellar attachment zone; FL, flagellum; FP, flagellar pocket; G, Golgi apparatus; K, kinetoplast; L, lysosome; LE, late endosomes; Mt, mitochondrion; N, nucleus; PFR, paraflagellar rod; PMT, pellicular microtubule; RE, recycling endosomes; SC, surface coat; VSG, variant surface glycoprotein. Modified from (Overath and Engstler, 2004)

2.11 Diversity of African trypanosome species

In sub-Saharan Africa, several different trypanosome species are the causative agent of fatal diseases in diverse animal species. *Trypanosoma brucei rhodesiense* and *T. b. gambiense* cause human sleeping sickness, whereas *T. vivax, T. congolense* and *T. b. brucei* cause nagana in domestic animals. By this trypanosomes have a major impact on public health as well as local agriculture and economy. Most research was focused on *Trypanosoma brucei brucei*, as this species was easily accessible to state of the art forward and backward genetics. This is in part due to the fact, that no reproducible experimental methods are currently available to maintain different stages of *T. vivax* and *T. congolense* in laboratory conditions. Only few procedures conducting *in vitro* cultivation of *T. vivax* and *T. congolense* are available (Trager, 1975; Hirumi and Hirumi, 1991; Otigbuo and Oyerinde, 1993), still long-term cultivation of these species is a difficult task. In the 1990 appropriate protocols were developed to maintain axenic cultures of *T. b. brucei*, *T. congolense* and *T. vivax*, by this *T. b. brucei* and *T. congolense* were genetically manipulated successfully (D'Archivio et al., 2011). Constitutive protein expression in *T. vivax* has been established about 15 years later (D'Archivio et al., 2011), however detailed analysis of fundamental processes in these species was unattended for years.

3 Results

Functional cell division is a prerequisite in eukaryotes to ensure segregation of all essential cell components. Trypanosomes have become a convenient model organism for investigating fundamental questions in cell biology (Overath and Engstler, 2004) as they display a highly polarised cell architecture and most of its organelles are present in single copy which simplifies the analysis of the cell division cycle. Since forward genetics became a routine method to investigate *Trypanosoma brucei* cell biology, many cell cycle phenotypes have been described (Muñoz-Jordán and Cross, 2001; Sheader et al., 2005; Chanez et al., 2006). Unfortunately, obtaining detailed information on the temporal events in the *T. brucei* cell division cycle has been difficult because of the apparent disadvantage that a proliferating trypanosome population cannot be synchronised efficiently. In order to circumvent this limitation we opted for an *in silico* synchronisation approach. Therefore, we developed a new approach by an unbiased screen using morphological well-described structures that change during cell division cycle progression. On the basis of a high significant number of cells we synchronised a natural growing trypanosome population based on these morphological markers.

The first step of this project was the identification of markers that would allow the positioning of a randomly picked cell from a growing culture within the cell division cycle, which in effect synchronised the cell population *in silico*. Afterwards the duplication events of the major organelles, such as the endoplasmic reticulum, the endoplasmic reticulum exit site, the Golgi apparatus, the endosomal apparatus, the lysosome, the glycosomes and the mitochondrion were analysed and pinpointed with high temporal resolution. Central to the analysis was the question whether these organelles are segregated or built *de novo*. Furthermore, we were interested in the chronology of organelle duplication. Is the duplication of the organelles precisely timed or temporally uncoupled from the cell division cycle? For this we used immunofluorescence analysis as well as high-speed live cell microscopy to investigate the dynamics of organelle duplication during the cell division cycle.

3.1 The cell division cycle of *T. brucei* can be timed precisely

Gathering information on the temporal events in the *T. brucei* cell division cycle was difficult because of the apparent disadvantage that a constantly proliferating trypanosome population cannot be synchronised efficiently. Besides technical problems in establishing long-term synchronously growing cultures we doubt the soundness of chemical approaches for analysis of such populations, as they are not synchronised in nature. The following characteristic and well-described events occurring in the cell division cycle were taken into account (1) duplication of the kinetoplast and nucleus, (2) the outgrowth rate of the daughter flagellum and (3) DNA synthesis. These data were correlated with the aim of creating a comprehensive temporal map to allow the determination of the exact cell cycle position of individual cells.

In *T. brucei*, the order and mode of kinetoplast and nucleus division are well described and allowed us to split the cell division cycle into rough sections (Woodward and Gull, 1990; Siegel et al., 2008). A trypanosome cell in G1/S-phase has a single kinetoplast (K) and a single nucleus (N) and is termed 1K1N. During S-phase, the kinetoplast segregates first, leading to a 2K1N cell. As segregation of the kinetoplast is well understood and described (Robinson and Gull, 1991; Hammarton et al., 2007; Gluenz et al., 2011), we further distinguished cells with a early dividing (v-shape; $1K^{V}$) and late dividing (bone-shaped; $1K^{B}$) kinetoplast (Figure 5A). In trypanosomes mitosis and cytokinesis are uncoupled, leading to a bi-nuclear 2K2N cell after mitosis, which is separated by scissiparity during cytokinesis (Woodward and Gull, 1990).

We first determined the percentage of cells in each section of the cell division cycle, based on the kinetoplast and nucleus content (Figure 5B). In an exponentially growing population of BSF trypanosomes, 72% of the cells displayed one kinetoplast. These could be further divided into

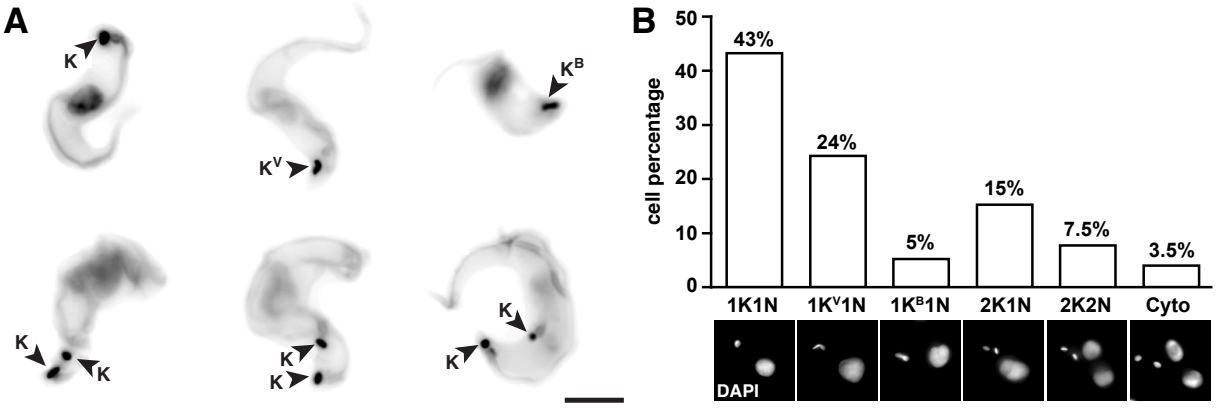

Figure 5. Cell division cycle stages based on kinetoplast and nucleus status. (A) Cells were stained with the inpermeable sulfo-NHS-AMCA dye, which binds to primary amines and hence labelees the cell surface; DNA was counterstained with DAPI. Arrows indicate the kinetoplasts at different stages in the cell division cycle. Early dividing ($1K^{V}1N$) and late dividing ($1K^{B}1N$) kinetoplasts are indicated (Jung, 2009). Scale bar = 4 µm. (B) Percentage of each cell cycle stage in the population based on kinetoplast and nucleus content as determined by DAPI labelling (n=2500).

43% of 1K1N cells prior to kinetoplast duplication, 24% cells with a kinetoplast during S-phase ($1K^V1N$) and 5% cells with a dividing kinetoplast ($1K^B1N$). About 26% of the cells in the population contained two separated kinetoplasts within 15% displaying one and 11% two nuclei. Late in the cell division cycle, cells performed cytokinesis (Cyto) a stage, which was represented by 3.5% of the cells. For a more precise classification of the cell division cycle we considered flagellum outgrowth as a further morphological marker.

It was reported, that the mature flagellum is a structure, which remains constant in length during the cell division cycle while the new flagellum grows, which hence, can be used as a timer (Tyler et al., 2001). The new daughter flagellum originates at the posterior cell pole within the flagellar pocket, immediately adjacent to the origin of the old flagellum (Kohl et al., 1999; Moreira-Leite et al., 2001; Hughes et al., 2013). The new flagellum is assembled at its tip and grows at a constant rate towards the anterior cell pole (Tyler et al., 2001). In cells displaying two flagella, we compared the length of the new, growing flagellum with the constant length of the mature flagellum (Figure 6). This ratio was termed *New Flagellum Ratio* (NFR) and encompassed values between 0 and 1. Cells displaying only one mature flagellum had an NFR of 0; the others were equally divided into 10 groups, each covering 10% of new flagellum outgrowth. Finally, cells with a value of 1 had two flagella, the mature and the new fully-grown flagellum.

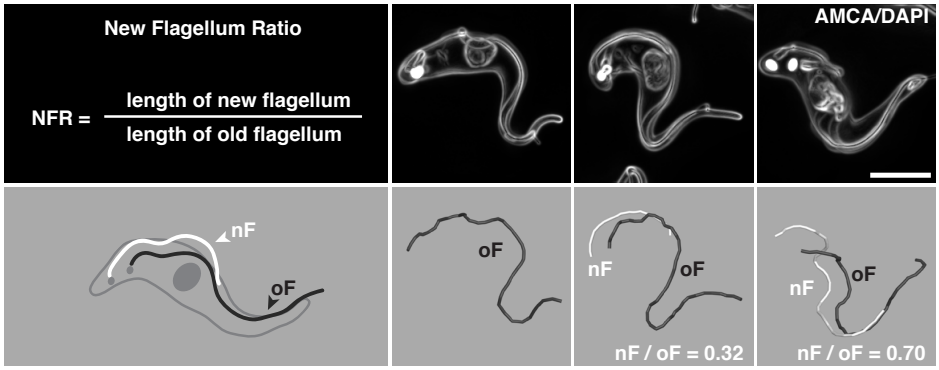

Figure 6. Determination of the New Flagellum Ratio. Deconvolved 3D-stacks of surface stained cells were analysed with the Imaris software package. The upper panel shows AMCA and DAPI stained cells. The ImageJ edges algorithm was used for better visualisation of the cell and flagellum surface. The lengths of the new (white line) and mature (black line) flagellum were determined and the NFR ratio calculated. Modelled cells with different NFR are depicted in the lower panel. Scale bar represents = 5 µm

If specific events, defining morphologically distinguishable cell types, are temporally ordered in an asynchronously growing culture, the timing of these events can be calculated from the proportion of cells representing each cell type. The duration of each event could be calculated by a method described by Williams (1971) if the following parameters were defined: (1) the time to accomplish the cell division cycle, (2) the proportion of cells in a particular cell division cycle step and (3) the order of these cell cycle steps.

$$x = t\,\frac{ln\left(1-\frac{1}{2}y\right)}{-ln(2)}$$

The equation contained *t* as the population doubling time, *y* as the cumulative proportion of cells representing a particular stage in the cell division cycle and *x*, the duration of the presence of a particular stage during the cell division cycle (Wheeler et al., 2011).

For the kinetoplast and nucleus as well as for the NFR, the Williams algorithm was used to calculate the duration of each morphological event (Woodward and Gull, 1990), with 5.9 hours as population doubling time (*t*). The time-period for each NFR group varied only slightly between 0.29 and 0.33 hours (Table 1A); thus confirming the constant growth of the new flagellum (Tyler et al., 2001). In Table 1B the duration of each stage based on the K/N status was calculated. The 1K1N stage showed the longest duration with 2.6 hours compared to the cytokinesis event, which was the shortest with 0.15 hours.

Table 1. Duration of morphological events based on NFR and K/N status. (A) Shows the time the new flagellum took to grow 10% in length (n = 500 in total). (B) Shows the duration of each cell cycle stage based on kinetoplast and nucleus content (n = 2500 in total).

A

NFR	proportion of cell cycle	time / hours	time [h:m]
10	0.10	0.32	0:19
20	0.10	0.31	0:19
30	0.10	0.32	0:19
40	0.10	0.33	0:20
50	0.10	0.33	0:20
60	0.10	0.32	0:19
70	0.10	0.33	0:20
80	0.11	0.34	0:20
90	0.09	0.31	0:19
100	0.10	0.29	0:18

B

stage	proportion of cell cycle	time / hours	time [h:m]
1K1N	0.43	2.60	2:36
$1K^{v}1N$	0.24	1.40	1:24
$1K^{B}1N$	0.05	0.30	0:18
2K1N	0.15	0.90	0:54
2K2N	0.075	0.45	0:27
Cyto	0.035	0.15	0:25

A first step towards the generation of the temporal map was to correlate the data obtained for new to old flagellum length ratio with distinct kinetoplast and nucleus conformations (Figure 7). The new to old flagellum ratios spanned from 0 to 0.5 (NFR=10 – 50) for $1K^V1N$ cells, 0.36 to 0.5 (NFR=40 – 50) for $1K^B1N$, 0.5 to 0.77 (NFR=50 – 80) for 2K1N and 0.75 and 1 (NFR=80 – 100) in 2K2N cells. We precisely matched an NFR value to a K/N status comparing the 25th and 75th percentile corresponding to the boxes in Figure 7. The 25th and 75th percentile ranged from 0.07 to 0.35 for $1K^V1N$ cells, 0.45 to 0.5 for $1K^B1N$, 0.55 to 0.65 for 2K1N and 0.75 to 0.85 for 2K2N cells. These values served as an internal control comparing the K/N status with the NFR.

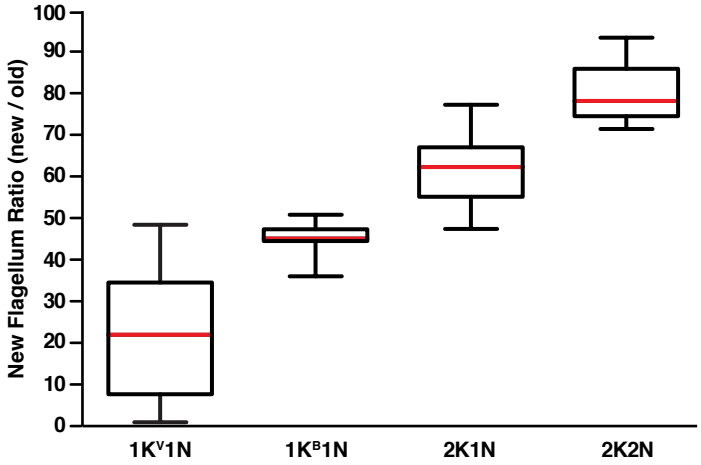

Figure 7. Cells with different kinetoplast and nucleus conformation show a characteristic range of NFR. The conformation of kinetoplast and nucleus was determined and plotted against the corresponding NFR value (n = 500 in total). The red line indicates the medium flagellum length for each stage. The box refers to the range defined by the 25th and 75th percentile; whiskers indicate the minimum and maximum NFR values.

In the next step, the classical description of the eukaryotic cell cycle based on G1, S-phase, G2 and mitosis, was used as an additional marker to refine the temporal cell cycle map. We used the incorporation of EdU (5-ethynyl-2´-deoxyuridine) into newly synthesized DNA to determine the duration of the kinetoplast and nucleus S-phase. Gull and colleagues showed, that for the trypanosome cell cycle, besides G2-phase, additional cytological post S-phase events have to be considered (Woodward and Gull, 1990). We have to consider, that the cell is binuclear after mitosis and has two kinetoplasts before the period of cell cleavage takes place. Taken together, 5 stages for both the kinetoplast (G1, S_K, G2, M_K and P_K) and the nucleus (G1, S_N, G2, M_N and P_N) had to be considered. Figure 8A shows the proportion of cells with either a single, dividing or post division kinetoplast and nucleus (n=600). 68% of cells showed a single kinetoplast compared to 82% with a single nucleus, this showed, that kinetoplasts segregate first leading to 2K1N cells which after mitosis led to the pre-cytokinesis 2K2N stage. The percentage of dividing organelles was similar, as we found 5% of dividing kinetoplasts and 6% of mitotic nuclei.

A

organelle	kinetoplast	nucleus
single organelle	0.68	0.82
dividing organelle	0.05	0.06
post-division	0.27	0.12

B

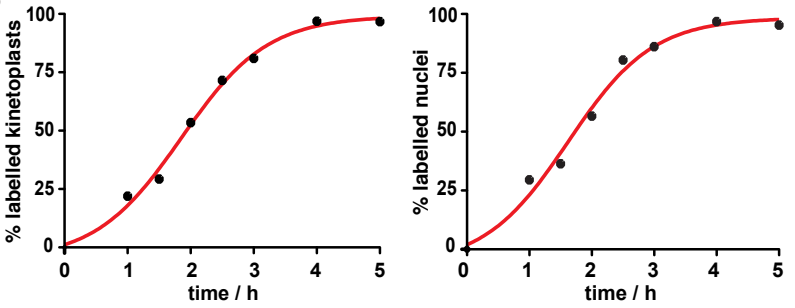

C

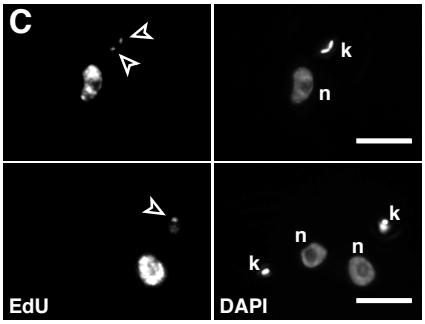

D

Kinetoplast		
stage	proportion of cell cycle	time / h
G1	0.36	2.12
S_K	0.14	0.81
G2	0.20	1.18
M_K	0.05	0.25
P_K	0.27	1.44

Nucleus		
stage	proportion of cell cycle	time / h
G1	0.37	2.17
S_N	0.21	1.20
G2	0.28	1.64
M_N	0.06	0.26
P_N	0.12	0.53

Figure 8. EdU incorporation into newly synthesized DNA was used for cell cycle analysis. (A) For both the kinetoplast and the nucleus the number of organelles in division was determined by counting DAPI stained cells for either a single organelle, dividing organelle and duplicated organelle. (B) Shows the percentage of labelled kinetoplasts and nuclei in dependance of the time period in which the cells were incubated in the presence of EdU (n≥1200). (C) EdU incorporation (left panel) into the kinetoplasts (arrowheads) and the nuclei. Cells were counterstained with DAPI (right panels). Scale bar = 5 µm. (D) Duration of the different cell cycle stages calculated based on the methods by Stanners and Till (Stanners and Till, 1959).

To define the start and duration of S-phase for kinetoplast and nucleus we used the labelled cell methodology of Till and Stanners (Stanners and Till, 1959) for which the post S-phase stages had to be determined. M and P were already known from the DAPI analysis (Figure 8A), whereas the duration of G2 was calculated by EdU incorporation into both the kinetoplast and nucleus. We cultivated 1390 BSF trypanosomes in the presence of 300 µM EdU and took samples every 30 minutes during the first 3 hours and then every hour at 4 and 5 hours. The number of cells with dividing and EdU labelled kinetoplasts and nuclei was determined for each sample (Figure 8B). Figure 8C shows images of representative cells after incubation in the presence of EdU for different time periods. The lower panel depicts cells from an early sample taken after 2 hours, here the cell on the right hand side incorporated EdU into the kinetoplast and the nucleus while the cell on the left hand side did not incorporate EdU, suggesting, that this cell had not yet entered S-phase. The upper panel shows a 2K1N cell at a late sampling time point in which both kinetoplasts and the nucleus showed incorporated EdU. While at an early time point only a small proportion of cells showed labelling of the kinetoplast and nucleus all cells were EdU positive after 4 hours of incubation (Figure 8B). The time passed until 50% of dividing organelles had incorporated EdU, was taken as the average duration of the G2-phase (Stanners and Till, 1959). This period corresponded to 1.18 hours for the kinetoplast and

1.64 hours for the nucleus (Figure 8D). The duration of the post S-phase for the kinetoplast and the nucleus, as well as the population doubling time allowed us to calculate the duration of the S-phase (Stanners and Till, 1959).

$$S = \frac{1}{\alpha}\ln\left[L + e^{\alpha(z)}\right] - (z + t)$$

The equation is composed of the following parameters: α is ln 2/*T, z* is the sum of *G2+M+P, T* is the generation time*, t* is the duration of the EdU labelling period and *L* represents the proportion of cells exhibiting a labelled organelle*.* Figure 8D shows the duration of each stage, calculated as described by Gull and colleagues (Woodward and Gull, 1990). The G1-phase for the kinetoplast was 0.05 hours shorter and overlapped with nuclear G1-phase. After 0.81 hours kinetoplast S-phase was accomplished and G2-phase commenced, while nuclear S-phase took 1.20 hours to complete. After 3.37 hours in the cell division cycle, cells were in G2-phase for both the kinetoplast and the nucleus. At 5.2 hours in the cell division cycle, nuclear mitosis led to a bi-kinetoplast and bi-nuclear 2K2N cell for further 0.45 hours until cytokinesis initiated. We summarised the order of events creating a temporal map (Figure 9) by combining the data obtained from the aforementioned analyses. This allowed the determination of the position of single cells in the cell division cycle with high temporal resolution (20 minutes for cells with an NFR from 10 - 100).

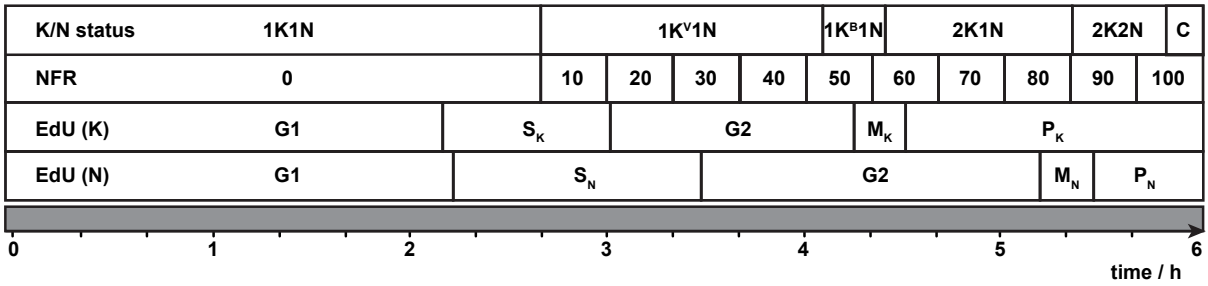

Figure 9. Temporal map of the *T. brucei* cell division cycle with respect to K/N status, NFR and DNA synthesis. Temporal map of the data obtained by (1) K/N status, (2) outgrowth of the daughter flagellum (*New Flagellum Ratio*) and (3) DNA synthesis (EdU analysis). For the kinetoplast and nucleus status (1) as well as for NFR (2) the Williams algorithm was used to calculate the duration of each morphological event. About 43% of cells displayed a single flagellum and represent an NFR of 0. Cells representing 2 flagella (57% of cells in a constant growing culture) were sequentially divided into 10 groups, each of 10% new flagellum growth. Here the NFR represents values from 10 (0 - 10% new flagellum growth) to 100 (90 – 100% new flagellum growth). The description of the eukaryotic cell cycle based on G1, S-Phase, G2 and mitosis was performed according to Gull and colleagues (Woodward and Gull, 1990) taking into account 5 stages for both the kinetoplast (G1, S_K, G2, M_K and P_K) and the nucleus (G1, S_N, G2, M_N and P_N). For cells, that showed an NFR from 10 – 100 the cell cycle position could be determined with an accuracy of 20 minutes. The grey bar shows the timeline through one cell division cycle in hours (population doubling time = 5.9 hours).

3.2 The dynamics of cell morphology hints towards a two-phase cell division cycle

The dynamics of cell morphology was investigated during the cell division cycle by following the increase in cell elongation and cell volume. As a marker for cell elongation the distance of the segregating kinetoplasts was measured dependent on the NFR. In order to determine the cell volume, cells were surface-stained with both sulfo-NHS-AMCA and sulfo-NHS-Rhodamine. Sulfo-NHS-dyes were used for labelling proteins, which have primary amines. The AMCA staining was well suited for visualising the trypanosome outline where structures such as the flagellar pocket or the flagellum showed a strong fluorescence signal. However, this staining was disadvantageous for rendering the whole cell surface area. Fortunately, staining the cell surface with rhodamine led to concolourously stained cells, where structures such as the flagellum or flagellar pocket were not enhanced.

We first investigated the dynamics of cell elongation and it became apparent, that the distance between the kinetoplasts showed a two-stage relation over the cell division cycle (Figure 10A). The kinetoplasts showed a steady state distance up to an NFR of 60 (4.6 h in the cell division cycle), this period included S-phase, G2 and M_K for the kinetoplast. During the $1K^B1N$ stage, the kinetoplast distance was varying between 0.5 to 1 µm. Starting at an NFR of 70, kinetoplast-to-kinetoplast distance increased and the distance between the nuclei became measurable. At an NFR of 80 to 100 both the kinetoplasts and the nuclei separated, to a maximum distance of 3.5 µm and 4.5 to 5 µm, respectively (Figure 10A,B). In order to answer the question when the cells are elongating, we compared the separation of the kinetoplasts with the cell length that was measured from the anterior pole to both, the posterior pole and to the old flagellar pocket. The distance between the anterior pole and the old flagellar pocket remained at a constant distance of 14 µm during the cell division cycle. Interestingly, the distance of the kinetoplasts increased at the same time as the distance between the cell poles, which grew from around 14 µm to 18 µm. Taken together, this indicates that cell elongation was concomitant with kinetoplast separation. The cell volume was assessed with the aid of surface-stained cells and revealed a marked increase in cells with an NFR between 80 and 90 (Figure 10C). Cells displaying an NFR lower than 80 showed a mean cell volume of 73.3 ± 16.2 μm^3, showing, that for a 5-hour interval of the cell division cycle, the cell volume stayed constant. Kinetoplast distance increase began about 20 minutes earlier at an NFR of 60. In cells with an NFR larger than 80, the cell volume increased to 105.1 ± 22.9 μm^3 which remained unchanged until the initiation of cytokinesis.

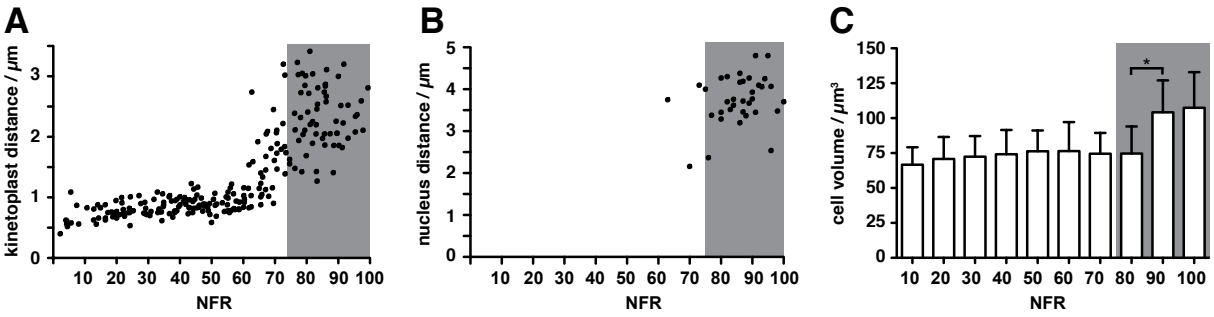

Figure 10. Cell growth is not constant; it is a two-phase process. Cell morphology traits such as kinetoplast (A) and nucleus distance (B) as well as cell volume (C), were followed during the cell division cycle. The distance (µm) of both the kinetoplasts (A) and nuclei (B) were measured and plotted against the corresponding NFR. Kinetoplast distance compared to NFR showed a two-step relation. Both kinetoplasts and nuclei repositioned after mitosis. (C) Mean cell volumes ± SD (μm^3) for different NFR-groups were determined to follow the increase in cell volume during cell division cycle progression (n = 168 cells in total). An ANOVA test was performed with the values of NFR 80 versus 90 and proved to be significant with a p-value of <0.001 (indicated with an asterisk).

The exact cell volumes determined for individual NFR groups are depicted in Table 2. The increase proved to be significant from NFR 80 to NFR 90, suggesting, that the cell volume increased rapidly in the cell division cycle. The mean cell volumes determined for cells with an NFR of 100 did not amount to twice the mean volume of a 1K1N cell only if the maximum values were considered. Therefore, we conclude, that in most cells the bulk of cell volume increase occured during cytokinesis. In summary, we suggest, that the cell division cycle shows two-phase dynamics regarding cell morphology. We are aware that investigations concerning cytoskeleton formation have not been performed yet. Therefore we plan to correlate these findings with dynamics of microtubule cytoskeleton dependent on our precise temporal cell division cycle map.

Table 2. Cell volume variations for different NFR groups.

NFR	**10**	**20**	**30**	**40**	**50**	**60**	**70**	**80**	**90**	**100**
Mean $_{(cell\ volume)}$ / μm^3	66.7	70.9	72.4	74.2	76.3	76.5	74.6	74.7	104.2	107.4
SD	12.4	15.7	14.8	17.4	15.0	20.8	14.8	19.4	22.8	25.6

3.3 VSG diffusion is constant during the cell division cycle

Trypanosomes have to maintain VSG coat functionality in order to be able to evade the host immune system at all times. As stated in the last chapter, cell volume increases in a very short period of time in the cell division cycle and thus we questioned whether VSG mobility is maintained during growth and elongation of the cell body. In order to determine the diffusion coefficient for VSGs on the surface we conducted FRAP analysis (Fluorescence Recovery After Photobleaching) on with sulfo-NHS-Atto488 surface-labelled and immobilised cells (according to Hartel 2013). Up to 10 frames were recorded (Pre-bleach) before fluorescently labelled proteins were irreversibly photo-bleached by a laser impulse in a region of interest (ROI) (Figure 11A, arrowhead). The recovery of fluorescence intensity within the bleached area was monitored over time until fluorescence was saturated in the ROI (Recovery). The z-projection of the time-lapse movie showed, that cells were completely immobilised during the experiment (Figure 11A). According to the fluorescence recovery rate in the bleached area the *Diffusion coefficient* (D) and *mobile fraction* (MF) were calculated from the diffusion equation. The diffusion coefficient for cells early in the cell division cycle with an NFR of 0-60 (Phase 1 / steady state cell morphology) was determined as 0.029 $\mu m^2 s^{-1} \pm 0.01$. This was consistent with diffusion coefficients assessed for different types of VSGs on living trypanosome cells in the 1K1N stage (Hartel, 2013). The diffusion coefficient determined for cells in Phase 2 (NFR 90 – 100) was 0.026 $\mu m^2 s^{-1} \pm 0.01$. The mobile fraction was determined to be 79%±6 for cells in both phases. A t-test showed no significant differences for diffusion coefficients and mobile fractions for Phase 1 compared to Phase 2 cells, which indicated that the fraction of mobile VSGs on the cell surface was constant for cells early and late in the cell division cycle.

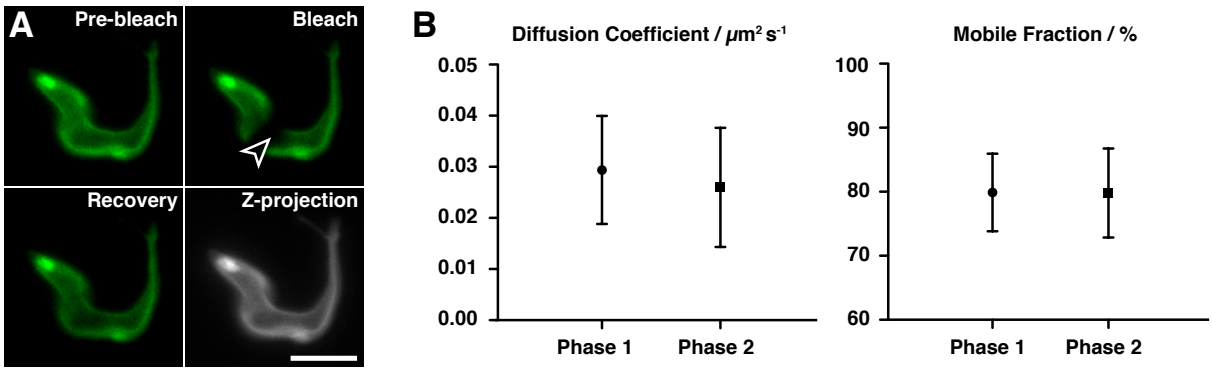

Figure 11. VSG surface coat mobility is constant during the *T. brucei* cell division cycle. FRAP analysis was performed in order to determine the diffusion coefficient and the mobile fraction of fluorescently labelled surface VSGs. (A) Shows representative images of an immobilised, surface-labelled cell during the course of a FRAP experiment. An arrowhead indicates the photo-bleached area (Bleach). Corresponding Z-projections of time-lapse movies show, that cells were immobile during data aquisition. (B) Shows the diffusion coefficient and mobile fraction (mean ± SD) of surface VSG for cells early in the cell division cycle (Phase 1, NFR 0 - 60) compared to cells late in the cell division cycle (Phase 2, NFR 90 - 100) (n = 56 cells in total). Scale bar = 5 µm

3.4 VSG mRNA abundance doubles during S-phase early in the cell division cycle

We showed, that VSG mobility on the trypanosome surface is constant during the cell division cycle; even during progression from Phase 1 to Phase 2 the VSG coat dynamics was maintained. This suggests, that protein expression is quickly adapted during cell volume increase and we therefore aimed at investigating if and when the expression of the active VSG, the major component of the cell surface, is changed during the cell division cycle. The *QuantiGene® ViewRNA ISH Cell assay* (Affymetrix) was used to detect the amount of VSG mRNA on single cell level, thus allowing us to monitor variations in mRNA amount during progression through the cell division cycle.

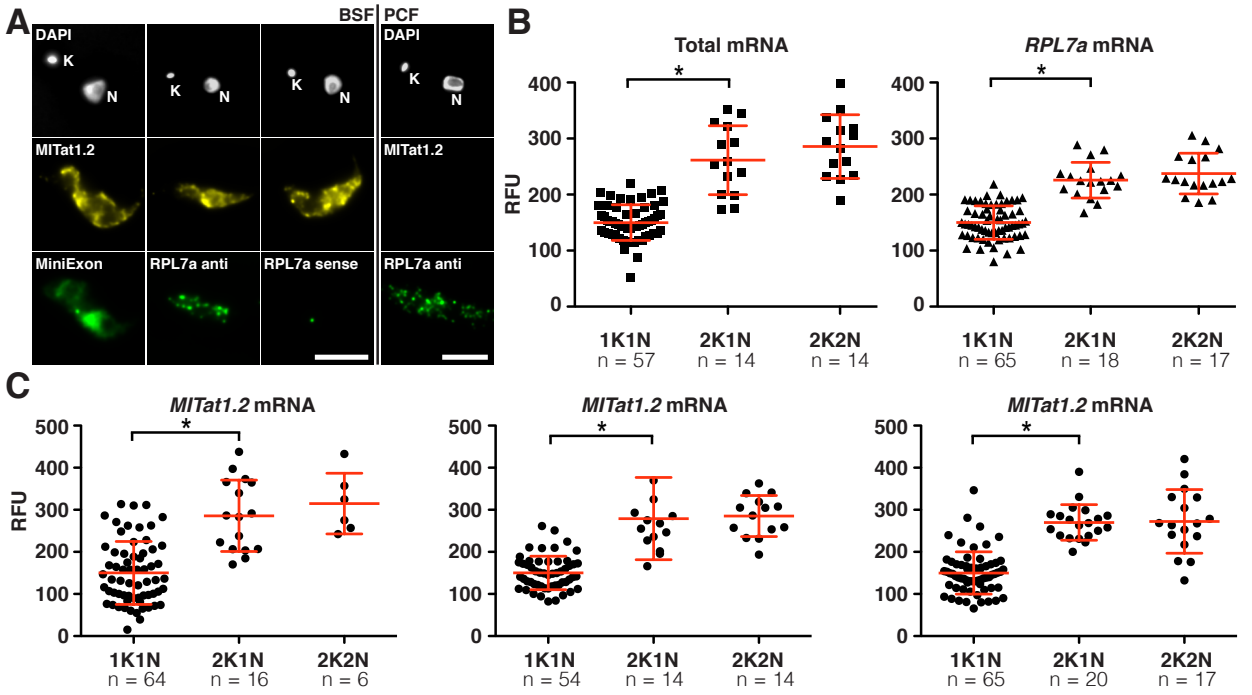

Figure 12. Variation in mRNA amounts during the cell division cycle. The *QuantiGene® ViewRNA ISH Cell assay* was used to follow changes in mRNA levels during the cell division cycle. (A) Shows images of representative cells in different cell division cycle stages with respect to *MITat1.2* mRNA (yellow). As a control the total mRNA (probe against the MiniExon), RPL7a anti-sense (positive control) and RPL7a sense probe (negative control) are shown in green. DNA was counterstained with DAPI (grey). (B) Shows the fluorescence intensity signals for 1K1N, 2K1N and 2K2N cells with respect to total mRNA and *Rbp7a* mRNA levels. (C) Shows fluorescence intensity signals in 1K1N, 2K1N and 2K2N cells for *MITat1.2* mRNA levels from three independent experiments. Black dots depict the individually measured values. Red lines indicate the mean fluorescence intensity per cell (RFU) and SD. A t-test was performed and significant differences between stages are indicated with * = P<0.0001. (n = 445 cells in total). Scale bars = 5 µm

The cell division cycle position of individual cells was determined by DAPI staining alone (Figure 12A) as the use of detergent during the course of the experiment did not allow for a further increase in the temporal resolution by determining the NFR. The BSF cells assayed with the *MITat 1.2* probe showed a strong fluorescence signal, distributed in the whole cell body. In

PCF *MITat 1.2* mRNA could not be detected, which served as a negative control for the *MITat1.2* probe. A double Cy3 labelled probe (RNAfish probe SKA48), directed against the Miniexon region was used to quantify the total mRNA amount. As further controls, mRNA levels of a gene expressed from another genomic context were quantified, RPL7a sense and antisense probes directed against the mRNA of the ribosomal binding protein RPL7a (accession number Tb427.08.1340) were generated by Susanne Kramer. The mean fluorescence intensity was set to 150 RFU (relative fluorescence units) for 1K1N cells and the levels detected in the other cell cycle stages calculated accordingly (Figure 12B,C). The mRNA amount increased significantly from 1K1N to 2K1N for both, total and *RPL7a* mRNA, of about 75% to 2614 ± 616 RFU and 50% to 2257 ± 319 RFU, respectively (Figure 12B). During progression from 2K1N to 2K2N no significant increase in mRNA levels was observed. The *MITat 1.2* mRNA levels from three independent experiments were quantified during the cell cycle progression, where the mean fluorescence intensity for 1K1N was 1500 RFU compared to around 2700 and 2900 for 2K1N and 2K2N cells, respectively (Figure 12C). The exact values for three independent experiments are summarised in Table 3. 2K1N cells showed an increase of fluorescence intensity by a factor of 2, thus indicating, that the amount of *MIT1.2* mRNA in 2K1N cells was doubled compared to 1K1N cells. The quantification of *MITat1.2* mRNA levels revealed, that about 25% of 1K1N cells displayed values beyond the mean ± SD value for 1K1N cells. These cells showed fluorescence intensities similar to 2K1N and 2K2N cells. This fact suggests, that the amount of *MITat 1.2* mRNA increased in late 1K1N. This trend was not observed in the case of total mRNA and *RPL7a* mRNA quantification. In summary, the amount of mRNA followed a two-stage fashion with a shift that occurred early, starting at 2.5 hours into the cell division cycle. $1K^{V}1N$ and $1K^{B}1N$ were not considered due to problems correlating cells to a definite cell cycle stage.

Table 3. Fluorescence quantification of single cell mRNA levels. Mean fluorescence values for different cell division cycle stages are shown ± SD for total mRNA (MiniExon), *RPL7a* mRNA and *MITat1.2* probe (replicates are indicated with numbers).

		1K1N	2K1N	2K2N
MiniExon	RFU Average	1500	2614	2858
	SD	318	616	569
RPL7a	RFU Average	1500	2257	2375
	SD	300	319	364
MITat1.2 (1)	RFU Average	1500	2857	3149
	SD	748	849	721
MITat 1.2 (2)	RFU Average	1500	2791	2853
	SD	399	976	489
MITat 1.2 (3)	RFU Average	1500	2699	2724
	SD	503	423	754

3.6 Visualisation of major *T. brucei* organelles

We now aimed at investigating the duplication of the major BSF trypanosome organelles with respect to our temporal map of the cell division cycle created by the *in silico* synchronisation approach. In this chapter the cloning of different organelle markers is described e.g. for the endoplasmatic reticulum exit site (ERES), the endoplasmic reticulum (ER), the flagellum and the glycosomes. Furthermore, we established protocols to stain the endosomal compartment, the lysosomes and the cell membrane by commercially available fluorescent dyes.

3.6.1 Visualisation tool for the endoplasmic reticulum

The endoplasmic reticulum was visualised by combining the GFP sequence with an ER import sequence derived from EP1 and an ER retention sequence. The ER import sequence fused to GFP was amplified by PCR using the 17_ERimp_GFP_u and the 18_ERrGFP_l oligonucleotides from the pLewLS.GFP.GPI vector obtained from Christopher Batram (Batram, 2013). The 18_ERrGFP_l oligonucleotide added the MDDL ER retention signal to the C-terminus, as described by Jay Bangs (Bangs et al., 1993). The obtained 940 bp fragment was cleaned up and digested with *Hind*III and *Bam*HI over night. For expression in *T. brucei* the pL82ΔOP(puro) vector was used, digested with *Hind*III and *Bam*HI and the resulting 4800 bp fragments was purified by gel extraction. The digested 940 bp fragment was integrated in the pL82ΔOP(puro) vector and after verification by sequencing, the pL82ΔOP(puro)LS::GFP::MDDL vector was linearised with *Not*I and transfected into BSF 1390 cells.

3.6.2 Fluorescence tagging of the endoplasmic reticulum exit-site

He and colleagues showed, that *Tb*Sec13p is a marker for the ER exit-site (ERES) in PCF (He et al., 2004). For visualisation of the ERES in BSF *T. brucei* we obtained the *Tb*Sec13p (Tb427.10.14180) sequence from the TriTrypDB website (http://tritrypdb.org) (Aslett et al., 2010) and amplified the gene, from genomic DNA taken from 1390 cells, via PCR, using the 26_HindIII_Sec13p and the 27_SalI_Sec13L oligonucleotides. The resulting 1100 bp fragment was purified and digested over night with *Hind*III and *Sal*I. The red fluorescent protein cherry was amplified from the p2705 plasmid obtained from Susanne Kramer via PCR using the 23_Cherry_Xho_Bam_l and the 24_Cherry_SalI_u oligonucleotides. The resulting 788 bp fragment was purified and digested over night with *Bam*HI and *Sal*I. For ectopic expression in *T. brucei* the T7-driven pL82ΔOP(puro) vector was used and digested with *Hind*III and *Bam*HI and the resulting 4800 bp fragment was isolated by gel extraction. Both digested PCR fragments were purified by gel extraction and ligated with the 4800 bp pL82ΔOP(puro) fragment. Correct integration was analysed by restriction digest and verified by sequencing. The resulting

pL82ΔOP(puro)*Tb*Sec13p::GFP vector was linearised with *Not*I and transfected into BSF 1390 cells. Six days after transfection clones were isolated and assayed for red fluorescence by microscopy.

3.6.3 Cloning of a flagellum marker

Staining of the flagellum was difficult during live cell microscopy, because most fluorescent dyes were phototoxic and caused fast cell death after fluorescence illumination. In order to visualise the flagellum in living cells we aimed at fusing GFP to a protein, that was shown to localise in the trypanosome flagellum without disturbing motility or growth. Luginbuehl and colleagues showed, that the N-terminus of a phosphodiesterase TbrPDEB1 is sufficient for targeting proteins to the flagellum (Luginbuehl et al., 2010). The DNA sequence corresponding to the N-terminal 70 amino acids of TbrPDEB1 (TB09.160.3590) was amplified from genomic DNA by PCR using the 21_PDEB1_u_HindIII and 19_PDEB1_212r oligonucleotides. The obtained 650 bp fragment was purified and digested with *Hind*III and *Sal*I over night. GFP was amplified by PCR with the 20_GFP_u_SalI and 22_GFP_XhoBam oligonucleotides from the pL82ΔOP(puro)*Tb*Sec13p::GFP vector. The 750 bp PCR product was purified and digested with *Sal*I and *Bam*HI. Both PCR products were inserted into the pL82ΔOP(phleo) vector, after digestion with *Hind*III and *Bam*HI. After sequencing the pL82ΔOP(phleo)PDEBI::GFP vector was linearised with *Not*I and transfected into BSF 1390 trypanosomes.

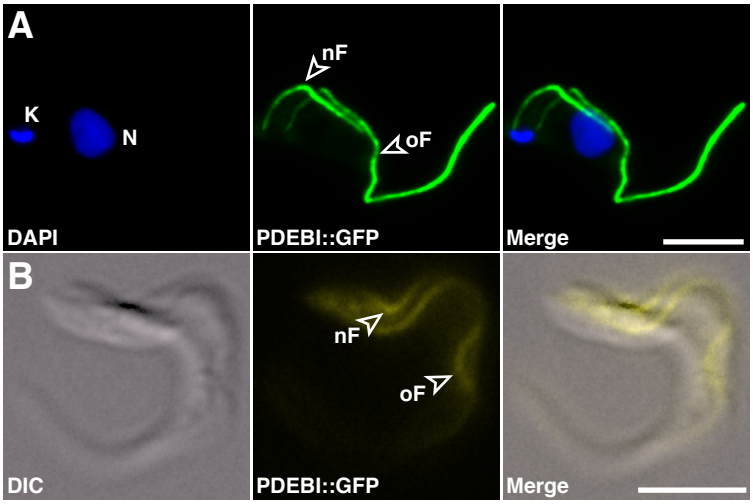

Figure 13. The *T. brucei* flagellum can be visualised in fixed and living cells. (A) Shows images of fixed cells expressing the PDEB1::GFP flagellum marker. The GFP is localised to the whole axonem also inside the flagellar pocket. (B) Shows 3D stacks of immobilized live cells. Scale bars = 5 µm

In the following the N-terminal 70 amino acids of TbrPDEB1 are referred to as PDEBI. The PDEB1::GFP localised exclusively to the flagellum as shown by Luginbuehl *et al*. This marker enabled the automation of NFR determination for high cell quantities, in contrast to the whole surface staining obtained by the sulfo-NHS-dyes coupled to different fluorescent molecules (AMCA, Atto488 or Rhodamine). Furthermore, this marker was well suited for live cell analysis with respect to cell cycle progression, due to the ability to determine the position of living cells in the cell division cycle as precisely as for fixed cells.

3.6.4 Fluorescence tagging of the glycosomes

Sampathkumar and colleagues identified the peroxisomal targeting signal PTS1, which is recognized by Peroxin 5 (*Tb*Pex5) in *T. brucei* and leads to the translocation of proteins across the glycosomal membrane (Sampathkumar et al., 2008). In order to visualise the glycosomes we fused the DNA sequence corresponding to the PTS1 (SKL) to the C-terminus of GFP and in parallel to cherry. *GFP* was amplified with the 10_CFP_u_HindIII and the 16_SKL_BamHI oligonucleotides from the pL82ΔOP(puro) *Tb*Sec13p::GFP vector whereas *mCherry* was amplified with the 28_Cherry_HindIII and the 29_Cherry_SKL oligonucleotides from the p2705 vector obtained from Susanne Kramer. The obtained 750 bp (GFP) and 790 bp (Cherry) fragments were purified and digested with *Hind*III and *Bam*HI over night. The PCR products were inserted into the pL82ΔOP(phleo) vector, that was digested with *Hind*III and *Bam*HI. After sequencing the vectors were linearised with *Not*I and transfected into BSF 1390 trypanosomes.
In PCF the glycosomes have been visualised with other marker proteins before. Michels and colleagues showed, that an internal sequence targets *T. brucei* Triosephosphat Isomerase to glycosomes (Galland et al., 2010). This sequence was added to the N-terminus of GFP by PCR. We amplified GFP using the 05_TPI_HindIII and the 04_GFP_BamHI_L oligonucleotides. The obtained 800 bp fragment was purified and digested with *Hind*III and *Bam*HI over night. For expression in *T. brucei* the pL82ΔOP(puro) vector and the pRib(puro) vector were used and digested with *Hind*III and *Bam*HI. The digested 800 bp fragment was integrated into the pL82ΔOP(puro) and into the pRib(puro) vector. The pL82ΔOP(puro) vector was linearised with *Not*I and the pRib(puro) vector was linearised with *Bgl*II prior to transfection. Figure 14 shows a cell expressing the GFP::PTS1 and TPI::GFP markers. GFP::PTS1 localised to the glycosomes as had been shown by immunofluorescence using glycosome specific antibodies (3.8.6). The TPI::GFP marker localised to the mitochondrion, not to the glycosomes (Figure 14B). Both kinetoplasts colocalised with green fluorescence indicating localisation in the mitochondrion. In addition a further glycosome marker protein GAT126 (Igoillo-Esteve et al., 2011) was generated, this marker, however, also localised to the mitochondrion in the BSF.

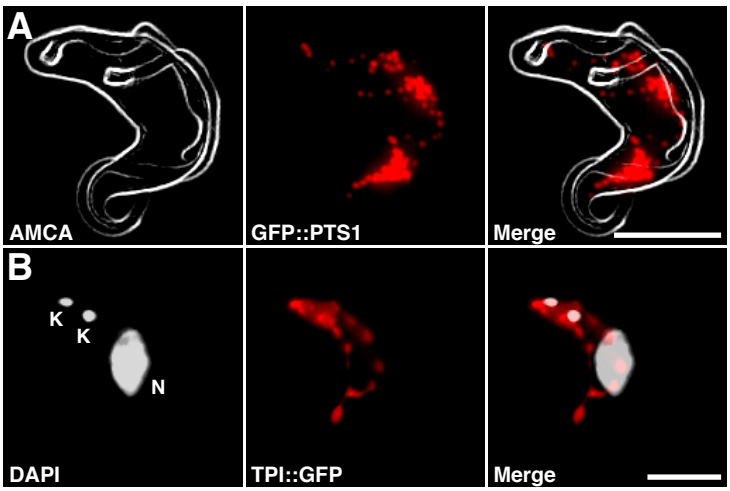

Figure 14. Potential glycosomal marker proteins show different localisation. (A) Shows images of fixed cells expressing the GFP::PTS1 glycosome marker. The GFP localises into the glycosomes. The ImageJ edges algorithm was used for better visualisation of the cell surface and flagellum. (B) Shows images of fixed cells expressing the TPI::GFP glycosome marker. GFP does not localise into glycosomes. GFP localises into the mitochondrion. Scale bars = 5 µm

3.6.5 Verification of the generated GFP markers by Western analysis

We performed western analysis to show, that the GFP in the trypanosome reporter cell lines was fused to the corresponding marker proteins (Figure 15). For western analysis protein samples were taken from exponentially growing cultures and the equivalent of $2x10^6$ cells was loaded per lane. The L13D6 antibody (Kohl et al., 1999) against PFR (1:20) was used as a loading control and a monoclonal antibody against GFP (1:2000; generated in mouse; Roche; Cat. 1181 4460 001) was used to detect GFP. 1390 BSF trypanosomes, not expressing any GFP, were used as a negative control, and a 1390 cell line expressing cytosolic GFP (C. Batram) served as a positive control (PK). In the latter, the signal derived from cytosolic GFP was found at a molecular weight of approximately 27 kDa. The GFP detected in the reporter cell lines corresponded to the expected protein size of the marker proteins (Figure 15, white asterisks). Western analysis revealed, that no further GFP band was detected in the reporter cell lines.

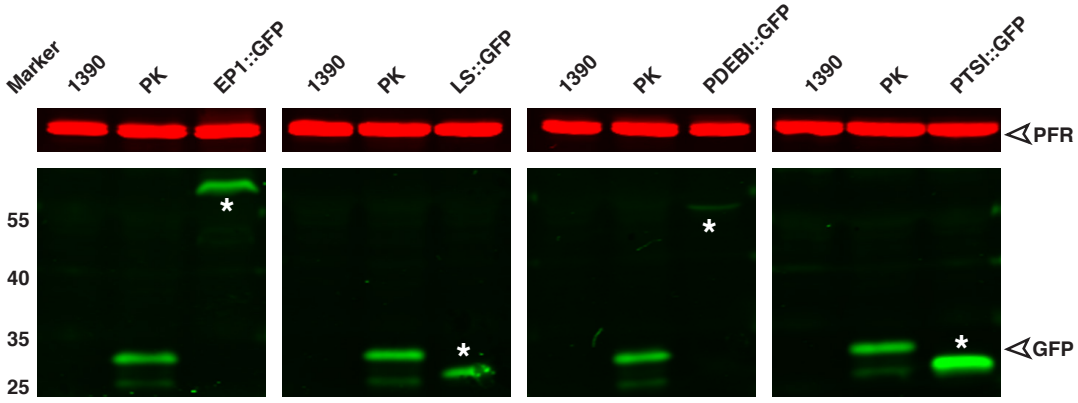

Figure 15. Western analysis of organelle marker reporter proteins. PFR (red) detected by the monoclonal antibody L13D6 was used as a protein loading control. For the detection of GFP proteins, the 1390 cells expressing cytosolic GFP were used as positive controls (PK) and 1390 BSF trypanosomes as a negative control. Asterisks indicate the expected signals for the reporter cell lines

3.6.6 The cellular organelles

We visualised most trypanosomal structures including the flagellum, the endoplasmic reticulum, the Golgi apparatus, the endosomal compartment, the lysosome, the mitochondrion and the glycosomes (Figure 16). Markers for the flagellum, the endoplasmic reticulum (Figure 16A), the glycosomes (Figure 16F) and the ERES were generated during this work; other markers were available from former lab members or other laboratories. We obtained a plasmid containing a putative GlcNAc transferase (GntB) fused with YFP, found to be a Golgi marker by Ho and colleagues (Ho et al., 2006) (Figure 16B). In the BSF EP1 localised to the endosomal compartment, as has been shown by colocalisation analysis using the *Tb*MBAP antibody (Engstler et al., 2005) (Figure 16C). P67::GFP was used as a marker protein for the lysosome, Bangs and colleagues showed, that the LAMP like protein p67 localised to the lysosomal membrane (Alexander et al., 2002), this marker was modified by Mark Günzel for use in BSF (Günzel, 2010). The p67::GFP was integrated into a pTsarib(blas) expression vector and transfected into 1390 BSF trypanosomes (Figure 16D). Mark Günzel also generated a marker for the mitochondrion by fusion of *GFP* to a mitochondrial leader sequence ligated with the pl61 expression vector, this marker was transfected into 1390 BSF trypanosomes (Figure 16E). An overview of the available organelle markers is shown in Figure 16.

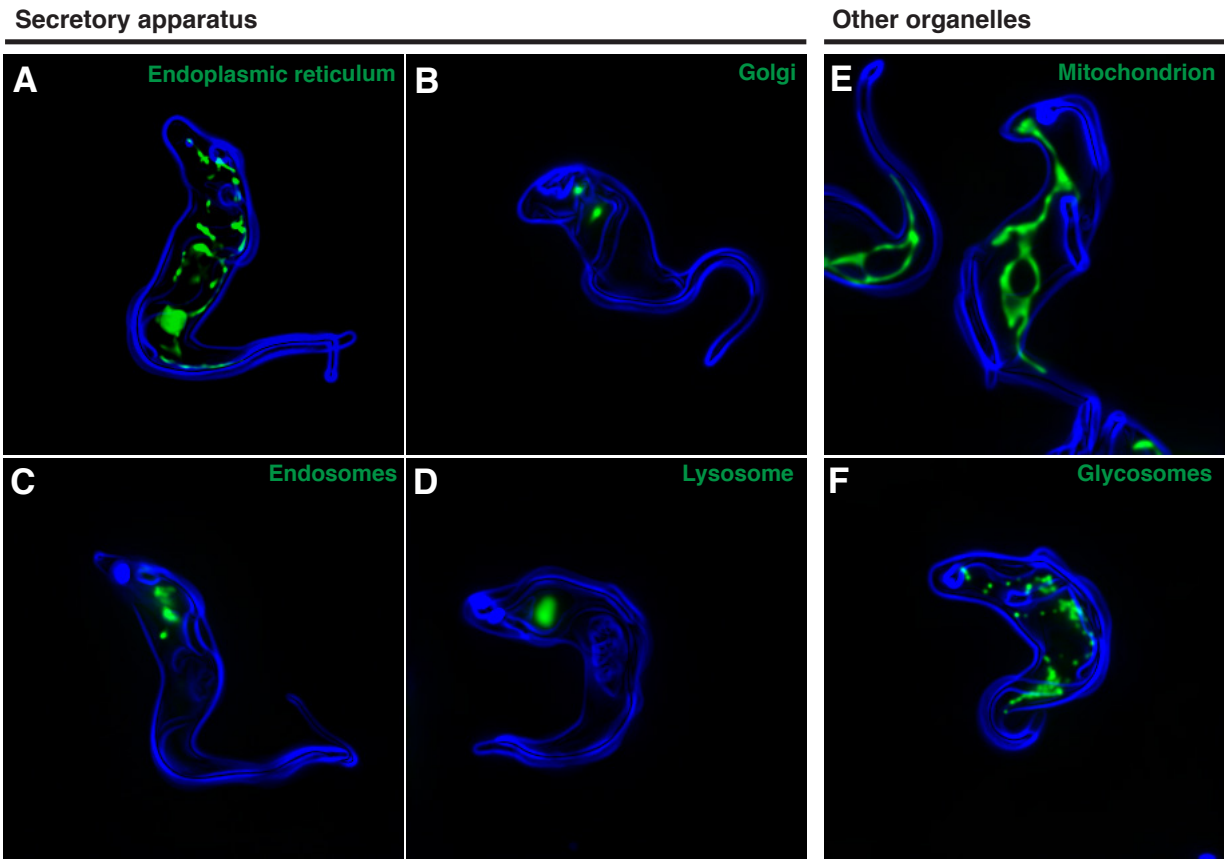

Figure 16. Visualisation of different BSF *T. brucei* cell organelles by fluorescent reporter proteins. Shown are images of surface-stained (blue), fixed cells expressing different organelle markers (green). They are divided into secretory organelles (A-D) and others (E-F). (A) Shows the LS::GFP::MDDL marker for the endoplasmic reticulum. (B) Shows the GntB::YFP Golgi marker cell line. (C) Shows the EP1::GFP endosome marker. (D) Shows the p67::GFP lysosome marker. (E) Shows GFP targeted to the mitochondrion. (F) Shows the GFP fused to the peroxisomal targeting signal 1 (PTS1) .

3.6.7 Fluorescence dyes for the staining of different trypanosomal compartments

Several commercially available fluorescence dyes were well suited for visualisation of cellular structures in trypanosomes, such as the mitochondrion, the endosomal compartment, the lysosome or the cell membrane. Especially for live cell microscopy the dyes were useful to circumvent problems due to bleaching and low signal intensities. In organisms, that are not accessible to genetic manipulation e.g. wild type cells or different trypanosome strains such as *Trypanosoma vivax* or *Trypanosoma congolense*, this approach was useful in order to visualise organelles or cell compartments. The *MitoTracker Red CMXRos* (Molecular probes) was used at a final concentration of 100 nM in HMI-9 medium wherein cells were incubated for 30 minutes at 37°C in the incubator in order to visualise the mitochondrion. Cells were washed once in TDB and prepared for live microscopy or fixed in formaldehyde (Figure 17A). The cell membrane was visualised with the *FM 4-64 FX* dye obtained from the company Molecular probes (Figure 17B), by adding the fluorescent dye to the cultivation medium. In order to stain

the endosomal compartment, cells were incubated in the presence of fluorescently labelled dextran at a final concentration of 0.1 mg/ml at 37°C for 30 minutes thus allowing its internalisation via fluid phase uptake. After incubation the fluorescent signal was detected in the flagellar pocket, the early, late and recycling endosomes, exocytic carriers, clathrin vesicles and the lysosome (according to Engstler et al., 2004). If only the lysosome was to be stained, cells were washed in TDB or HMI-9 after the incubation period, to prevent further uptake of dextran and incubated for an additional 10 to 15 minutes at 37°C. This allowed the fluorescence signal to accumulate in the lysosome (Figure 17C).

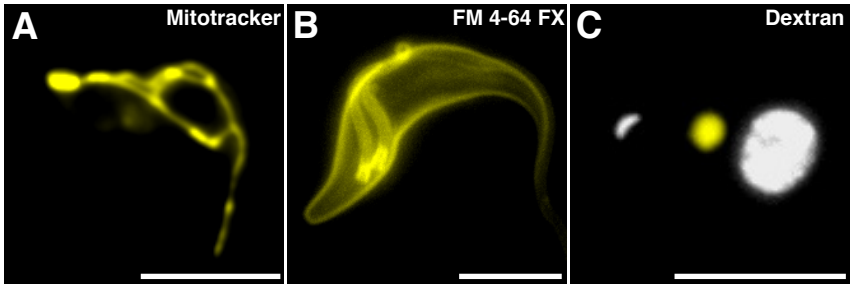

Figure 17. Commercially available fluorescence dyes to visualise structures in *T. brucei*. Shown are images of fixed cells stained with commercially available fluorescence dyes (yellow), namely the MitoTracker Red CMXRos to visualise the mitochondrion (A), the FM 4-64 FX dye in order to stain lipid membranes (B) and the Alexa564 conjugated Dextran to mark the lysosome (C). In (C) the cells were counterstained with DAPI (white). Scale bars = 5 µm

3.7 Duplication of the *T. brucei* organelles

We precisely timed the cell division cycle of BSF trypanosomes with high temporal resolution and provided markers to visualise the major organelles in *Trypanosoma brucei*. With the aid of these tools we followed the duplication events of organelles with respect to the temporal position in the cell division cycle.

Questions to be addressed were:

(A) Can we provide hints for the mode of organelle formation in trypanosomes?

(B) Can we correlate the formation of organelles with the cell division cycle?

(C) Can we define an order of organelle formation?

(D) Are organelle formation events controlled by cell cycle checkpoints?

(E) Lastly, is the orchestration of organelle formation related to VSG coat maintenance?

3.7.1 Formation of a new ER takes place by continuous growth and late segregation

The endoplasmic reticulum has been well analysed, in the host laboratory, concerning the structure and location in the trypanosome cell body. Electron tomography showed the endoplasmic reticulum to be a flat, lobate, perforated and continuous membrane system (Karo, 2008). We investigated whether this network was maintained during the cell division cycle or whether it dissolves and is rebuilt during duplication. The ER was visualised using the LS::GFP::MDDL reporter cell line generated in the course of this project. In general the ER always spanned through the cell body from the posterior pole at the flagellar pocket to the anterior tip of the cell (Figure 18). In fixed 1K1N cells a branch of the ER was always located at the side adjacent of the attached flagellum (Figure 18A). In 1K1N two different situations were found, on the one hand cells, which contained one single branch, spanning through the cell body, and on the other hand cells, that showed an additional slim branch (Figure 18A). The additional branch was always located on the opposite of the flagellum and did not reach to the poles of the old branch. However, both branches were connected with each other in the posterior and anterior part of the cell as well as with the nuclear envelope as identified by manual tracing of 3D stacks (Figure 18A). In 2K1N cells the ER kept the same morphology in the anterior cell part, whereas ER complexity increased in the posterior cell part, as further branching and interconnections were detected (Figure 18B,C). Both ER branches showed small interconnected structures, that increased in number, leading to two ER branches in 2K2N cells, which followed the new and old flagellum, respectively (Figure 18C). We identified sheet-like patches in the ER close to the nuclear envelope, that were found in fixed but not in living cells. We concluded, that these structures were artefacts due to fixation and conducted live cell microscopy of immobilized cells to reconstruct ER morphology from 3D stacks (87 slices; 0.07 µm step size). Cells were harvested and mixed with gelatine as described for the FRAP experiments and cooled at 4°C prior to microscopy. The microscope stage was adjusted to 21°C in order to maintain the immobilization during data acquisition, afterwards cells were warmed to 37°C, in order to confirm viability.

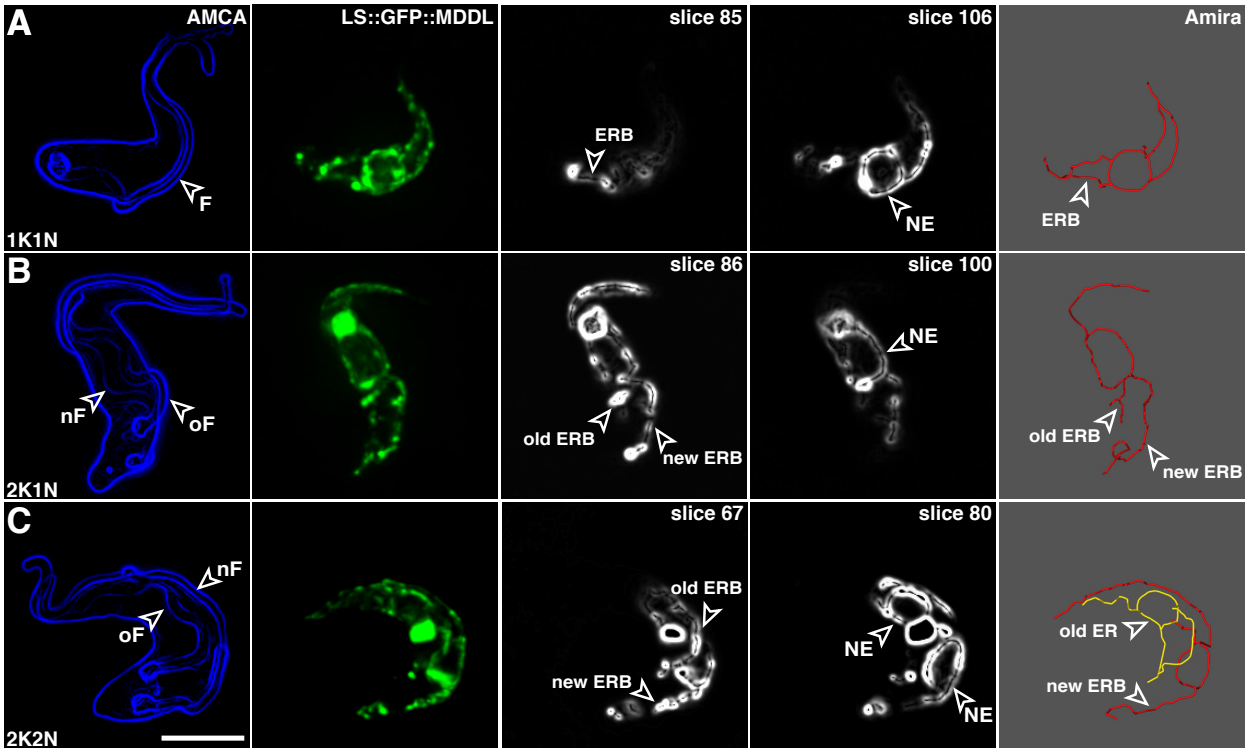

Figure 18. Visualisation of the endoplasmic reticulum in fixed cells. Shown are images of fixed cells at different stages of the cell division cycle expressing the LS::GFP::MDDL ER marker (green). Cells were surface-stained with AMCA to detect the flagellum (blue). The flagellum is indicated with F, the old and new flagellum with oF and nF. Shown are single slices of a 3D stack to visualise the ER branches (ERB) and the nuclear envelope (NE). The endoplasmic reticulum was manually traced using the Amira software package. In (C) the old ER is shown in yellow and the new ER in red. The ImageJ edges algorithm was used for better visualisation of the cell surface and flagellum. Scale bar = 5 µm

Figure 19 illustrates ER morphology in immobilized living cells during cell division cycle progression. In 1K1N cells the morphology of the ER did not differ compared to fixed cells (Figure 19A), as the ER spanned through the cell body from the posterior pole at the flagellar pocket to the anterior tip of the cell. In 1K1N cells the ER was always located at the cell side where the flagellum is attached. This main ER branch showed multiple small extensions and was contiguous with the nuclear envelope enclosing the nucleus (Figure 19A). During cell cycle progression the complexity of the ER structure constantly increased as the extensions formed multiple interconnections. In 2K1N cells a network providing a second ER branch was identified in the posterior of the cell (Figure 19B), which we suggest is built by continuous growth and connection of the ER extensions. Later in the 2K2N phase the enlarged ER network was also identified in the anterior cell pole (Figure 19C).

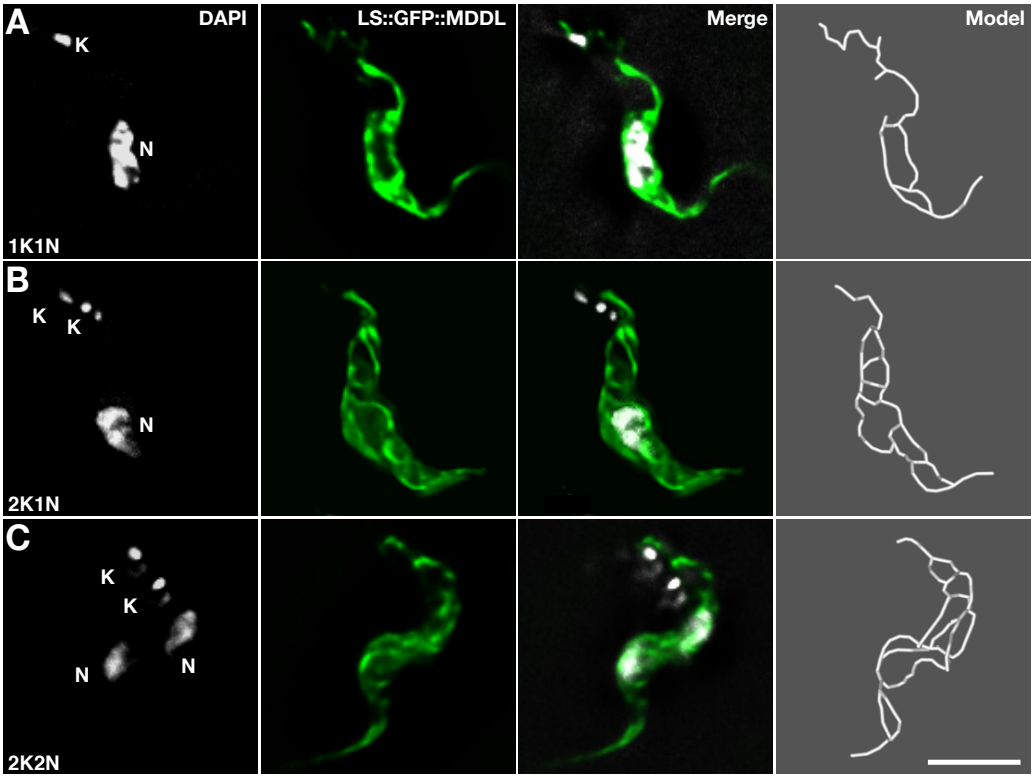

Figure 19. Visualisation of the endoplasmic reticulum in living cells. Shown are z-projections of deconvolved 3D stacks of immobilized cells at different stages of the cell division cycle expressing the LS::GFP::MDDL ER marker (green). DNA such as kinetoplast (K) and nucleus (N) was visualised with DAPI. The ER was manually traced using the Amira software package and is depicted as a model (white). The complexity of the ER increases with progression through the cell division cycle. Scale bar = 5 µm

To simplify the identification of the two major ER branches both structures were modelled separately and overlaid with the ERES (Figure 20). In living cells we were not able to localise the ER in parallel with the two flagella, due to phototoxic effects of AMCA staining during microscopic observations, nevertheless, the data obtained from fixed cells support this observation.

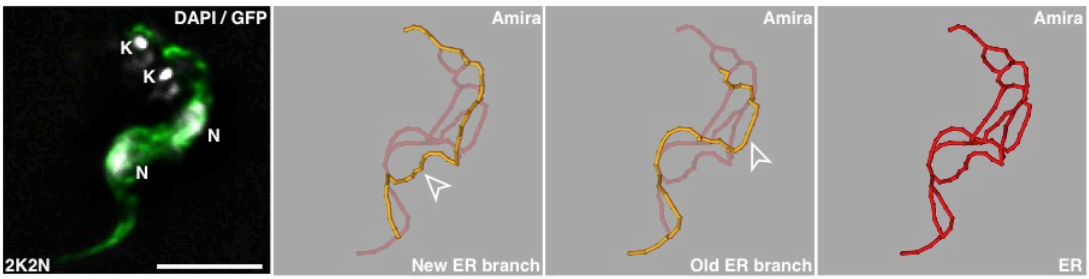

Figure 20. Visualisation of the old and new ER branch in a 2K2N cell. Shown is a z-projection of a deconvolved 3D stack of an immobilized cell expressing the LS::GFP::MDDL ER marker (green). DNA was visualised with DAPI (white). The ER was manually traced using the Amira software package and is shown as a model (red). For better visualisation, the new and old ER branches are depicted in separate images (yellow). Scale bar = 5 µm.

We investigated the extending structures of the ER in the posterior cell part in 1K1N and 2K1N cells in more detail, as we hypothesised, that these might be starting points for further interconnections of the ER. An array of images taken from 1K1N cells supported the suggestion of ER branching (Figure 21). Several 1K1N cells displayed only a single ER branch in the posterior part of the cell (Figure 21A, arrowhead), others showed up to two invaginations, one at the major ER branch and another one at the nuclear envelope (Figure 21B, asterisk). In Figure 21C a larger extension, that could be observed in 1K1N cells is shown. The number and location of these different extensions varied, but most cells showed at least invaginations at the nuclear envelope and on the main ER branch. In 2K1N cells a triangular structure was generally identified, that was composed of the major ER branch (arrowhead), the new ER branch (asterisk) and the nuclear envelope, shown enlarged in the inset of Figure 21D. Later in the cell division cycle, in 2K2N cells, the ER showed varying numbers of interconnections also in the anterior part of the cell (Figure 19C).

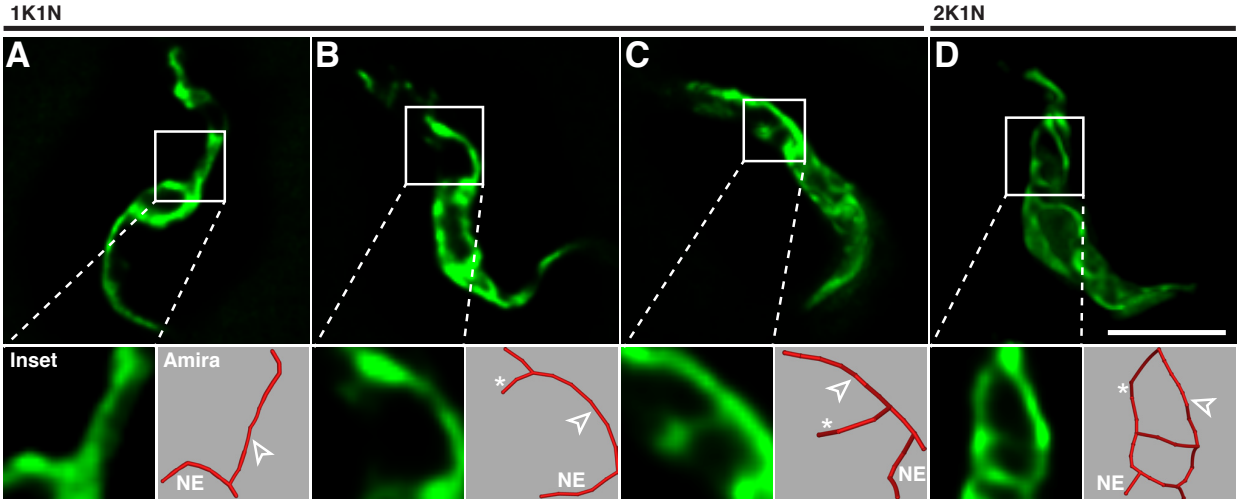

Figure 21. The posterior ER branch interconnects in 1K1N cells. Shown are z-projections of deconvolved 3D stacks of immobilized cells in stages 1K1N and 2K1N, expressing the LS::GFP::MDDL ER marker (green). The area posterior to the nuclear envelope (NE) is enlarged in the insets. The ER was manually traced using the Amira software package (red). Arrowheads point to the major ER branch, asterisks indicate new ER structures identified in the posterior part of the cell. Scale bar = 5 µm

We suggest, that the ER starts to expand in late 1K1N and/or early 2K1N where two ER branches are established, formed through ER extensions. In 2K2N the complex ER network was interconnected and remained as such in later stages, suggesting that the ER only gets separated during cytokinesis, resulting in two distinct ER structures after cell division.

3.7.2 Appearance of an early new Golgi indicates increase in secretory capacity

The duplication of the Golgi apparatus has been well described in PCF trypanosomes (He et al., 2004). We investigated whether Golgi duplication differs in the bloodstream form. To visualise the Golgi apparatus we used the Golgi marker GntB::YFP, generated by Warren and colleagues, that was modified for expression in BSF trypanosomes (Günzel, 2010). Cells in the 1K1N stage showed at least one Golgi structure (Figure 22, filled arrowheads) between the nucleus and the kinetoplast in the posterior part of the cell (27%), while 65% showed an additional Golgi close to the nuclear envelope (G^N) (Figure 22B) and about 8% more than two Golgi structures. A new Golgi structure appeared more posterior to the main, mature Golgi at an NFR of 20 and grew during the period of kinetoplast duplication (Figure 22, bottom panels). We did not identify a new Golgi structure at an NFR smaller than 20; but missing earlier structures due to the small size of the new growing Golgi could not be excluded. The distance between the old and new Golgi remained constant during a long period of time and increased only late in the cell division cycle. The appearance of a new Golgi structure and the duplication event in 1K1N1G compared to 1K1N2G cells followed the same pattern, only differing in the total number of Golgi structures (n=100) (Figure 22, bottom panel).

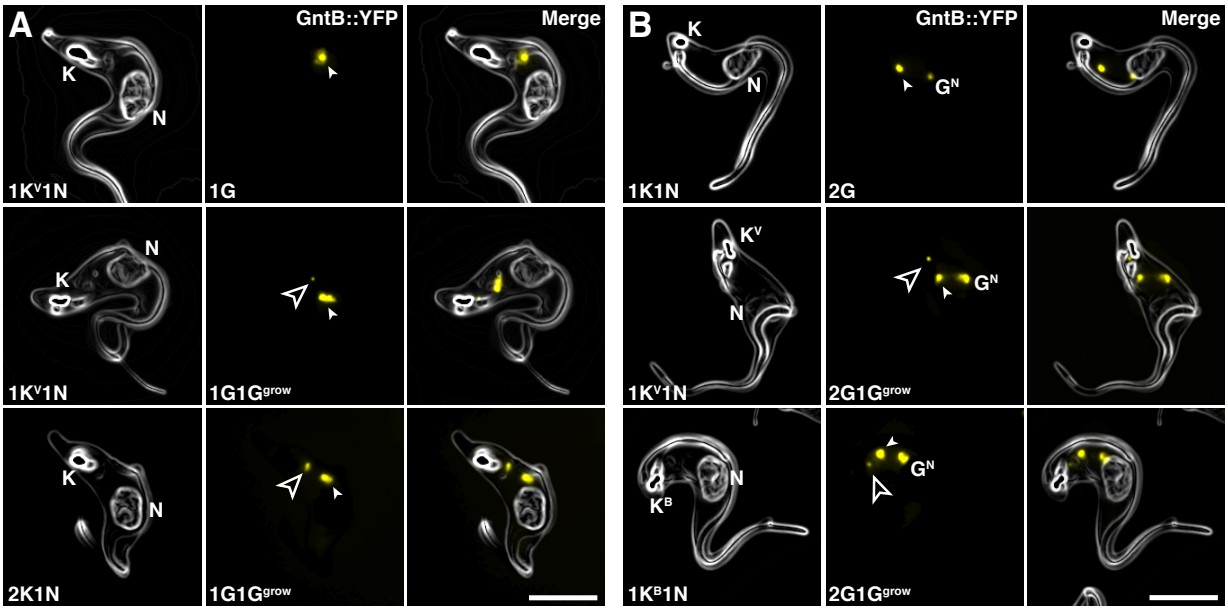

Figure 22. A new Golgi is built *de novo* in BSF trypanosomes. Shown are representative images of fixed cells at different stages of the cell division cycle expressing the GntB::YFP Golgi marker (yellow). (A) Shows the *de novo* Golgi appearance for cells with one Golgi (1K1N1G), (B) for cells with two Golgi (1K1N2G). The mature Golgi is indicated by filled arrowheads (➤), the new growing Golgi is indicated by open arrowheads (➢) and G^N marks the additional Golgi, located at the nucleus. The cell surface was visualised with AMCA and DNA was counterstained with DAPI. The ImageJ edges algorithm was used for better visualisation of the cell surface and the flagellum. Scale bars = 5 µm.

We investigated the location of the newly growing Golgi compared to the mature Golgi and measured their distance in relation to cell division cycle progression determined by the NFR (Figure 23). The new, growing Golgi appeared at an NFR of 20 (3.3 hours into the cell division cycle) and remained at a mean distance of 1 µm up to an NFR of 60, indicating that the new Golgi was in constant proximity to the mature Golgi for 1 hour and 20 minutes. Late in the cell division cycle the Golgi distance increased up to a maximum distance of 3.8 µm. Figure 23B shows the two situations, in the upper panel Golgi separation had not started, so the new Golgi was about 1 µm away from the mature Golgi, in contrast to the lower panel where the Golgi started to separate and showed a distance of 2.5 µm at an NFR of 70 (Figure 23B). The relation of Golgi distance and NFR was the same for 1K1N1G and 1K1N2G cells.

We showed, that the new Golgi appeared *de novo* in BSF trypanosomes at an NFR of 20 and kept a constant distance to the old Golgi in phase 1 (NFR 0-60) and separated in phase 2 (NFR 70-100) of the cell division cycle. This early appearance of a new Golgi indicates, that the secretory capacity is potentially increased early in the cell division cycle.

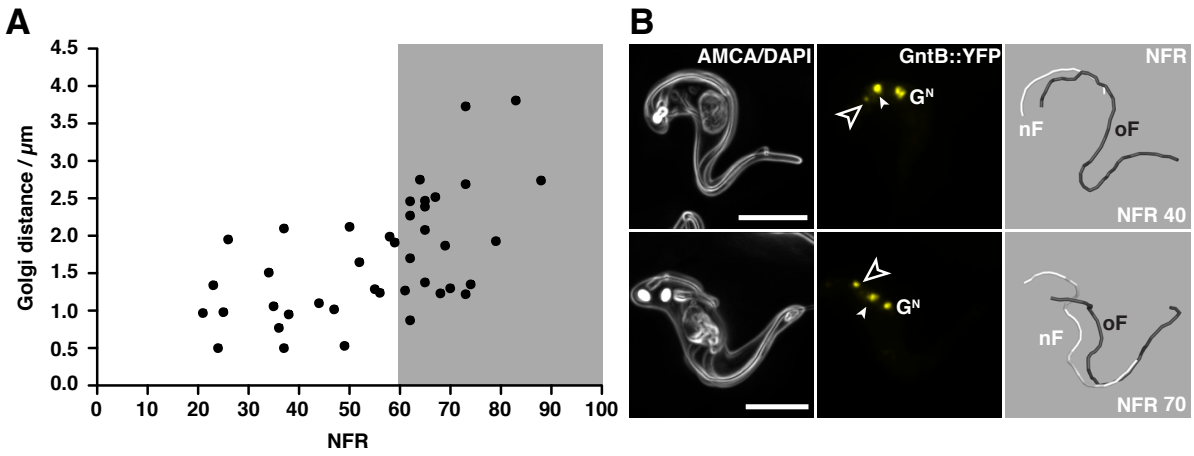

Figure 23. The new Golgi shows a constant distance to the mature Golgi in phase 1 and separates in phase 2 of the cell division cycle. (A) Shows the Golgi distance between the growing and mature Golgi, plotted against the NFR (total n = 42). (B) Images of fixed cells expressing the GntB::YFP Golgi marker (yellow) at different stages of the cell division cycle with a cell prior to Golgi separation (upper panel) and a cell during Golgi separation (lower panel). The surface was visualised with AMCA and DNA was counterstained with DAPI. The ImageJ edges algorithm was used for better visualisation of the cell surface and flagellum. The new (nF, white) and old flagella (oF, black) were manually traced using the Amira software package for the determination of the NFR. The mature Golgi is indicated by filled arrowheads (➤), the newly growing Golgi is indicated by open arrowheads (➢) and G^N marks the additional Golgi, located at the nucleus. Scale bars = 5 µm.

3.7.3 Early appearance of new ER exit-site indicates doubling of ER performance

We showed, that the endoplasmic reticulum network remained connected during the progression through the cell division cycle; therefore we aimed at investigating when the ER exit-site (ERES) is duplicated and where it is located on the ER complex. Furthermore, we aimed at elucidating whether the new ERES appeared with the same kinetics observed for the new Golgi. The ERES was visualised using the *Tb*Sec13p marker protein (Accession number Tb 427.10.14180) involved in COPII vesicle formation in *T. brucei*. Reported by He, this marker accumulated in the inter-ERES-Golgi space, highlighting the ERES (He et al., 2004). Electron microscopy images of 1K1N cells were screened for the inter-ERES-Golgi space and showed, that the ERES was always associated with a Golgi structure (Figure 24A). Fluorescence microscopy of fixed 1K1N cells revealed, that the mature ERES was located in the posterior part of the cell, always between nucleus and kinetoplast (Figure 24B,C). Early in the cell cycle, in several 1K1N cells but almost in all cells with an NFR of at least 10, a new *Tb*Sec13p positive structure was identified posterior to the mature ERES (Figure 24B,C open arrowhead) increasing in size during progression through the cell division cycle Figure 24B,C bottom panel). In 1K1N cells we found variations in ERES numbers with 18% of 1K1N cells displaying one ERES located between the nucleus and the kinetoplast, 71% had an additional ERES^{N}, located close to the nucleus, and 11% showed three to five ERES (n = 86). Similar ratios were true for 2K2N cells, with 29% displaying two compared to 71% with four ERES structures. In both cases the duplication event followed the same pattern, only differing in the total number of ERES.

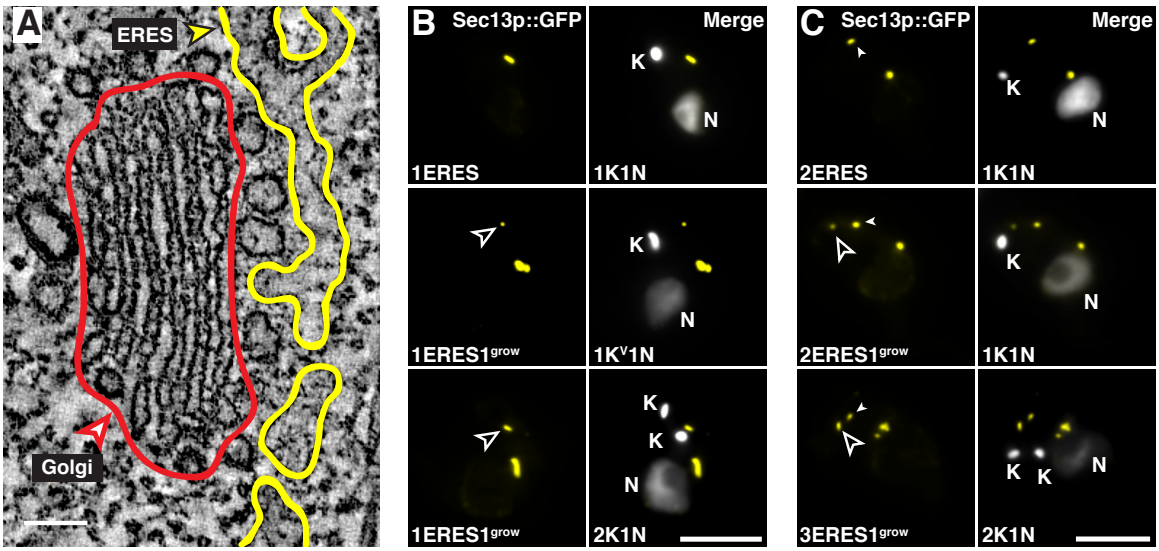

Figure 24. A new ERES appears *de novo* early in the cell division cycle. (A) Electron microscopy image of the ER exit-site (yellow) in close proximity to the Golgi (red). Scale bar = 100 nm. (B-C) Shown are representative images of fixed cells, counterstained with DAPI to determine the different cell division cycle stages, expressing the *Tb*Sec13::GFP ERES marker (yellow). (B) Shows *de novo* ERES appearance in 1K1N1ERES cells. (C) Shows *de novo* ERES appearance in 1K1N2ERES cells. Arrowheads (➤) indicate the mature ERES; the newly ERES is indicated by open arrowheads (➢). Scale bars = 5 µm.

We immobilized living cells and acquired 3D stacks in order to reconstruct the ER morphology and to identify the location of the ERES on the ER. Parallel labelling of ERES (cherry) and ER (GFP) revealed, that all ERES are located on the ER network; the mature ERES (Figure 25A), the additional ERES located close to the nuclear envelope (Figure 25B) as well as the newly growing ERES (Figure 26). The mature ERES was always located on the main ER branch in the posterior part of the cell, whereas the additional ERES^{N} was located either on the main ER branch or on the part of the ER that was spanning the nucleus (Figure 26). This localisation pattern of the mature and nuclear ERES was similar to the localisation of the Golgi structures and thus reinforced the observation of the associated appearance of ERES with the Golgi.

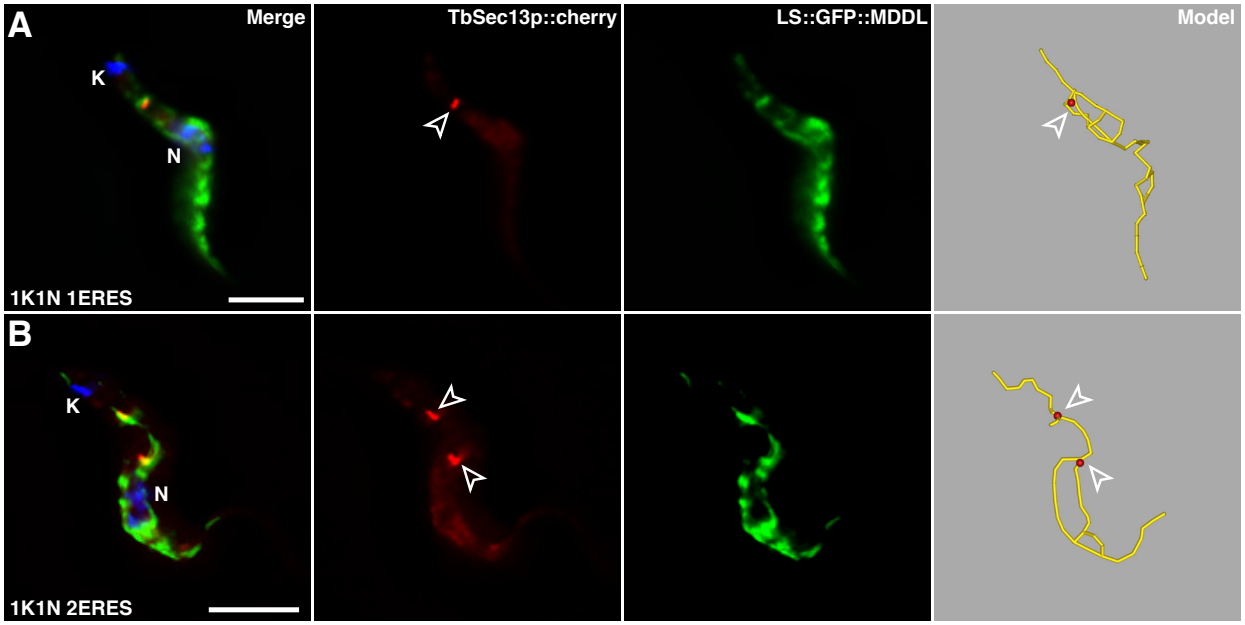

Figure 25. 1K1N cells possessing either one or two ER exit-sites. Immobilised 1K1N cells expressing both the *Tb*Sec13p::cherry ERES marker (red) and the LS::GFP::MDDL ER marker (green). DAPI visualised the kinetoplast and nucleus (blue). The cells in the 1K1N stage showed either (A) on mature or (B) two ERES, the mature and the nuclear one. The endoplasmic reticulum in each cell was manually traced using the Amira software package and is shown as a model (yellow) colocalised with the ERES marker in red. Arrowheads indicate the ER exit sites. Scale bars = 5 µm.

By tracing the new and old ER branch, we were able to assign one ERES to each ER branch (Figure 26). Following cytokinesis this cell would have given rise to two cells, each representing a 1K1N1ERES cell, where the mature ERES would have been located between the nucleus and the kinetoplast. Cells with an additional ERES close to the nucleus, the 2K2N4ERES cells, would have resulted in 1K1N2ERES cells, each with a mature ERES and additional nuclear ERES. This led to the conclusion that duplication of the ERES showed similar kinetics compared to the Golgi duplication in BSF *T. brucei*. We propose, that two ER branches are established, each containing one or two ERES in proximity to a corresponding Golgi. Even in late 2K2N the ER network was connected, resulting in two distinct ER structures after cell division, either with one or two ERES. However, the early appearance of a new ERES and new Golgi indicates, that ER performance is increased early in the cell division cycle.

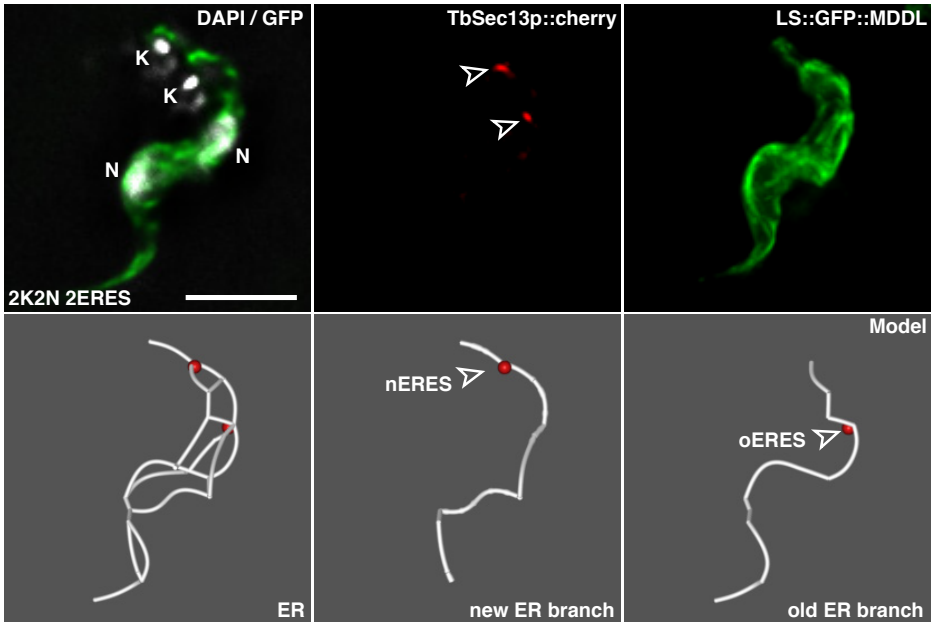

Figure 26. 2K2N cell displaying two ER exit-sites. An immobilised 2K2N cell expressing the *Tb*Sec13p::cherry ERES marker (red) and the LS::GFP::MDDL ER marker (green) is shown. DAPI (white) visualises the kinetoplasts (K) and nuclei (N). The new and old ER branches were manually traced using the Amira software package and the position of the corresponding ERES (red) is marked by arrowheads. Scale bar = 5 µm.

3.7.4 *De novo* formation of a new endosomal apparatus

In trypanosomes endo- and exocytosis are limited to only 5% of the cell surface area, the flagellar pocket (Engstler et al., 2004). Previous work showed, that endosomal membrane trafficking occurs at a very high rate and a lower level of complexity than in mammalian cells (Overath and Engstler, 2004). We investigated how the endosomal capacity is increased during the cell division cycle in order to maintain the high rates of membrane recycling by endo- and exocytosis. Trypanosomes perform endocytosis exclusively via clathrin-coated vesicles (Allen et al., 2003), this allowed to estimate the relative endocytosis capacity by determining the amount of clathrin protein. We quantified the amount of clathrin in cells expressing a YFP::CLC (clathrin light chain) marker protein (Heddergott, 2006). 1K1N and 2K1N cells showed a similar mean fluorescence intensity, 458.3 ± 18.3 RFU (relative fluorescence units) for 1K1N and 530 ± 28.4 RFU for 2K1N cells (Figure 27A). During mitosis in 2K1Nm cells, the signal increased to 955.4 ± 68.8 RFU reaching 968.3 ± 61.6 RFU in the 2K2N stage. The increase proved to be significant from 2K1N to 2K1Nm, suggesting, that the amount of clathrin rose rapidly in the cell division cycle within 40 minutes. In 2K1N cells clathrin was mainly localised in the area between the nucleus and the old flagellar pocket (Figure 27B), however, it was also detectable at the new flagellar pocket (Figure 27E). Proceeding in the cell division cycle, at the onset of mitosis in 2K1Nm cells, clathrin was detectable at both flagellar pockets and a second endosomal compartment developed between the old and new flagellar pocket (Figure 27C). In 2K2N cells, two clathrin labelled compartments were detected, both spanning from the flagellar pocket to the nucleus, new and old respectively (Figure 27D-E).

Since the amount of clathrin was only doubled after the onset of mitosis, we suggest, that endocytic activity was shared between both flagellar pockets in the 2K1N stage. This implicates that flagellar pocket activity was independent of the appearance of the new endosomal compartment.

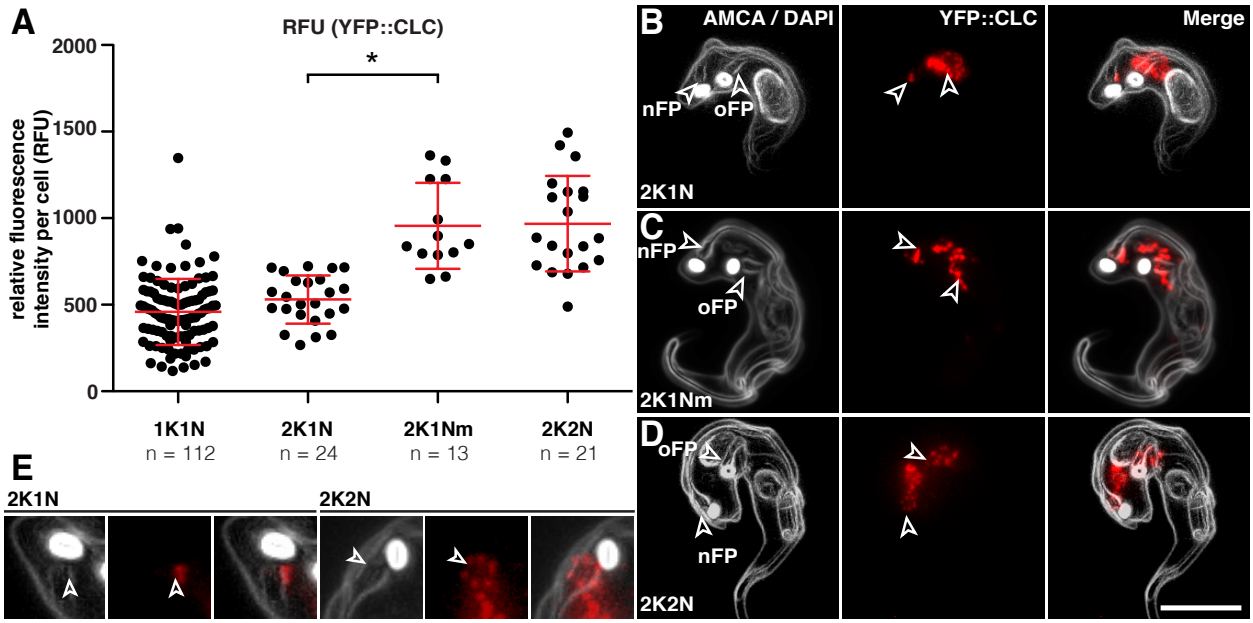

Figure 27. The amount of clathrin doubles during nuclear mitosis. To visualise the duplication of the endosomal compartment the fluorescence intensity of YFP fused to the clathrin light chain (CLC) was quantified for different cell cycle stages and compared. (A) Shows the fluorescence intensity signal for 1K1N, 2K1N, 2K1Nm (mitotic nucleus) and 2K2N cells. The individually measured values are shown as black dots. Red labels indicate the relative fluorescence intensity per cell (RFU) ± SD (n = 170). An ANOVA test was performed and significant comparisons between different stages are indicated with * = $P < 0.0001$. (B-D) Shows the distribution of CLC in different cell division cycle stages. Arrowheads indicate the new (nFP) and old flagellar pocket (oFP). The surface was visualised with AMCA and DNA was counterstained with DAPI (white). The ImageJ edges algorithm was used for better visualisation of the cell surface and flagellum. Scale bar = 5 µm. (E) The insets show the new flagellar pockets in 2K1N and 2K2N cells. As indicated by arrows endocytosis takes place at the new flagellar pocket for both, 2K1N and 2K2N cells.

As EP1 fused to GFP colocalises with endocytosed surface-biotinylated VSG in BSF cells it was used as a marker for the recycling compartment (Engstler and Boshart, 2004). This marker allowed the modelling of the volume and the area of the recycling compartment in different cell division cycle stages (Figure 28A). 1K1N cells showed a volume of 3.04 ± 0.12 µm^3 and an area of 14.99 ± 0.38 µm^2 (Figure 28B). In comparison, EP1::GFP was localised in two equal compartments in 2K2N cells (Figure 28A), covering a volume of 6.6 ± 0.66 µm^3 and an area of 30.03 ± 2.15 µm^2 (Figure 28B).

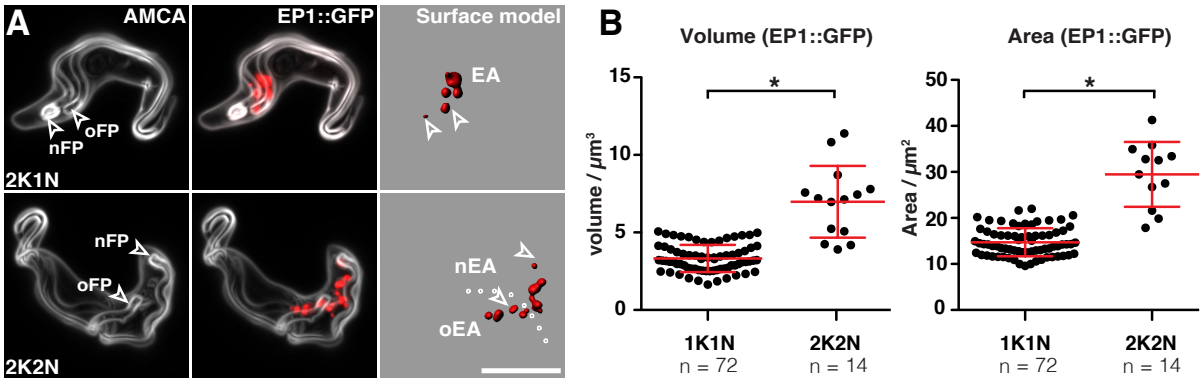

Figure 28. Volume and area of the EP1::GFP covered recycling compartment doubles during mitosis. (A) Shows representative images of fixed cells expressing the EP1::GFP marker (red) at different stages of the cell division cycle. The surface was stained with AMCA (grey). Arrowheads indicate the new (nFP) and old flagellar pocket (oFP). The ImageJ edges algorithm was used for better visualisation of the cell surface and flagellum. The surface of the recycling compartment was modelled using the Amira software package and is shown in red. Scale bar = 5 µm. (B) The volumes and areas of the endosomal compartment were determined from the surface models obtained from the EP1::GFP fluorescence signal. Individually measured values are shown as black dots. Red labels indicate the mean values of the volume (left graph) and area (right graph) for 1K1N and 2K2N cells, respectively. A t-test was performed and significant comparisons between different stages are indicated with * = $P < 0.0001$

A t-test showed significant increase between 1K1N and 2K2N cells for both, the volume and the area of the endosomal compartment. We separated the two compartments in 2K2N cells into two groups based on the localisation, the first compartment between the nucleus and the old flagellar pocket and the second compartment between the new nucleus and the new flagellar pocket, and determined the volume and area separately. The volume determined for each endosomal compartment matched the volumes determined for a single endosomal compartment in 1K1N cells (3.36 µm^3 and 3.59 µm^3 compared to 3.04 µm^3). Compared to the quantification of clathrin, the secretory capacity increased late in the cell division cycle during mitosis.

The data revealed, that the endocytosis and recycling capacity was doubled during the progression from 2K1N to 2K2N, at around 5.3 hours in the cell division cycle, by the appearance of a new endosomal and recycling compartment, located in the area between the new nucleus and new flagellar pocket. Consistent with the YFP::CLC fluorescence both flagellar pockets performed endo- and exocytosis.

3.7.5 Formation of a new lysosome late in the cell division cycle

Trypanosomes remove host-derived antibodies from their cell surface via hydrodynamic flow-mediated antibody clearance (Engstler et al., 2007). The Ig-VSG complexes are internalized and the immunoglobulins (Ig) are degraded in the lysosome. This indicates the importance of the lysosome for the parasites protection against complement-mediated immune destruction by the mammalian host (Engstler et al., 2007). We investigated when and how the single lysosome gets duplicated during the cell division cycle. The lysosome was visualised by immunofluorescence analysis using the monoclonal mAB280 antibody, directed against the LAMP like protein p67, obtained from Bangs and colleagues (Alexander et al., 2002).

In 1K1N cells the lysosome showed a spherical shape and was located in the posterior, adjacent to the nucleus (Figure 29). An elongated extension (Ex) was identified at the mature lysosome with different orientations in $1K^V1N$ and $1K^B1N$ during kinetoplast duplication (Figure 29). This extension was either directed towards the posterior cell part, close to the new flagellar pocket or anterior towards the nucleus. Rare images could be captured from 2K1N cells where we identified two spherical lysosomes, that were connected, this might suggest, that a new lysosome could be built at the tip of one of these extensions in 2K1N cells in close proximity to the old flagellar pocket (Figure 29, right-hand panels). In 2K2N two separate lysosomes were detected in most of the cells analysed (Diplomarbeit J. Jung, 2009).

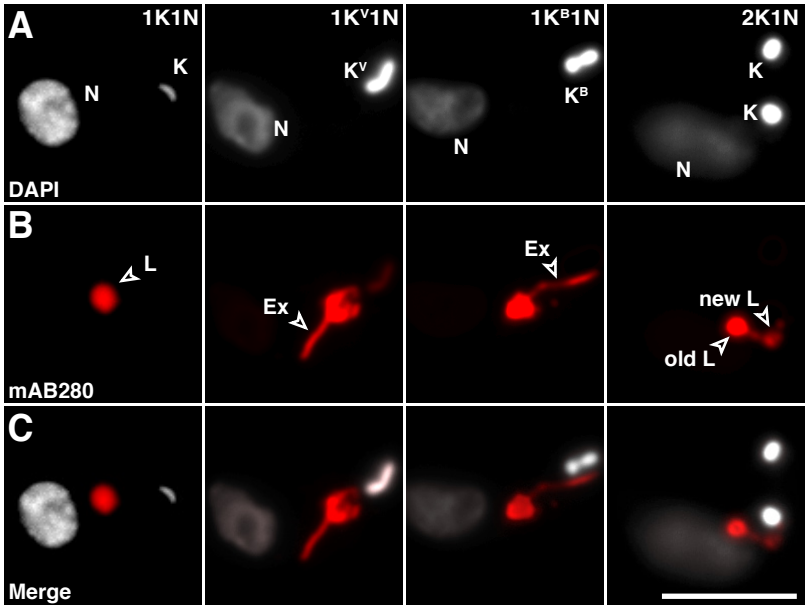

Figure 29. The lysosome forms an extension early in the cell division cycle. Immunofluorescence against the LAMP like protein p67 using the monoclonal mAB280 antibody (red) on fixed cells, (Alexander et al., 2002) at different stages of the cell division cycle (IF performed by M.Engstler). DNA was counterstained with DAPI (white). Arrowheads indicate the lysosome (L) or the lysosome extension (Ex). Images suggest, that the new lysosome (new L) grew at an extension built at the mature lysosome (old L). Scale bar = 5 µm

We further aimed at investigating the segregation of the lysosome using the p67::GFP expressing marker cell line derived by Mark Günzel. Unfortunately the fluorescence signal of p67::GFP was not sufficient for live cell microscopy. Furthermore the p67::GFP marker protein showed background fluorescence in the cytoplasm and in the ER. To monitor lysosome dynamics in single living cells, fluorescently labelled dextran was left to accumulate in the lysosome. Trypanosomes internalize dextran via fluid phase uptake and transport it to the lysosome (Engstler et al., 2004), allowing the endosomal compartment and/or lysosome to be labelled in this way. Fluorescently labelled dextran was added to the cells, which were incubated for 30 minutes at 37°C, to allow uptake into the endosomal compartment. After washing and further incubation at 37°C the dextran accumulated in the lysosome. Movies, taken at 200 fps from immobilised living cells, revealed, that tubular structures extending from the lysosome were highly flexible. Up to three tubular extensions were identified simultaneously (Figure 30) and the tubule tip showed bending of up to 90 degrees. Furthermore the tubules appeared and disappeared at different sites of the lysosome indicating, that the lysosome tubules are highly dynamic structures. None of these highly flexible structures showed similar length compared to the extension identified by IF, still these structures might be the origin of those observed by IF. We have no prove on how the lysosome is duplicated, still we propose that the new lysosome might grow at the tip of an extension built by the old lysosome. Tubular structures extending from the mature lysosome are highly flexible and dynamic and could explain how lysosomal membranes are separated from the lysosome and are recycled by a structure known as the retromer complex. This needs further investigations e.g. by colocalisation analysis of the lysosome with marker proteins for the retromer complex. Super resolution microscopy could reveal the appearance of a new lysosome either by *de novo* formation or at the tip of an extension formed by the mature lysosome.

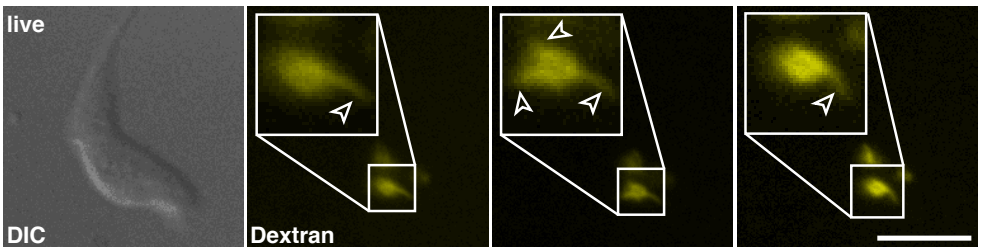

Figure 30. The lysosome shows highly flexible tubular extensions. Cells were incubated with fluorescently labelled dextran to visualise the lysosome and immobilised for high-speed video microscopy. Shown are representative frames of the high-speed time-lapse movie taken from the same cell (DIC image) at 200 fps. The inset shows the lysosome and arrowheads point at the tubules extending from the lysosome. Up to three tubular structures were detected in parallel. Scale bar = 5 µm.

3.7.6 Duplication of the glycosomes

Trypanosomes have compartmentalized the process of glycolysis into membrane-surrounded organelles that are related to peroxisomes. These so-called glycosomes and their correct duplication is important due to the fact, that glycolysis is the main ATP-generating source for BSF trypanosomes (Hart et al., 1984). We investigated how and when glycosomes are duplicated, in order to answer the question how the cells generate the energy levels necessary for the enormous changes occurring during the cell division cycle. In order to visualise glycosomes, we used the peroxisomal targeting signal 1 (PTS1) fused to GFP as Michels and colleagues showed that the PTS1 was sufficient for the translocation of proteins into glycosomes by Peroxin 5 (Sampathkumar et al., 2008). First, we investigated if the fusion protein covers the whole population of glycosomes or if the protein composition of glycosomes varies in terms of enzyme subpopulations. Immunofluorescence analysis against different glycolytic enzymes in the background of the PTS1::GFP marker cell line was performed. Aldolase (ALD), Hexokinase (HXK) as well as Glyceraldehyde 3-phosphate dehydrogenase (GAPDH) showed complete colocalisation with the PTS1::GFP marker and therefore we conclude that there are no subpopulations of glycosomes and all glycosomes share equal content (Figure 31).

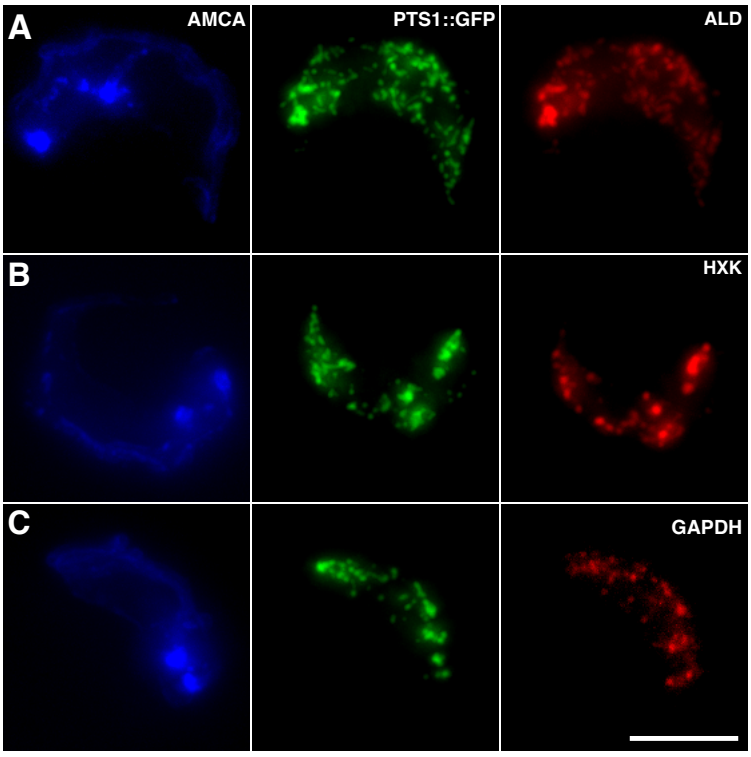

Figure 31. The PTS1::GFP marker colocalises with glycolytic enzymes of the glycosomes. Immunofluorescence images of surface stained (AMCA), fixed cells expressing the PTS1::GFP glycosome marker. Antibodies used were directed against (A) Aldolase (ALD), (B) Hexokinase (HXK) and (C) Glyceraldehyde 3-phosphate dehydrogenase (GAPDH). PTS1::GFP fluorescence colocalised with the three glycolytic enzymes, indicating equal enzyme composition in the different glycosomes. Scale bar = 5 µm.

We further investigated when glycosomes duplicate in the cell division cycle. Therefore, we counted the number of glycosomes per cell in each cell division cycle stage and realised that glycosomes continuously increase in number during the cell division cycle (Figure 32). The number of glycosomes was counted during progression through the cell division cycle. A comparable number of 33.6 ± 1.2 glycosomes per cell in 1K1N cells and 34.2 ± 2.5 in 1K^{V}1N cells was maintained until kinetoplast duplication. A t-test showed no significant difference in glycosome number for 1K1N cells compared to 1K^{V}1N. During further progression through the cell division cycle the glycosome number increased up to 47.3 ± 1.1 in 2K1N and 64.2 ± 2.8 in 2K2N cells. The differences in glycosome numbers for 1K^{V}1N, 2K1N and 2K2N proved to be significant by t-test. This suggested a continuous increase in glycosome number during progression through the cell division cycle. In Figure 32B the localisation of glycosomes in cells at different cell cycle stages is shown. Glycosomes were located in the whole cell from the anterior to the posterior cell pole and for all cell division cycle stages elongated glycosomes were identified. In z-projections of the fluorescent glycosomes marker glycosomes seemed to be randomly distributed in the cytoplasm (Figure 32B,C). The elongated structures could indicate glycosomes during division; still the resolution of light microscopy cannot prove this hypothesis. Therefore high-resolution light microscopy could reveal, whether these elongated structures show glycosomes in close proximity or during division. Unfortunately to date we could not identify dividing glycosomes by EM.

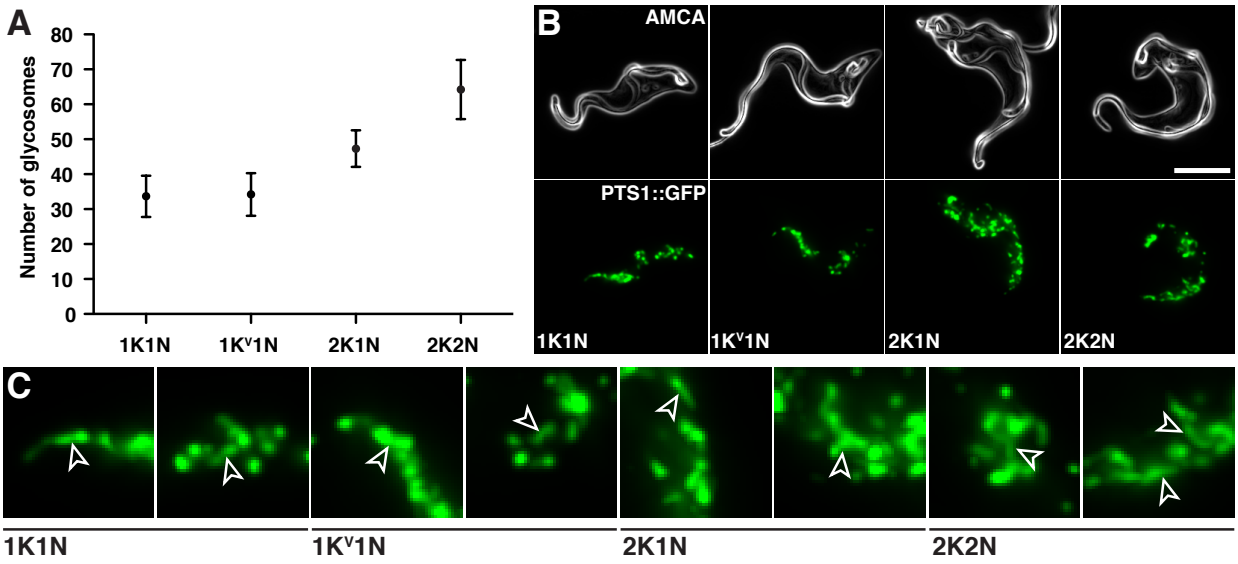

Figure 32. Glycosome division occurs continuously during the cell division cycle. (A) Amount of glycosomes counted for different cell division cycle stages (n= 66 in total). (B) Fixed cells expressing the PTS1::GFP glycosome marker at different stages of the cell division cycle. Glycosomes are distributed in the whole cell from the posterior to the anterior pole. The surface was visualised with AMCA and DNA was counterstained with DAPI. The ImageJ edges algorithm was used for better visualisation of the cell surface and flagellum. Scale bar = 5 µm. (C) Detailed view of cells at different cell division cycle stages. The arrowheads show clustered and elongated glycosomal structures indicating glycosomes in division.

It has been suggested that peroxisomes could be attached to the ER membrane (Agrawal and Subramani, 2013) and therefore we analysed glycosome movement using high-speed microscopy. The chain-like array of glycosomes suggested that they are ordered and could be located close to the ER, hence, also following the structure of the flagellum.

Cells expressing the PTS1::GFP marker were surface labelled with sulfo-NHS-Atto488 to visualise glycosomes and cell surface in parallel. Movies taken at 200 frames per second allowed the investigation of the movement of the glycosomes in the cell body (Figure 33). The cell diameter was marked in representative frames of the high-speed time-lapse movie along which the fluorescence intensity profile was extracted (Figure 33B). In principle, the profile plot displays a two-dimensional graph of the intensities of pixels along a line drawn through the cell. The peak in the plot displaying the maximum fluorescence intensity (Figure 33B, red line) indicated the position of the glycosomes in the cell (Figure 33A, red arrowheads). The position of the flagellum was indicated with a green spot in the fluorescence intensity plot (Figure 33B). As the distance between glycosomes and flagellum was always around 0.5 µm we hypothesised a coordinated movement of the glycosomes with the flagellum but the reason for the chain-like assembly of glycosomes still remains unclear. On ultrastructural level we could not identify glycosomes attachment to any cellular structure. Therefore, coordinated movement of glycosomes and the flagellum could be a passive effect due to the crowded environment in the cytoplasm.

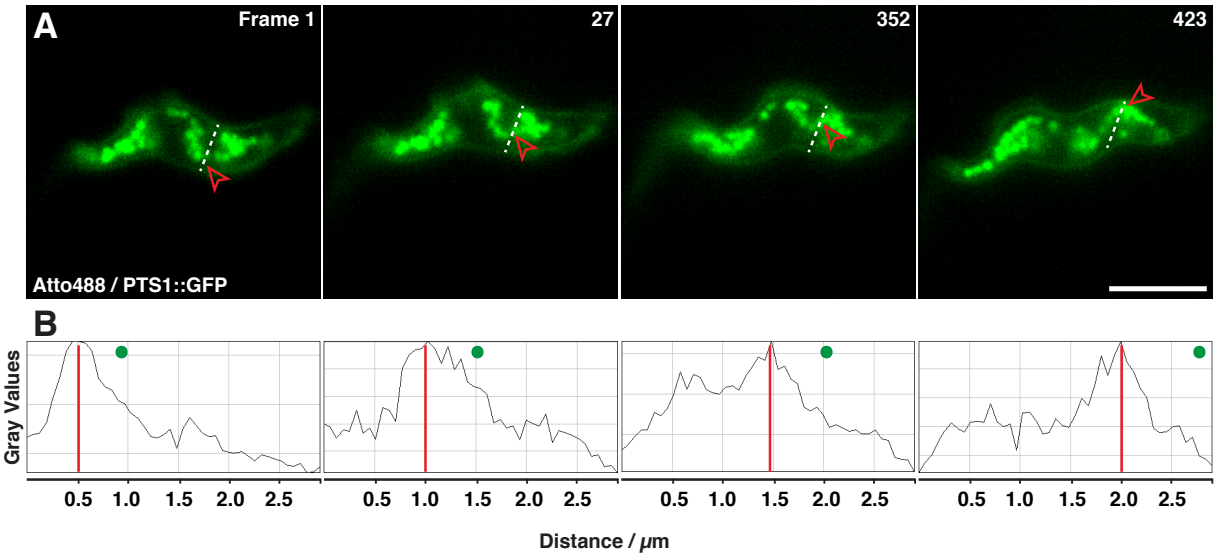

Figure 33. Glycosomes move in a recurrent fashion with the flagellum. (A) Representative frames from high-speed movies (200 fps) taken of surface labelled cells (Atto488 dye) expressing the PTS1::GFP glycosome marker. The dashed line was drawn alongside the cell diameter immediately before the nucleus and determined the region from which the fluorescence intensity profile plot (B) was generated. The red arrows indicate the intensity maxima determined from the profile plot. Red bars indicate fluorescence intensity maxima and green dots mark the position of the flagellum. Scale bar = 5 µm.

3.7.7 The mitochondrion grows continuously and segregates during cytokinesis

We further investigated the mitochondrion, which is a single copy organelle and, as in the case for the ER, spans through the whole cell body. In contrast to the ER, the mitochondrion is not essential for energy metabolism in the BSF. Previous work performed by Tyler and colleagues suggested that the mitochondrion segregates prior to cytokinesis using a rather rough time-scale (Tyler et al., 2001). Observations in our lab indicated that the mitochondrion was still connected during cytokinesis and we therefore aimed at investigating mitochondrion duplication in regard to the detailed cell division cycle time map. In 1K1N cells the mitochondrion appeared as a tubule spanning through the whole cell, always located opposite of the flagellum (Figure 34). At the posterior end of the mitochondrion, a bulge containing the kinetoplast that increased in size was identified during kinetoplast duplication. During cell division cycle progression, the mitochondrial tube expanded and showed multiple extensions (Figure 34). In 2K2N cells both kinetoplasts located in the same tubular structure, this is why we concluded that the two tubules did not represent two mitochondria prior to separation.

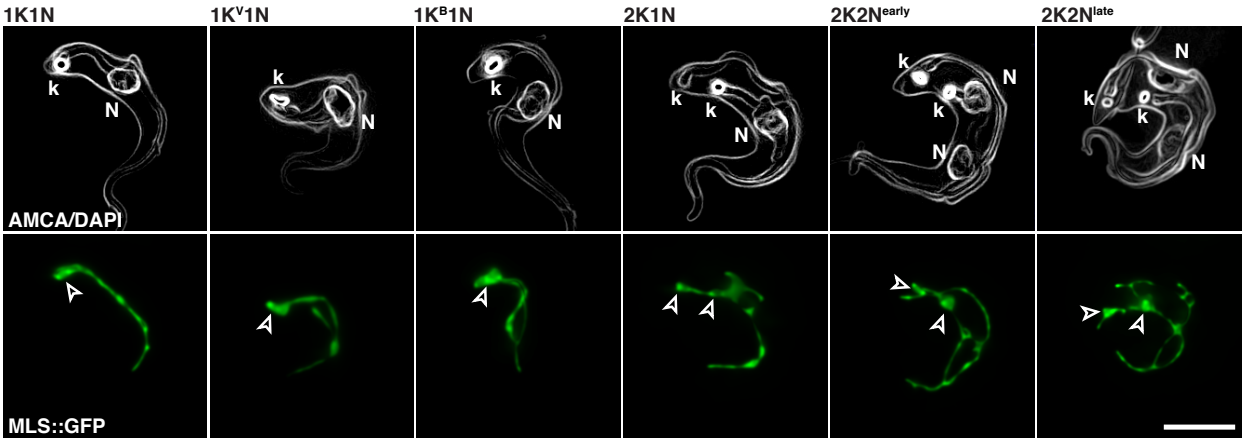

Figure 34. The mitochondrion stays connected until late 2K2N stage. Shown are representative images of fixed cells expressing the MLS::GFP mitochondrion marker (green) at different stages of the cell division cycle. During progression through the cell cycle the mitochondrion structure becomes more and more complex and shows variable interconnections. (A) DAPI and AMCA staining (white). The ImageJ edges algorithm was used for better visualisation of the cell surface and flagellum. (B) MLS::GFP mitochondrion marker staining. Arrowheads point to the location of the kinetoplasts. Scale bar = 5 µm.

We conducted live cell microscopy in order to follow mitochondrion separation and partitioning in the dividing cell, where the dynamics of the mitochondrion enabled us to detect whether the tubules were connected or separated. Trypanosomes expressing the MLS::GFP mitochondrion marker were immobilised and the temperature was adjusted to allow moderate movement of the cells to follow organelle dynamics. Mitochondrion morphology was the same compared to fixed cells, with 1K1N cells showing a single tubule spanning through the cell body. Two tubules with interconnections were detected in 2K2N cells and as observed in fixed 2K2N cells, the mitochondrion network showed interconnections during initiation of the cleavage furrow (Figure 35). During the furrowing process, one mitochondrion tubule was located in each daughter cell while still being connected at the very posterior end up to the final abscission (Figure 35B).

We noticed that besides tubular morphology of the mitochondrion in 1K1N cells, some cells also showed structured mitochondria with extensions. We suggested that after cell cleavage and thus mitochondrion separation, the extensions remained and were retracted during 1K1N. These data indicate that the mitochondrion is separated with the furrowing process during cytokinesis.

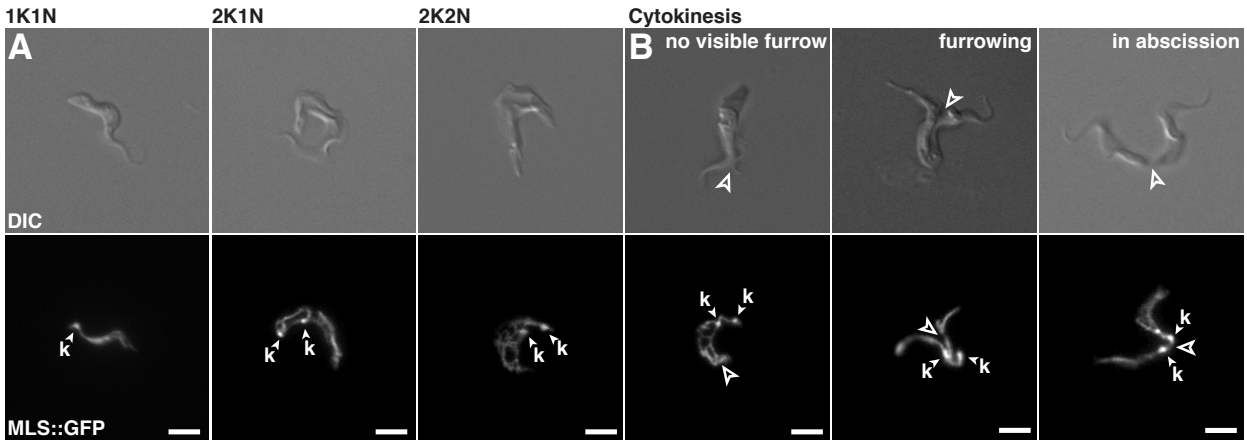

Figure 35. Live cell microscopy revealed that the mitochondrion is connected up to the very end of cytokinesis. During furrowing each cell contains a mitochondrion tubule connected at the posterior cell pole. Open arrowheads indicate cleavage furrows while filled arrowheads indicate the position of the kinetoplasts in the mitochondrion. For live cell microscopy trypanosomes were mounted in 5% gelatine and the climate chamber was adjusted to a temperature range between 24°C and 30°C to allow cell motility and the cytokinesis process was recorded. During microscopy the excitation was switched from DIC to eGFP. Scale bars = 5 µm.

3.8 *In silico* synchronisation as a tool for drug screening

Identifying temporal and spatial effects of a potential drug is challenging. At first glance it seems impossible to temporally resolve drug effects in an asynchronously growing culture. The group of Prof. Holzgrabe synthesised a library of quinolone-type molecules inspired by recent reports, which showed anti-trypanosomal activity using quinolones such as ciprofloxacin (1999; Keiser and Burri, 2001; Nenortas et al., 2003). The quinolone-type molecules were then tested in our laboratory for anti-trypanosomal activity and cytotoxicity, following which two compounds were chosen to be assayed with our *in silico* synchronisation approach. The effects of compounds 19 and 29 (Hiltensperger et al., 2012) on different organelles were tested and showed no alteration of the endoplasmic reticulum, Golgi apparatus, endosomal compartment and lysosome. However, after incubation with compound 19 (0.54 ± 0.04 µM) and compound 29 (0.023 ± 0.004 µM), the morphology of the mitochondrion was changed and sheet-like patches could be observed (Hiltensperger et al., 2012). We then performed a cell cycle analysis with the MLS::GFP marker cell line treated with compound 19 and 29 for 42 hours to investigate whether cells accumulated in a specific cell division cycle stage (Figure 36). Both untreated and DMSO (1%) treated cells showed a typical distribution of cell division cycle stages based on their K/N status. Cells treated with ciprofloxacin were compared to control cells and all showed a 1K1N to 1K^{seg}1N ratio of 2:1.

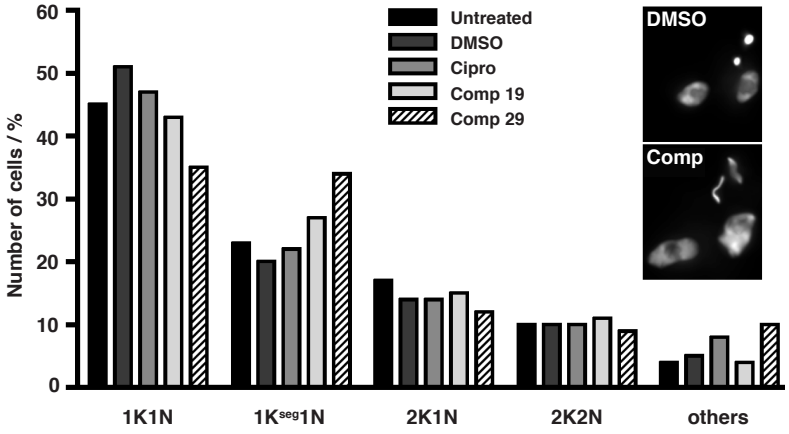

Figure 36. Quinolone-like molecules 19 and 29 lead to aberrant kinetoplast segregation. Cell cycle analysis of the *T. brucei* MLS::GFP mitochondrion marker cell line before and after treatment for 42 h with either DMSO, Ciprofloxacin, Compound 19 and 29 (n = 300 each condition). The figure insets show representative cells stained with DAPI, the upper image shows cells from the DMSO control, whereas the lower figure (comp) depicts an example of two cells displaying a segregation defect in their kinetoplasts (Hiltensperger et al., 2012).

Treatment with compound 19 and 29 led to a shift in the ratio of 1K1N to 1K^{seg}1N cells, from 2:1 for control cells, to 3:2 and 1:1, respectively (Figure 36). Changes in kinetoplast morphology were also caused by the treatment with compounds 19 and 29 leading to elongated kineto-

plasts and indicating a defect in their segregation (Figure 36, insets). Other cell division cycle stages were unaffected after treatment with DMSO, ciprofloxacin or compound 19 and 29, all showed a morphologically normal nucleus and kinetoplast. It has been shown that ciprofloxacin targets the mitochondrial topoisomerase II, hence we wanted to investigate the possibility that compound 19 and 29 target the trypanosomal topoisomerase II, *Tb*TopoII$_{mt}$. We used an inducible RNA-interference (RNAi) approach to knock down *Tb*TopoII$_{mt}$ in BSF trypanosomes in order to compare the phenotypes. The efficiency of *Tb*TopoII$_{mt}$ silencing was verified by Northern blot, which proved that the mRNA is absent at 24 hours after tetracycline induction (Figure 37A). Furthermore, the proliferation rate was investigated in non-induced versus induced cells, which showed that cell growth decreased at 96 hours after induction and cells started to die (Figure 37A). Then, cells were stained with DAPI at different time points in the course of the RNAi experiment to investigate the morphology of DNA-containing structures. Starting from 48 hours after induction, a continuous loss of kDNA could be detected, leading to a majority of dyskinetoplastid cells by 72 hours. After 120 hours no cell with kDNA could be found. The phenotype after *Tb*TopoII$_{mt}$ knock-down was consistent with previous work performed in the PCF form (Wang and Englund, 2001; Lindsay et al., 2008). Comparing the phenotype after RNAi against *Tb*TopoII$_{mt}$ with the one resulting from treatment with compound 19 and 29 we can conclude that the two processes are independent.

Taken together, we could show that our marker cell lines could be used to investigate the target location of potential drugs or agents and used to pinpoint changes in the cell division cycle using the developed *in silico* synchronisation approach.

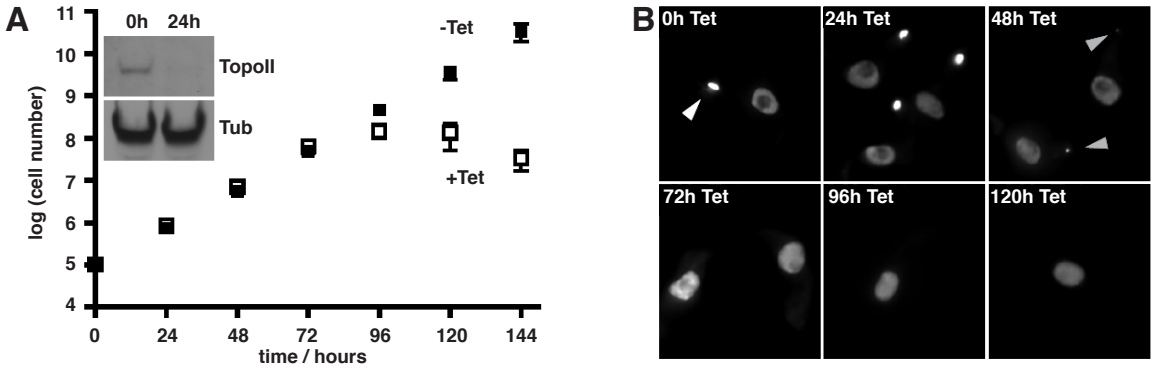

Figure 37. Knockdown of mitochondrial *T. brucei* topoisomerase II. (A) Knockdown of *Tb*TopoII$_{mt}$ in BSF *T. brucei* affects cell growth beginning at 72 h after induction of RNAi with tetracycline (Tet). Three independent clones were analysed, and average cell numbers are shown in the growth curves with their standard deviation. The inset shows the Northern blot results of one clone to confirm knockdown of topoisomerase II (TopoII) using a tubulin probe as loading control. (B) Images illustrating the shrinkage of the kinetoplast after RNAi induction. At 0 h and 24 h, kinetoplasts are clearly visible, while kDNA loss in DAPI stained cells is first detected after 48 h of induction. By 72 h post induction, the majority of induced cells are dyskinetoplastid (Hiltensperger et al., 2012).

3.9 Evolution of cell division cycle dynamics in different trypanosome species

We established the flagellum as a precise timer of the BSF *Trypanosoma brucei* cell division cycle and described the duplication of the cellular compartments with high temporal resolution. The next step is to apply this knowledge in order to decipher similarities and differences in different trypanosome species. Most freshly isolated trypanosome species are delicate to handle and are not amenable to genetic manipulation; for this reason new non-invasive protocols had to be developed. In collaboration with Dan Masigas group at the *International Centre of Insect Physiology and Ecology* (ICIPE) in Nairobi we applied the knowledge gained from *in vitro* BSF *T. brucei* cultures, to trypanosomes isolated in the field as well as on other animal infective strains obtained from mouse infections. About 5 ml blood was collected from the jugular vein of infected cattle and parasites were purified by centrifugation (200x*g*, 5 min). We surface stained *T. brucei*, *T. evansi*, *T. vivax* and *T. congolense* and visualised the cell surface and the flagellum (Figure 38). The *MitoTracker Red CMXRos* (Molecular probes), the *FM 4-64 FX* dye (Molecular probes) and fluorescently labelled dextran allowed us to stain the mitochondrion, the endosomal compartment as well as the lysosome in previously uncharacterized trypanosomes freshly isolated from infected animals. This work builds a solid basis for investigating different trypanosome species in order to reveal evolutionary conserved mechanisms or species-specific differences in organelle maintenance during the cell division cycle.

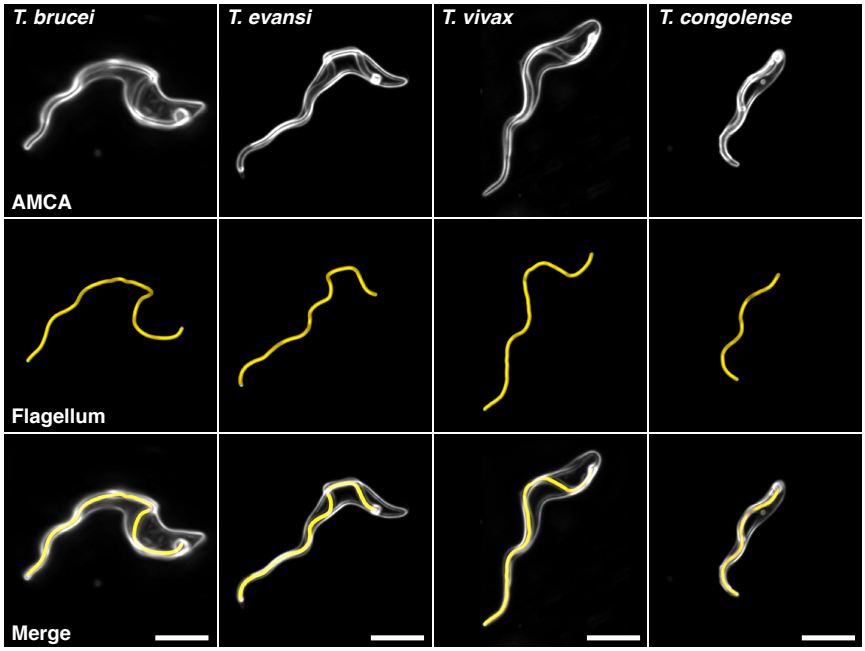

Figure 38. Surface staining allows flagellum tracing in different trypanosome species. The surface of different trypanosome species was visualised with AMCA (white) and the deconvolved 3D stacks are shown as z-projections. The ImageJ edges algorithm was used for better visualisation of the cell surface and flagellum. The flagellum was manually traced (yellow) using the Amira software package allowing the determination of the NFR for different trypanosome species (flagella traced by Tim Krüger). Scale bars = 5 µm.

3.10 Conclusion

During this work we established a non-invasive *in silico* synchronisation approach to determine the cell division cycle position of single cells in asynchronously growing cultures with high temporal accuracy. We divided the cell division cycle into 11 stages based on K/N status and outgrowth rate of the new flagellum. In addition, we generated fluorescent marker cell lines for all major trypanosomal organelles and followed their duplication events with respect to the position in the cell division cycle. As a proof of principle we showed that this approach is well suited for pinpointing the effect of potential drug targets (Hiltensperger et al., 2012).

This work answered the following questions:

(A) Can we provide hints for the mode of organelle formation in trypanosomes?

We clearly could give hints on how major organelles are duplicated in BSF trypanosomes. The architecture of organelles, sensitive to fixation, such as the ER and the lysosome was described in detail by live cell 3D microscopy of immobilised cells and motile cells.

(B) Can we correlate the formation of organelles with the cell division cycle?

(C) Can we define an order of organelle formation?

The spartio-temporal correlation of organelle formation was described in detail. We proved, that all organelles analysed are duplicated at a specific time point during the cell division cycle. We identified two cell division cycle phases based on cell morphology dynamics. In the steady state cell morphology phase (Phase I), organelles of the secretory apparatus are duplicated while cell morphology remains constant. In phase II, the new secretory organelles are functional and cell morphology dynamics, such as cell volume increase and cell elongation is initiated.

(D) Are organelle formation events controlled by cell cycle checkpoints?

(E) Lastly, is the orchestration of organelle formation related to VSG coat maintenance?

We found that cell growth and formation of secretory organelles is temporally separated and we speculate that this orchestration ensures a functional VSG coat during cell growth and cell division cycle progression. This dependency on a functional VSG coat could serve as an important cell cycle checkpoint.

4 Discussion

4.1 *In silico* synchronisation of the BSF *T. brucei* cell division cycle

During this work we performed a detailed analysis of the BSF *Trypanosoma brucei* cell division cycle. This detailed analysis was only possible due to an efficient synchronisation approach that was developed and established during this project. Well-described events occurring during the cell division cycle were taken into account in order to generate a precise temporal map of the cell division cycle. This data allowed us to determine the position of individual cells in a population with high accuracy whilst not affecting their natural growth. So far timing of the *T. brucei* cell division cycle has been difficult due to the lack of availability of efficient cell synchronisation tools. For most eukaryotes harsh chemical treatment has been used to force synchronous growth. Hydroxyurea (HU) induced cell cycle arrest has been applied in the PCF of *T. brucei* (Brun, 1980; Chowdhury et al., 2008) and this was further adapted for use in the BSF by Hammarton and colleagues and is the only successful approach published that conduces cell synchrony in *T. brucei*. Even so, there are limitations in establishing long-term synchronously growing cultures. Englund and colleagues showed that 0.2 mM hydroxyurea was sufficient to arrest PCF trypanosomes near the end of S-phase (Chowdhury et al., 2008). The hydroxyurea concentration sufficient for arresting PCF trypanosomes was one order of magnitude lower compared to other kinetoplasts (Galanti et al., 1994; Mutomba and Wang, 1996; Soto et al., 2000; Zick et al., 2005). 0.1 mM hydroxyurea could not arrest PCF trypanosomes and 0.25 mM hydroxyurea was toxic (Mutomba and Wang, 1996). After hydroxyurea removal, growth resumed to normal after 6 hours but synchrony was gradually lost after 20 hours. Hammarton and colleagues obtained similar results for BSF *T. brucei*, as 0.1 µg ml^{-1} led to an S-phase block, which was released after HU removal, still synchronous growth could not be achieved as cell synchrony was gradually lost within 2 hours after HU removal (Forsythe et al., 2009). Taken together HU induced synchronisation approaches can be used for enrichment of cell division cycle stages but does not result in cell division cycle synchronisation of living cultures. Furthermore it is questionable whether this approach might affect cell division cycle regulated events as it was shown that HU treatment in PCF did not affect kinetoplast replication but inhibited the repair of minicircle gaps in the kinetoplast, which could lead to accumulation of defects in the mitochondrial genome (Chowdhury et al., 2008). Even though cell synchrony was achieved for a short time, we aimed for a non-invasive cell cycle synchronisation approach. In the green algae chlamydomonas a non-invasive synchronisation approach has been adapted to achieve synchronous growth by circadian dark/light adaption (Rooney et al., 1971; Lemaire et al., 1999) but this non-invasive approach is not suited for most eukaryotes. The question remains of how a cell population can be synchronised without harsh treatment therefore remains.

Barford and Hall established an approach to estimate the duration of different stages in the cell division cycle, provided the position of the stage in the cell cycle was known, the generation time was constant and the culture was truly asynchronous (Barford and Hall, 1976). Due to the age distribution in asynchronous cultures the estimation of the duration of a particular phase will not be accurate unless the position of this phase has been determined. There is always a greater probability for a cell to be less progressed in the cell division cycle (Barford and Hall, 1976). To overcome this bias the frequency of cells at different positions in the cell division cycle can be estimated for an ideal, exponentially growing culture by the equation: $y = 2^{(1-x)}$; where (y) is the relative frequency of cells at a particular stage of the cell cycle (x). This bias was considered in the calculations of Williams (Woodward and Gull, 1990) and was used by Gull and colleagues to estimate the duration of kinetoplast and nucleus duplication in PCF *T. brucei* (Woodward and Gull, 1990). Sherwin and Gull precisely determined the order of events leading to kinetoplast and nucleus duplication, and used this to roughly time the cell division cycle of PCF *T. brucei*. During this project it was shown that for the BSF the events for duplication of the kinetoplast and nucleus follow similar kinetics concerning DNA synthesis phase for both, the kinetoplast and the nucleus. The duration of S-phase was slightly faster in the BSF with 0.81 hours in BSF compared to 0.99 hours in PCF for the kinetoplast and 1.20 hours in BSF compared to 1.51 hours in PCF for the nucleus (compare (Woodward and Gull, 1990)). In contrast the actual segregation of the duplicated organelles was about twice as fast in BSFs than in the PCFs lasting 0.25 hours and 0.26 hours in BSF compared to 0.72 hours and 0.69 hours in PCF for the kinetoplast and nucleus, respectively. Differences in living environment could account for faster organelle segregation in the BSF, due to increased cellular motility at 37°C compared to 27°C for PCF trypanosomes. This is consistent with our idea that physical forces due to cell motility support segregation and separation processes in trypanosomes. For the BSF of *T. brucei* cell motility is essential, not only *in vivo*, but also *in vitro* (Broadhead et al., 2006), thus emphasising motility as an important factor. This leads to the conclusion that life cycle stage specific differences could arise from different living environments. This is why it is important to conduct experiments on different trypanosome species and their life cycle stages in order to investigate common features and specific differences due to adaption to the environment and evolution.

4.2 Duplication events of major organelles can be pinpointed precisely

One important question to answer was, if organelle duplication is temporally controlled or occurs randomly during the cell division cycle. Furthermore we investigated whether organelles duplicate in a specific order, this could indicate new cell cycle checkpoints. Especially for single copy organelles active segregation and organelle separation appeared to be necessary to maintain organelle integrity during cell multiplication. Trypanosomes have been introduced as a model system for analysing basic principles of eukaryotic cell biology; e.g. flagellum biogenesis, Golgi duplication and membrane recycling (Engstler et al., 2004; He et al., 2004; Morgan et al., 2005; Morga and Bastin, 2013) but tools for precise timing of the *T. brucei* cell division cycle were not yet available. Due to our precise temporal map of the cell division cycle we could perform a detailed analysis of the BSF *T. brucei* cell division cycle with respect to duplication of all major organelles with high temporal resolution. We generated cell lines expressing GFP, YFP or mCherry tagged versions of marker proteins in order to localise and follow duplication events of the ERES, Golgi, ER, endosomal apparatus, lysosome, glycosomes and the mitochondrion.

By the use of our *in silico* synchronisation approach we divided the cell division cycle into 11 stages (NFR 0 – 100). In stage 1 (1K1N), the cells showed a single flagellum with an NFR of 0. Cells with an NFR of 10, proceeded through S-phase for kinetoplast and nucleus, later, at an NFR of 20, kDNA synthesis was completed while the nucleus S-phase was still in progress. At the end of the 1K1N stage, coinciding with the ER network beginning to increase, the new ERES appeared; therefore the ER was found to be the first of the secretory organelles to start duplication. With a delay of over 30 minutes a new Golgi appeared in close proximity to the new ERES. It was shown for PCF that the new Golgi was built *de novo* from the new ERES but also received material from the old Golgi that stayed in close proximity (He et al., 2004). The delayed onset of new Golgi appearance in BSF supports a similar mechanism in both life cycle stages where the new ERES is built first and following which a new Golgi is established. It was reported that duplication of the ERES appeared to be different in PCF compared to BSF (Bangs, 2011). Due to our detailed temporal map we could correlate the findings for PCF (He et al., 2004) and BSF (Bangs, 2011) and suggest that PCF and BSF share a similar duplication mechanism for the ERES and Golgi. It was indicated that the duplication of the ERES is not tightly coupled to the cell division cycle in BSF trypanosomes, due to the fact that the growing Golgi and bilobe structures are spatially apart in the BSF (Bangs, 2011). The bilobe is a cytoskeletal structure that was proposed to mediate biogenesis of the Golgi in PCF (He et al., 2005), however, the function of the bilobe is still unclear (Esson et al., 2012). We suggest that despite the localisation and function of the bilobe, the association of the new ERES and Golgi

with the ER could be sufficient for correct distribution of these organelles during cell division (Bangs, 2011). We argue that the role of the bilobe in ERES duplication remains unclear and that the ER to FAZ association may play an important role in ERES duplication and maintenance during cell division.

Bangs suggested that typical 1K1N cells showed 2 ERES and that a lack of tight coupling of ERES duplication with cell cycle progression could account for all less prevalent ERES copy numbers (Bangs, 2011). We propose the concept that a core Golgi is maintained and additional Golgi appear during cell division cycle progression, this has been suggested previously for PCF (Yelinek et al., 2009). We found that the time point when a new Golgi appeared was similar, independent of the number of Golgi structures found in 1K1N cells (1K1N1G or 1K1N2G). We clearly find cells where a new structure appeared at an accurately defined moment in 1K1N1G as well as 1K1N2G cells. By this we conclude that 2G are not mandatory for BSF 1K1N cells, still the majority of cells presented 2 Golgi indicating that this was the favoured configuration. The number of 1K1N cells that showed less than two ERES and Golgi corresponded with the number of 1K1N1ERES cells determined by Bangs (Bangs, 2011). The second ERES and Golgi in 1K1N cells were located close to the nucleus and were termed $ERES^N$ and G^N (N = location at nucleus), respectively. We did not find a new growing Golgi close to the G^N. We suggest that as mentioned by He et al., these additional structures are not part of the core duplication complex. We assume that this structure correspondes to the late Golgi described in PCF (Yelinek et al., 2009). How this additional Golgi is duplicated and distributed remains unclear. Therefore, we will conduct *Correlative Light Electron Microscopy* (CLEM) in order to further investigate this additional Golgi structure.

Parallel labelling of both the ERES and the ER indicated that irrespective of the number of ERES and Golgi, theses organelles were always associated with the ER network. In 1K1N the ER started to grow and the complexity of ER morphology increased during cell division cycle progression, until finally the ER was separated during cytokinesis. Although the structure and maintenance of the ER has been investigated in many organisms trypanosomes may provide a suitable new model to study ER duplication. In trypanosomes the ER is associated with the flagellum by a distinct cytoskeletal structure called FAZ (flagellum attachment zone). When the new flagellum grows in parallel a new FAZ is assembled from the posterior pole of the cell close to the flagellar pocket (Sunter et al., 2015). Due to this association of the ER with the FAZ, we could use colocalization of these structures to distinguish which part of the growing ER will develop to the new and old ER, even before ER separation was completed. We plan to use FRAP to investigate how these ER branches communicate and how exchange of components is managed. How spatial organisation of ER morphology and localisation is performed is under investigation in other model organisms. In the early 1990s immunofluorescence based

investigations revealed the ER structure in *S. cerevisiae* and in recent years molecular markers were identified that recruit and organise the ER throughout cell division (Preuss et al., 1991; Fehrenbacher et al., 2002; 2003; Wolf et al., 2012). These findings indicated that in yeast the ER is a highly dynamic membrane system that interacts with cytoskeletal structures; these interactions assist recruitment of the organelle during budding (Fehrenbacher et al., 2003; West et al., 2011). In *C. elegans* a similar connection was identified, where the actin cytoskeleton facilitated the dispersal of the ER during mitosis (Rolls et al., 2002; Poteryaev et al., 2005). We suggest that the association of the *T. brucei* ER with the FAZ shows a trypanosome specific mechanism of linking the ER to the cytoskeleton in order to ensure correct portioning during cell division. Despite the late separation of the ER, the early appearance of a new ERES and Golgi indicated that the performance of the ER was increased early on in the cell division cycle in the 2K1N stage. We conclude that the complex ER membrane system grows throughout the cell division cycle, is assigned to the new growing FAZ and finally separates by fission during the cytokinesis stage.

Duplication of the endosomal compartment occurred late in the cell division cycle. Appearance of a new endosomal compartment was observed about 5.2 hours into the cell division cycle during mitosis and following ERES and Golgi duplication. Doubling of the amount of clathrin (endocytosis) and EP1::GFP (recycling compartment in BSF) indicated that the capacity of the endosomal and recycling compartment was duplicated. The endosomal compartment was localised in the area between the nucleus and the old flagellar pocket. During transition from the 2K1N to 2K2N stage, a new endosomal and recycling compartment, located in the area between the new nucleus and new flagellar pocket, appeared. The localisation of theses compartments suggests that the new endosomal compartment is built *de novo* rather than by fission. The flagellar pocket, the only place for endo- and exocytosis in trypanosomes (Engstler et al., 2004), divides during transition from 1K1N to 2K1N; this event took place before duplication of the endosomal compartment. The question remained whether both flagellar pockets performed endo- and exocytosis at the same rates; this would indicate increased membrane turnover performance along with flagellar pocket duplication, as these processes can be found on both FPs. It seems that the high rates of membrane turnover (Engstler et al., 2004) remain constant for 5.2 hours of the cell division cycle and are finally doubled during 2K1N to 2K2N transition. By this we could exclude that each endosomal compartment is strictly associated with a definite flagellar pocket. The ultrastructure of the endomembrane system in BSF trypanosomes was described in detail and showed how complex the endosomal compartment is (O. Karo, unpublished), these data could now be correlated with the precise temporal map of the cell division cycle in order to investigate *de novo* formation of a new endosomal compart-

ment with high temporal and spatial resolution. Therefore we will use different Rab antibodies to characterise the appearance of new endosomal components more precisely.

In order to complete duplication of the secretory and recycling organelles biogenesis of the new lysosome was investigated. To date little is known about lysosome biogenesis, though recently potential regulators of autophagosome to endolysosome fusion have been identified (Diao et al., 2015). It remains unknown whether new lysosomes emerge from pre-existing or maturate from precursor organelles. Our findings revealed highly flexible and dynamic tubular structures extending from the mature lysosome. These structures could explain how lysosomal membrane is separated from the lysosome either to develop a new lysosome by fission or to detach parts of the membrane from the lysosome for recycling by the retromer complex. The retromer is a complex of proteins that has been shown to be important in recycling of receptors that mediate transport of hydrolases to the lysosome (Pfeffer, 2001; Seaman, 2005). In trypanosomes conserved subunits of the retromer complex were identified and immunofluorescence analysis revealed its role in endosomal targeting (Koumandou et al., 2011), comparative immunofluorescence analysis might reveal a potential connection of the extending structures of the lysosome with the retromer complex.

The organelles of the secretory apparatus start to duplicate in an early stage of the cell division cycle, thus we asked when the glycosomes, the organelle that compartmentalises glycolysis, the main energy source of BSF, are duplicated in order to supply sufficient amounts of ATP for these energy consuming processes. We found that the number of glycosomes in 1K1N cells was constant (33.6 ± 1.2 glycosomes per 1K1N cell); this number was similar in $1K^V1N$ cells (34.2 ± 2.5 glycosomes per $1K^V1N$ cell) suggesting that glycosome duplication has not been initiated. During a 3 h period, between the $1K^V1N$ and 2K2N stage glycosome numbers increased to 47.3 ± 1.1 in 2K1N and 64.2 ± 2.8 in 2K2N cells. We suggest that glycosome numbers are controlled in 1K1N cells and duplication is initiated in $1K^V1N$ until twice the number of glycosomes is present in 2K2N cells. Glycosomes are related to peroxisomes that are widespread between various species. In the literature two main mechanisms have been described for peroxisomes duplication, either *de novo* formation or growth and subsequent fission (Purdue and Lazarow, 2001; Hettema and Motley, 2009). In the 1980s, it was reported that peroxisome membrane proteins (peroxins) were synthesised on free ribosomes and then targeted to pre-existing peroxisomes, this supported the growth and fission model, where pre-existing peroxisomes grow and divide (Lazarow and Fujiki, 1985; Imanaka et al., 1987). In recent years several peroxins (PEX) have been identified and described in *S. cerevisiae* (Stein et al., 2002; Nair et al., 2004). It has been reported that the *S. cerevisiae* Pex11p was involved in peroxisome division (Erdmann and Blobel, 1995); reduced expression of the *T. brucei* homologue *Tb*PEX11 resulted in trypanosomes with fewer, but larger, organelles (Lorenz et al., 1998). The-

se reports indicate that glycosomes divide by elongation and fission in trypanosomes, this agrees with our findings, that elongated glycosomes were identified in every cell division cycle stage. In other organisms association of peroxisomes with the ER has been described (Ma et al., 2011; Agrawal and Subramani, 2013), these associations could explain the movement of glycosomes observed during high-speed microscopy. Theses findings are preliminary and need further investigation in order to determine what ensures correct distribution of glycosomes during cell division in trypanosomes.

The last major organelle analysed was the mitochondrion. Even so the mitochondrion is silent referring to metabolic function in the BSF, it still undergoes massive structural changes. Communication and membrane exchange between the mitochondrion and the ER is a discussed topic in eukaryotic cell biology as it is thought to be important for mitochondrial activity and cell homeostasis (Tatsuta et al., 2014). In yeast an ER-mitochondrion tethering complex has been identified (Kornmann et al., 2009) and *in silico* work indicates similar functions are conserved in metazoans (Kornmann et al., 2009). Our observation, that mitochondrion shape was reduced with a simultaneous increase of ER complexity in 1K1N cells, could arise from membrane traffic and exchange between these two organelles that in BSF have close proximity at the flagellar pocket. This is purely speculative; none of the tethering complex factors have been identified in *T. brucei*, yet. Structurally the mitochondrion was located always on the opposite of the ER; we suggest that this may support confining the compartment for each daughter cell and assist orchestration of correct organelle distribution. By this the ER and mitochondrion could assist the correct distribution of all cellular compartments during cell division. In conclusion we pinpointed the duplication event of all major organelles in BSF *T. brucei*, these discoveries will form a solid basis for further investigations.

4.3 Cell growth is separated from formation of new secretory organelles

Having in hand our precise temporal map and the exact time point of organelle duplication events we could now compare these data in order to discover interesting links between organelle duplication and morphological changes during the cell division cycle. We found that the cell division cycle could be divided into two phases, in the first phase, at an NFR from 0 – 60, cell volume and morphology stayed constant, in the second phase, at an NFR of 80 – 100, cell volume increased rapidly and cell elongation as well as kinetoplast and nucleus separation took place. Secretory organelle duplication (ER, ERES, Golgi, endosomal apparatus and lysosome) was completed during phase 1 of the cell division cycle similar to transition from phase 1 to 2. Organelles that did not participate in secretory function (glycosomes, mitochondrion) completed duplication later in the cell division cycle. Glycosomes increased in number throughout the cell division cycle from 1K1N to 2K2N and mitochondrion growth was completed during cytokinesis. We are aware that we only focused on volume increase by investigating the cell membrane; in future we want to correlate cell volume increase with the growth of the microtubule cytoskeleton. However in contrast to immunofluorescence-based analysis of cytoskeleton formation, the use of cell membrane staining was best suited for live cell analysis.
The BSF of *T. brucei* is dependent on the protective VSG surface coat that shields the cell membrane from the host immune attack (Cross, 1975). Taking into account that the rates of membrane turnover found in trypanosomes were extremely high compared to other eukaryotes (Engstler et al., 2004), we can speculate that the temporal separation of cell volume increase and the completion of secretory organelle duplication could serve as a mechanism to ensure VSG coat maintenance (high membrane turnover) during cell growth. For a parasite such as *T. brucei* it may provide an evolutionary advantage to have no spare secretory capacity. At the moment this is purely speculative, as we first of all need to understand how the exact temporal order for organelle duplication is defined and maintained. Interestingly, the PCF, that is not dependent on a protective VSG coat, showed significant cell volume increase earlier in the cell division cycle, from 1K1N to 2K1N transition (Rotureau et al., 2011), compared to 2K1N to 2K2N transition in BSF. Unfortunately, the exact order of organelle duplication and therefore completion of the secretory apparatus in PCF remains unknown. Golgi duplication has been well described in PCF (Ho et al., 2006); these data suggest that duplication of the Golgi is completed during the 2K1N stage, thus following the onset of cell volume increase. This leads to the hypothesis that separation of secretory organelle duplication and cell growth could be a unique feature of the BSF of *T. brucei*. In BSF the dependence on a functional VSG coat could orchestrate cell volume increase and secretory organelle formation. In trypanosomes the strict spatial organisation of organelle positioning could orchestrate correct organelle distribution

during cell division. It has been reported that due to the connection of the basal body with cytoskeletal structures this organelle orchestrates flagellar pocket separation in PCF (Lacomble et al., 2010) and therefore is an important factor to ensure correct cell division cycle progression. For secretory organelles it had been speculated that plasma membrane and organelles itself regulate their size and function (Sealey-Cardona et al., 2014). It has been shown that *Tb*Sec16, the trypanosome homologue of Sec16, that is part of the COPII vesicle formation complex, can regulate Golgi size and flux through the secretory pathway. In other systems Sec16 can be regulated by phosphorylation or cargo load (Farhan et al., 2008; Zacharogianni et al., 2011), these findings could reveal regulatory control mechanisms for correct organelle size and duplication. Therefore the dependence on functional membrane turnover and VSG coat maintenance could serve as a further important factor orchestrating cellular organisation and cell division in the BSF of *T. brucei*.

4.4 Does VSG coat dynamics orchestrate the BSF cell division cycle?

We speculated that the separation of secretory organelle formation and cell volume increase could be caused by dependence on a functional VSG surface coat. We now correlated the dynamics of secretory organelle formation, cell volume increase and VSG mRNA synthesis in order to strengthen the hypothesis of VSG coat maintenance as a factor orchestrating cellular functions. Therefore we investigated when the amount of VSG mRNA is increased during cell division cycle progression as to date no single cell mRNA quantification has been performed and no information on VSG mRNA amount in different cell division cycle stages was available. We showed that the amount of mRNA increased early in the cell division cycle during progression from the 1K1N to the 2K1N stage during S-phase of the nucleus. VSG expression site transcription is mediated by RNA polymerase I in a discrete nuclear site named the expression site body (ESB) (Navarro and Gull, 2001) and this ESB remains associated with the active ES during cell division cycle progression (Landeira et al., 2009). The separation of the sister chromatid containing the actively transcribed expression site is delayed compared to the remaining chromatid; leading to separation of ESB associated chromatids during mitosis (Landeira et al., 2009), whereas the other chromatids are separated during S-phase/G2. Nevertheless all mRNA analysed increased in the same time, during 1K1N to 2K1N transition, unfortunately no $1K^{V}1N$ and $1K^{B}1N$ cells could be taken into account, due to the harsh permeabilisation conditions during the assay. We conclude that variations in mRNA amount follow the same kinetics independent of ESB association. It was hypothesised that the ESB limited the amount of VSG mRNA transcripts and by this is the limiting factor for VSG transcription. Our data suggest that as soon as S-phase is completed and two transcription templates are available, the amount of

mRNA is increased. This suggests the number of chromatids, copy number of VSG templates, would limit the amount of actively transcribed VSG mRNA.

Correlation of these temporal data with the appearance of a new ERES and Golgi suggest, that the increase in mRNA amount is immediately processed due to increased capacity of the ER early in the cell division cycle at an NFR of 20 (appearance of new Golgi). Still the increase in cell volume and completion of the new secretory apparatus starts about 2 hours later at an NFR of 80 in the 2K2N stage. This led to two possible fates of the VSG mRNA, either the mRNA is stored until cell growth is initiated, but so far VSG storage granules in the BSF have not been identified, or the mRNA is processed immediately after transcription. VSG mRNA in single cells showed a similar localisation as the ER, suggesting that the VSG mRNA is processed directly. Bangs and colleagues showed by pulse chase labelling that after synthesis on membrane-bound ribosomes the halflife for VSG modifications, (a) removal of the N-terminal signal sequence, (b) addition of oligosaccharides and (c) addition of the GPI anchor is 15 minutes (Bangs et al., 1986). We have no information on the exact number of ribosomes available for translation of VSG mRNA, still processing of around 5 x 10^6 VSG dimers has to be completed before cell growth is initiated. These data postulate that VSGs ready for transport to the cell surface have to be stored within the cell; which structure accomplishes this storage remains unclear.

FRAP experiments revealed that the VSG dynamics are constant during cell cycle progression, allowing us to conclude that the density of surface VSGs is not changed. Furthermore, this implies that with increasing amount of VSG the quantities of lipid membrane have to be increased in parallel. Trypanosomes use an alternative pathway of fatty acid synthesis compared to most other eukaryotes. By the enzymology of the elongase (ELO) pathway fatty acids are synthesized. This pathway seems to be well suited for trypanosomes. The modular ELO system allows synthesis of different fatty acid products dependent on the trypanosome environment. It is speculated that the ELO can be upregulated when the parasite enters the cerebrospinal fluids, where fatty acid concentrations are much lower compared to the blood (Lee et al., 2007). We think that this variability also allows the modulation of fatty acid synthesis in different cell division cycle stages. By this the parasite could increase fatty acid synthesis dependent on the requirements during cell division cycle progression; when more lipid membranes are needed during e.g. organelle formation and cell growth.

In summary our data strengthen the hypothesis that the dependence on a functional VSG coat orchestrates cellular functions in order to maintain VSG coat functionality, by the separation of secretory organelle formation and cell volume increase.

4.5 Linear order of events in the *T. brucei* cell division cycle allows non-invasive *in silico* synchronisation of a parasite cell population

Due to the precise temporal map developed during this project we pinpointed the duplication events of all major organelles. We showed that the duplication of the major organelles is ordered, displayed by the consecutive construction of a new secretory apparatus. Correlation of the duplication events of the secretory organelles and the dynamics of cell morphology led to the hypothesis that the dependence of BSF trypanosomes on maintaining their protective VSG coat could be orchestrating these cellular processes. This temporal and spatial information allowed us to screen for potential drugs affecting the order of events. Since we precisely determined when and where organelle formation takes place we can identify by which chemical components organelle formation is impaired. This increases the temporal resolution of our cell division cycle map, because we can take into account the order and timing of organelle formation. Furthermore, this allows us to compare organelle formation and cell division cycle progression between different life cycle stages as well as different trypanosome species. The non-invasive staining protocols developed during this project allowed us to visualise cell morphology in different trypanosome species such as *T. evansi*, *T. vivax* and *T. concolense*, which will allow us to generate the same temporal map for these species and identify conserved motifs and differences.

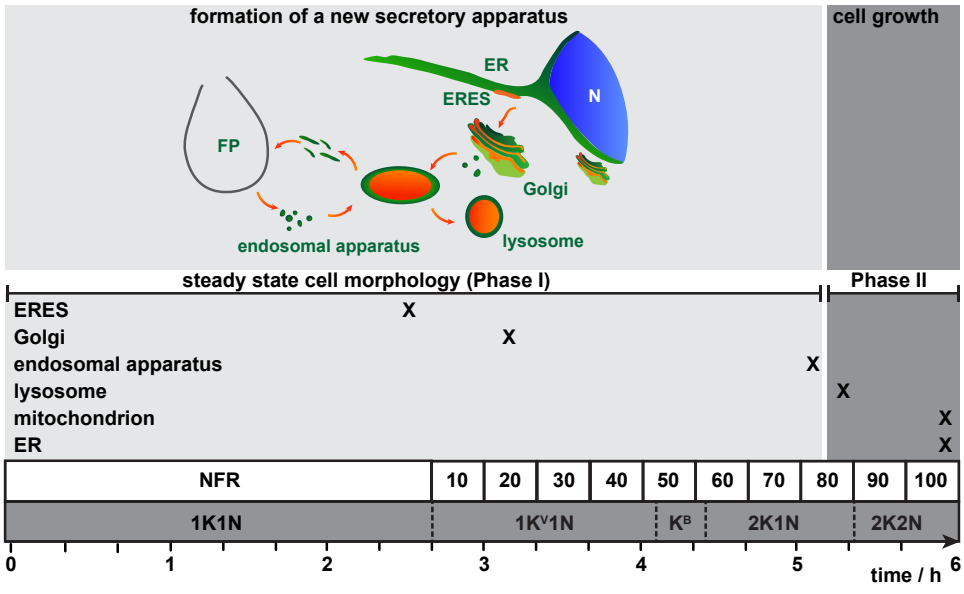

Figure 39. Temporal map of the BSF *T. brucei* cell division cycle. Temporal map of the data obtained by K/N status, outgrowth of the daughter flagellum (NFR) was correlated with the duplication events for the major organelles in BSF *T. brucei*. For each organelle a specific time point was identified when the duplication was initiated or took place, these events are indicated by (X) for the ERES, Golgi, endosomal apparatus, lysosome, mitochondrion and ER. The steady state phase, in which cell volume remained constant and the phase of cell volume increase (Phase II) are indicated by a light and dark grey box, respectively. In Phase I a new secretory apparatus was built. The grey bar shows the timeline through one cell division cycle in hours (PDT=5.9 hours).

5 Material and Methods

5.1 Materials

5.1.1 Oligonucleotides

Table 4. Oligonucleotides used during this work

Name	Sequence (5' > 3')	Source
01_EcVGFP	GATATCATGGTGAGCAAGGGCGAG	MWG
02_BclG126	TGATCAGTTATCTAGATCCGGTGG	MWG
03_GFP_SphI_U	GCCAAAGCGCATGCTGAGCAAGGG	MWG
04_GFP_BamHI_L	GACCCTGGATCCAATTACTTGTACAGCTC	MWG
05_TPI_HindIII	AGCTTATGGCTGTTGTTGTGCTCACACAGATCGCTGCTATTGCTA	MWG
06_TPI_SphI	CCCGCTTTGGCCCAGTCAGCCTTCTTCAGTTTCTTAGCAATAGCA	MWG
10_CFP.U.HindIII	TTGAAGCTTAATGGTGAGCAAGGGCGAG	MWG
11_PIP39HindIII	AGTCAAGCTTAATGGTGAGGACGACACG	MWG
12_PIP39SphI	AAGCATGCGGCTTTAGGGAAGTCTTGAAGGAG	MWG
13_GFP_ERr_Bam_L	ACAGGATCCAATTACAGATCGTCCATCTTGTACAGC	MWG
16_SKL_BamHI	CAGGATCCAATTATAACTTGGACTTGTACAGC	MWG
17_ERimp_GFP_u	GTACAAGCTTAGAATTCAATGGCACCTC	MWG
18_ERrGFP_l	ACAGGATCCAATTACAGATCGTCCATCTTGTACAGCTCGTCCA	MWG
19_PDEB1_212r	CGGTCGACAGTTGATTCTCGCTTCCTC	Sigma
20_GFP_u_Sal1	CTAATCCGTCGACAATGGTGAGCAAGGGCGAG	Sigma
21_PDEB1_u_HindIII	TAATCCAAGCTTATGTTCATGAACA	Sigma
22_GFP_XhoBam	GACCCTGGATCCCTCGAGAATTACTTGTACAGCTC	Sigma
23_Cherry_Xho_Bam_l	GACCCTGGATCCCTCGAGATTTATGCGGTACCAG	Sigma
24_Cherry_SalI_u	CTAATCCGTCGACAATCCGGTGGCGGAATGGC	Sigma
25_GFP_u_Sal1	CTAATCCGTCGACTAATGGTGAGCAAGGGCGAG	Sigma
26_HindIII_Sec13P	TAATCCAAGCTTATGCTTCATTCAACTAG	Sigma
27_SalI_Sec13L	ATGTCGACAGTGAACCCGCTG	Sigma
28_Cherry_HindIII	CGATCAAGCTTAATCCGGTGGCGGAATGGC	Sigma
29_Cherry_SKL	GACCTCGGATCCATTTATTATAACTTGGATGCGGTAC	Sigma
30_TbRab11_SalI	GCATGGTCGACGACAGCACCCGCCAC	Sigma
31_TbRab11_HindIII	GCTACAGTAAGCTTATGGAAGACATGAACC	Sigma
32_Rab11_SalI_u	CTAATCCGTCGACTAATGGAAGACATGAAC	Sigma
33_Rab11_XhoBam_l	GACCCTGGATCCCTCGAGAATTAACAGCACCCGCC	Sigma
34_GFP_SalI_l	GCATGGTCGACGCTTGTACAGCTCGTCC	Sigma
42_Cherry_NheI_l	GATGCTAGCTTTATGCGGTACCAG	Sigma
43_Ald3UTRNhe_u	CGTGCTAGCTGCCCATTTAGTTGG	Sigma
44_Act5UTRHind_l	TGCAAGCTTGCTTATTTTATGG	Sigma

5.1.2 Kits

Table 5 Kits used during this work

Basic Parasite Kit 2	Lonza
Click-iT EdU Alexa Fluor 488 Imaging Kit	Life Technologies
NucleoSpin Gel and PCR clean-up Kit	Macherey-Nagel
Plasmid Midi Kit	Qiagen
Plasmid Mini Kit	Qiagen
QIAEX II Gel Extraktion Kit	Qiagen

5.1.3 Enzymes

All enzymes used were ordered from Thermo scientific. Special orders by other manufacturers are referred in the text.

5.1.4 Antibodies

Table 6. Antibodies used during this work

Primary antibodies for immunofluorescence			
anti-p67 (mAB280)	Mouse, monoclonal	1:500	(Alexander et al., 2002)
anti-Bip	Rabbit, polyclonal	1:500	J. Bangs, Madison, USA
anti-GAPDH (Do403)	Rabbit, polyclonal	1:1500	P. Michels, Brussels, Belgium
anti-HXK (Do408)	Rabbit, polyclonal	1:2000	P. Michels, Brussels, Belgium
anti-ALD (Do423)	Rabbit, polyclonal	1:1500	P. Michels, Brussels, Belgium
anti-BrdU	Mouse, monoclonal	1:1500	Sigma Aldrich
Secondary antibodies for immunofluorescence			
anti-Mouse IgG Alexa488-conjugate	Goat, polyclonal	1:2000	Life Technologies
anti-Rabbit IgG Alexa488-conjugate	Goat, polyclonal	1:2000	Life Technologies
anti-Rabbit IgG Alexa594-conjugate	Goat, polyclonal	1:2000	Life Technologies
Primary antibodies for Western Blot			
anti-PFR L13D6	Mouse, monoclonal	1:20	(Kohl et al., 1999)
anti-GFP (Cat.No. 11814460001)	Mouse, monoclonal	1:2000	Roche
Secondary antibodies for Western Blot			
anti-mouse IgG IRDye680LT (Lot# C20927-05)	Goat, polyclonal	1:20.000	LI-COR Bioscience

5.1.5 Buffers and solutions

DNA analysis

TAE buffer

40 mM Tris-HCL, 40 mM Acetic acid, pH 8.0, 1 mM EDTA

DNA loading dye (10x)

0.1 M EDTA, pH 8.0, 0.05% Bromophenol blue, 0.05% Xylencyanol, 40% Saccharose

DNA size markers

GeneRuler DNA ladder mix ready-to-use (100-10.000) (Thermo scientific)

RNA analysis

Denhardts solution (50x)

1% Ficoll 400, 1% Polyvinylpyrrolidone, 1% BSA

RNA buffer (50x)

0.5 M NaH_2PO_4, pH 6.9

SSC (20x)

3 M NaCl, 0.3 M Tri-sodium citrate, pH 7.0

Northern blot hybridization solution

5xSSC, 5xDEN, 0.1% SDS, 0.1% Tetra-sodium pyrophosphate, 0.01% heparine

Northern blot wash solution

0.1% SDS, 0.1xSSC

Glyoxal solution

75.4% (v/v) DMSO, 21.5% (v/v) Glyoxal (deionized), 15 mM NaH_2PO_4, pH 6.9

RNA fish hybridization solution

2% BSA, 5xDenhardt, 4xSSC, 5% Dextran sulfate, 35% deionized formamide, 0.5 mg/ml yeast tRNA, 40 U/ml Ribolock

RNA fish permeabilization solution

0.5% Saponin, 2% BSA in ddH_2O

Protein analysis

2x Lämmli sample buffer

120 mM Tris-HCl, pH 6.8, 4% SDS, 20% (v/v) Glycerol, 2% (v/v) ß-mercaptoethanol

Lämmli running buffer

25 mM Tris-Base, 192 mM Glycerol, 0.1% SDS

Stacking gel

1 ml Acrylamid solution (30%; 37.5:1 Acrylamide:Bisacrylamide), 1.8 ml stacking gel buffer (0.5 M Tris-HCl, pH 6.8, 0.4% SDS), 4.5 ml H_2O, 37 µl 10% APS, 7 µl TEMED

Running gel (12.5%)

2 ml Acrylamid solution, 1.5 ml running gel buffer (1.5 M Tris-HCl, pH 6.8, 0.4% SDS), 2.5 ml H_2O, 20 µl 10% APS, 5 Ml TEMED

Western blot cathode buffer

0.25 M Tris, pH 7.6, 20% methanol, ddH_2O

Western blot anode buffer

0.3 M Tris, pH 10.4, 20% methanol, 40 mM e-Aminocapron acid, ddH_2O

5.1.6 Chemicals

Chemicals used were ordered from AppliChem (Darmstadt, Germany).

5.1.7 Cultivation media

LB medium for E. coli

10 g tryptone, 5 g yeast extract, 5 g NaCl. Add 1 l ddH_2O, pH 7.0. 100 µg/ml ampicillin was added for selection of transformed bacteria. For agar plates 17 g agar was added to 1 l LB medium.

HMI-9 medium for BSF T. brucei *(according to Hirumi and Hirumi, 1989)*

For 1 l medium: 17.66 g Iscove's modified Dulbecco's Medium (IMDM), 3.024 g $NaHCO_3$, 136 mg Hypoxanthin, 82.2 mg Bathocuproinsulfonat, 14 µl ß-mercaptoethanol, 39 mg thymidine, 100.000 U penicillin, 100 mg streptomycin, 182 mg cysteine, 10% (v/v) fetal calf serum (Sigma Aldrich)

5.1.8 Devices and Equipment

Table 7. Devices used during this work

AMAXA Nucleofector II	Lonza
DMI6000 wide-field microscope	Leica
Eclipse TS100 microscope	Nikon
FACScalibur Flow Cytometer	BD Bioscience
iMIC	FEI Munich GmbH formerly TILL Photonics GmbH
Infinite M200 Plate Reader	Tecan
Odyssey Infrared Scanner	LI-COR Biosystems

Table 8. Cameras used during this work

PCO Sensicam qe	(6.45 µm pixelsize)	PCO, Kelheim
PCO edge	(6.50 µm pixelsize)	PCO, Kelheim
Leica DFC 365 FX	(6.45 µm pixelsize)	Leica, Wetzlar

5.1.9 Software

Table 9. Software used during this work

4Peaks	Macentosj
Amira	Visage Imaging
CLC Main Workbench 6	CLC bio
Fiji	rsbweb.nih.gov/ij/
Huygens Essential	Scientific Volume Imaging
iControl	Tecan
ImageJ64	rsbweb.nih.gov/ij/
Imaris Pro	Bitplane
LA Aquisition	FEI Munich GmbH formerly TILL Photonics GmbH
Leica Application suite AF	Leica
Odyssey	LI-COR Biosystems
Papers	Macentosj
Prism 5	GraphPad Software
Zeiss ZEN	Zeiss

5.1.10 Plasmids

All expression vectors used express constitutively.

Table 10. Expression vectors used during this work. *BLE, Phleomycin resistance; ES, Expression Site; NEO, Neomycin resistance; PUR, Puromycin resistance*

Vector	Name	Source	Genomic locus	Res
pKD4	pKD4	(Muñoz-Jordán et al., 1996)	221 ES	*NEO*
pLew82ΔOP(phleo)	pL82ΔOP	(Best et al., 2005)	rRNA spacer	*BLE*
pLew82ΔOP(puro)	pL82ΔOP	(Best et al., 2005)	rRNA spacer	*PUR*
p2675	p2675	M. Carrington	*In situ* tagging	*PUR*
pTsarib(puro)	pRib	M. Günzel	rDNA promotor	*PUR*
p2T7-177	p2T7	(Wickstead et al., 2002)	177bp-region	*BLE*
pLew61	pL61	M. Günzel	rRNA spacer	*BLE*

5.1.11 Trypanosomes

Trypanosome species and strains

In the Nairobi facility the following trypanosome species were used:

T. congolense IL 1180 (originally isolated from a lion in the Serengeti National Park, Tanzania (Geigy and Kauffmann, 1973), *T. congolense* IL 3000 and *T. congolense* KETRI 3827; *T. vivax* IL 1392 and *T. vivax* IL 2136; *T. b. brucei* IL Tat 1.4; *T. evansi* KETRI 4009 and *T. evansi* KETRI 2479 (type b). *T. congolense* IL 1180, *T. congolense* IL 3000, *T. vivax* IL 1392, *T. vivax* IL 2136 and *T. b. brucei* IL Tat1.4 were obtained from the trypanosome bank at the International Livestock Research Institute (ILRI, Nairobi, Kenya), while *T. congolense* KETRI 3827, *T. evansi* KETRI 2479 and *T. evansi* KETRI 4009 were obtained from Kenya Agricultural and Livestock Research Organization- Biotechnology Research Institute (KALRO-BRI, Kikuyu, Kenya) trypanosome bank.

Ethical statement

Permit to conduct the experiments at KALRO-BRI and *ICIPE* were granted and approved by the Kenya Veterinary Board and the KALRO-BRI Institute Animal Care and Usage Committee (IACUC, Ref: C/TR/4/325/125). Experiments were reviewed and carried out in conformity with the local and international standards of animal care and welfare.

Transgenic lines

In the Würzburg facility the following trypanosome species were used:

MITat1.2 bloodstream form 13-90 (referred to as 1390 in the text)

This cell line is based on MITat 1.2 wt and constitutively expresses the T7 RNA polymerase and the tetracycline repressor (Wirtz et al., 1999), which allows for expression of T7 promotor driven genes in inducible vectors upon induction with 1 µg/ml tetracycline. Cells were selected with 5 µg/ml hygromycin and 2.5 µl/ml neomycin (G-418).

Organelle markers

Table 11. Cloned organelle markers. B, Blasticidine; CCV, Clathrin coated vesicles; CL, Cell line; ER, endoplasmic reticulum; EA, Endosomal Apparatus; G, G-418 (Neomycin); H, Hygromycin; P, Puromycin; Phl, Phleomycin, Selection given in µg/ml.

Name	Organelle	Vector	Source	CL	Selection
117tVSG	ER	pRib(b)	M. Günzel	1390	5 H, 2.5 G, 3 B
LS::GFP::MDDL	ER	pL82ΔOP(p)	J. Jung	1390	5 H, 2.5 G, 0.3 P
GntB::YFP	Golgi	pRib(p)	G.Warren	1390	5 H, 2.5 G, 0.3 P
EP1::GFP	EA	pKD4	M. Günzel	1390	5 H, 30 G
YFP::CLC	CCV	p2675(p)	N. Heddergott	1390	5 H, 2.5 G, 0.3 P
p67::GFP	lysosome	pRib(b)	M. Günzel	1390	5 H, 2.5 G, 0.3 B
MLS::GFP	mitochondrion	pL61	M. Günzel	1390	5 H, 2.5 G, 2.5 Phl
PDEBI::GFP	flagellum	pL82ΔOP(phl)	J. Jung	1390	5 H, 2.5 G, 2.5 Phl
PTS1::GFP	glycosomes	pL82ΔOP(phl)	J. Jung	1390	5 H, 2.5 G, 2.5 Phl
Sec13::GFP	ER exit-site	pL82ΔOP(phl)	J. Jung	1390	5 H, 2.5 G, 2.5 Phl

5.2 Methods

5.2.1 Working with *T. brucei*

In vitro *cultivation of* T. brucei

T. brucei bloodstream form strains were cultured in HMI-9 medium at 37°C in a humidified environment containing 5% CO_2. Cell densities were regularly determined by counting in a Neubauer chamber and kept below $1x10^6$ cells/ml by dilution with fresh pre-warmed medium.

Freezing and thawing of trypanosomes

For long-term storage approximately $4x10^6$ cells were harvested by centrifugation (1400x *g*, 4°C, 10min), resuspended in 500 µl HMI-9 medium and mixed with 500 µl 2x freezing medium (20% glycerol in HMI-9). Stabilates were thawed quickly in a 37°C water bath and washed once with 10 ml of HMI-9 medium. After centrifugation (1400x *g*, 4°C, 10min) the supernatant was aspirated and cells were taken up in 10 ml fresh pre-warmed HMI-9 medium. After cultivation for 45 - 60 minutes the cell density was determined and cells were diluted. Antibiotic selection was added if required.

Quick'n'easy "Kipp-Schütt" dilution

For quick and easy cell dilutions discard the volume of a T-25 flask ($1-5x10^5$ cells/ml) and refill the flask with 10 ml of fresh pre-warmed HMI-9. This dilution is adequate for the next day. Quick and easy dilutions over the weekend work by repeating the dilution steps a second time. Due to the high price of HMI-9 medium use PBS for the first dilution step. Not recommended for growth curves.

Transfection

For stable transfection of BSF trypanosomes the *AMAXA Nucleofector II (Program X-001)* and the *Basic Parasite Solution 2* was used. For electroporation, $3x10^7$ cells were harvested by centrifugation (1400x *g*, 37°C, 10min) and resuspended in 100 µl nucleofector solution. 10 µg of linearised DNA in 10 µl sterile ddH_2O was mixed with 100µl cell suspension and transferred to an electroporation cuvette. After transfection, cells were transferred to 30 ml of pre-warmed HMI-9 medium. Serial dilutions were plated onto 24-well plates. After 6-8 hours (approximately the population doubling time) cultures were supplemented with the final antibiotic selection.

EdU labeling

EdU stock solution was prepared in sterile ddH_2O (10 mM) and stored at 4°C. Cells were incubated in the presence of 300 µM EdU (5-ethynyl-2'-deoxyuridine) and samples were taken

every hour. Control cells were incubated with the same volume ddH_2O. Cells were fixed with 2% formaldehyde in 0.2 M HEPES for 1 hour at RT washed once and resuspended in PBS. Permeabilization was performed with 0.1% Triton-X100/PBS for 10 minutes. EdU incorporation was visualised using the Click-iT EdU Alexa Fluor 488 Imaging kit (Molecular probes). EdU reaction cocktail was prepared just prior to use by mixing the Click-iT reaction buffer with $CuSO_4$, the Alexa fluor 488 azide and reaction buffer additive.

1X Click-iT reaction buffer	430 µl
$CuSO_4$	20 µl
Alexa fluor 488 azide	1.2 µl
Reaction buffer additive	50 µl
Volume	500 µl

Cells were incubated for 30 minutes at room temperature protected from light. DNA was counterstained with DAPI (4', 6-diamidino-2-phenylindole) 0.5 µg/ml.

5.2.2 Working with *E coli*

E. coli strains

E. coli TG1 recO

Genotyp: K12 Δ (*lac-proAB*) *supE thi hsd* D5/F' *tra D36 proA⁺B⁺ lacI*^{q} *Lac Z* ΔM15 *recO*::Tn5

E. coli Top10

Genotyp: *mcr*A, Δ(*mrr-hsd*RMS-*mcrBC*), Phi80*lacZ(del)*M15, Δ*lacX74*, *deoR*, *recA1*, *araD139*, Δ(*ara-leu*)7697, *galU*, *galK*, *rspL*(SmR), *endA1*, *nupG*

Chemical competent bacteria

LB medium was inoculated with the appropriate *E. coli* strain and incubated overnight at 37°C. 1 ml of the overnight culture was added to 100 ml fresh LB medium and incubated until the absorbance at 600 nm was between 0.3 and 0.4. Cells were harvested by centrifugation (900x *g*, 4°C, 10min) resuspended in 2.5 ml TSS (LB medium with 10% PEG 3350, 5% DMSO, 50 mM $MgCl_2$) and aliquots were frozen in liquid nitrogen. Bacteria were stored at -80°C.

Transformation of chemical competent E. coli

Cells were thawed on ice mixed with 10 µl ligation mix and incubated on ice for 30 minutes. The cells were heat shocked at 42°C for 50 seconds and plated on LB ampicilin agar plates and incubated overnight at 37°C.

Isolation of plasmid DNA from E. coli

Small amounts of DNA for analytical digests were extracted from 1 ml of an overnight culture using a standard alkaline lysis protocol. Higher quantities of plasmid DNA were isolated with *QIAGEN Plasmid mini-* or *midi-kits* following the manufactures' instructions. The concentration of nucleic acid in the eluted solution was determined with the *Tecan Infinite M200 Plate reader* by measuring the absorbance at 260 nm.

5.2.3 Working with DNA

DNA Gel electrophoresis

DNA fragments were separated by agarose gel electrophoresis (0.8% agarose in TAE buffer for fragments up to 300 bp and 1.5% agarose in TAE buffer for fragments below 300 bp). Agarose gels were incubated in an ethidium bromide water bath (3 µg/ml) and DNA was visualised by UV-light (312 – 350 nm).

Extraction of DNA from Agarose gels

After DNA Gel electrophoresis fragment of interest was excised from agarose gels and isolated using the *QIAEX II gel extraction kit* following the manufacturer's instructions. DNA was eluted in Elution buffer (5 mM Tris HCl, pH 8.5).

DNA modification

In order to prevent religation blunt ended vectors and those opened with one enzyme were incubated with 1 unit of calf intestine alkaline phosphatase (CIAP) for 30 minutes at 37°C. CIAP treated fragments were gel extracted or isopropanol-precipitated prior to ligation.

Isopropanol precipitation of DNA

Precipitation was performed by adding 0.1 volume of 3 M sodium acetate, pH 7.0 and 1 volume of isopropanol and centrifugation for 20 minutes at 20.000x *g* at 4°C. The sediment was washed twice with 70% ice-cold ethanol (20.000x *g*, 4°C, 10min). The dried DNA was dissolved in elution buffer (5 mM Tris HCl, pH 8.5). For subsequent transfection of *T. brucei* the ethanol was decanted under sterile conditions and the dried DNA was dissolved in filter-sterilized ddH_2O.

PCR

Amplification of DNA fragments was performed using the *Phusion High-Fidelity DNA Polymerase* (Thermo scientific) 10 pmol of oligonucleotides and 10 ng of plasmid DNA or 1 µg of genomic DNA was used as template. DNA fragments were cleaned up using the *NucleoSpin Gel and PCR clean-up Kit* (Macherey-Nageland sequenced by *GATC Biotech* (Konstanz, Germany).

Digestion of PCR fragments

PCR fragments were digested prior ligation if required. Therefore fragments were cleaned up using the *NucleoSpin Gel and PCR clean-up Kit* (Macherey-Nagel) and eluted in 20 µl elution buffer (5 mM Tris HCl, pH 8.5). Digestion was performed over night at 37°C. Tubes were sealed with *Parafilm* (Bemis, Neenah, USA) to avoid vaporization.

5.2.4 Working with RNA

Single Cell mRNA quantification

In order to visualise the mRNA in individual trypanosome cells Susanne Kramer adapted the original protocol. A 1000 nt fragment of the gene of interest was chosen and a corresponding probe mix was generated by Affymetrix *assay* (Affymetrix, Santa Clara, USA). The probe consisted of a mixture of up to 100 oligonucleotides each covering a 20 nt fragment of the target mRNA thereby leading to a highly amplified as a 1000 nt mRNA fragment could be hybridized with up to 50 oligonucleotides in parallel. A further advantage of the *QuantiGene® ViewRNA ISH Cell assay* was the high signal-to-background ratio by the intrinsic stepwise signal amplification. For the detection of the *VSG MITat 1.2* mRNA a 1000 nt fragment ranging from nt 213 to 1289 of the *MITat 1.2* open reading frame (Accession number X56762) was used. The probe mix obtained 40 oligonucleotides covering the *MITat 1.2* mRNA.

BSF trypanosomes were harvested by centrifugation (1400x *g*, 4°C, 10min), washed two times in ice-cold TDB and fixed in 4% formaldehyde for 30 minutes at room temperature on a rotary table. Afterwards cells were washed in PBS and resuspended at a concentration of $4x10^7$ cells/ml in PBS. PCF trypanosomes were harvested by centrifugation (1400x *g*, 10min) and fixed in 4% formaldehyde for 30 minutes at room temperature on a rotary table. Cells were washed in 13 ml PBS and resuspended in 1 ml PBS. Cells were settled on Superfrost® Plus slides (Thermo scientific). Fixed BSF cells were applied on Poly-L-lysine slides (Thermo scientific) and allowed to settle for 60 minutes (100 µl per circle). During the procedure the pap pen gets destroyed, therefore only one probe can be used on one slide. Cells were washed once in PBS (coplin jar) and the residual PBS was removed using a tissue. The *detergent solution QC* was applied to the cells (100 µl per circle) for 5 minutes at room temperature. Cells were washed twice in PBS (coplin jar). Afterwards 100µl of *protease solution* (diluted 1:2000 in PBS) was added to each circle for 10 minutes at room temperature. Then slides were washed three times in 40 ml PBS (coplin jar). The RNA probes were diluted in *probe set dilutent* (1:100) in RNAse free eppendorf tubes and prewarmed to 40°C. Probes were set on the slides (100 µl per circle) and incubated for 3 hours at 40°C in a humid chamber in the oven. Afterwards cell were washed three times in 20 ml *washing buffer* (250ml wash buffer: 0.75 ml component 1, 1.25 ml component 2, 248 ml ddH_2O) for 2 minutes each. Afterwards slides were incubated with *PreAmplifier Mix solution* (806.4 µl *Amplifier Dilutent QF*, 33.2 µl *PreAmplifier Mix*) for 30 minutes at 40°C in a humid chamber (80 µl per circle) and washed three times in 20 ml of *washing buffer*. Then slides were incubated (80 µl per circle) with *Amplifier Mix solution* (806.4 µl *Amplifier Dilutent QF*, 33.2 µl *Amplifier Mix*) for 30 minutes at 40°C in a humid chamber and washed three times in 20 ml of *washing buffer*. Then cells were incubated with the

Label Probe mix (806.4 µl *Label Probe dilutent QF*, 33.2 *Label Probe mix*) for 30 minutes at 40°C in a humid chamber protected from light. After three washes in 20 ml washing buffer *DAPI solution* was added (1:100 in PBS) for 1 minute at room temperature and slides were additionally washed in PBS (coplin jar). Cells were embedded with Prolong Gold antifade (15 µl per circle) and covered with a cover slip.

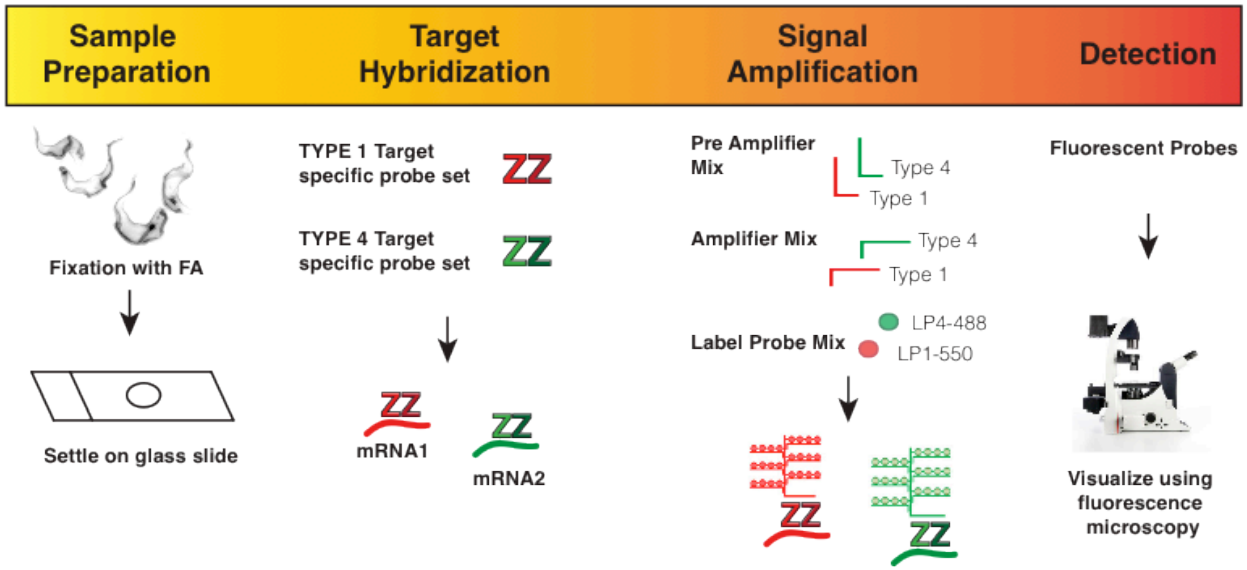

Figure 40. Schematic of QuantiGene ViewRNA ISH Cell assay. Label probes were detected with the corresponding filter sets (EX: LP4-488 = 488 nm, LP1-550 = 550 nm). (Schematic modified from Affymetrix, Santa Clara, USA).

RNA-FISH

BSF trypanosomes were harvested by centrifugation (1400x *g*, 4°C, 10min), washed once in HMI-9 without serum and fixed in 4% formaldehyde for 30 minutes at room temperature on a rotary table. Afterwards cells were washed in 12 ml PBS and resuspended in 1 ml PBS. For mRNA detection cells were applied on Poly-L-lysine slides (Thermo scientific) and allowed to settle for 60 minutes (3 circles per slide with a PAP pen, Kisker, Steinfurt). After washing in 25 mM NH_4Cl for 10 minutes cells were permeabilized with 0.5% saponin/ 2%BSA for 60 minutes. Prehybridization was performed with *Hybridization solution* (2%BSA, 5x Denhart, 4x SSC, 5%Dextran sulphate, 35%deionized formamide, 0.5 mg/ml yeast tRNA, 40 U/ml Ribolock, H_2O) for 2 hours. Oligonucleotides were diluted 1:100 in *Hybridization solution* and applied on the cells (over night, room temperature, humid and dark chamber). Slides were washed once in 4x SSC + 35% formamide and then washed once in 4x SSC, 2x SSC and PBS. For DNA staining a 1:1000 DAPI dilution (5mg/ml stock) was applied on the slides for 10 minutes. Cover slips were mounted with 80% glycerol in PBS.

RNA isolation

1x10^8 cells were harvested by centrifugation (1400x *g*, 4°C, 10min), washed once in HMI-9 without FCS. Supernatant was removed the sediment was resuspended in a residual volume and immediately frozen in liquid nitrogen. Samples were stored at -80°C until extraction was performed. RNA was extracted using the *RNeasy Mini kit* (QIAGEN). Samples were thawed and resuspended in 600 µl RLT buffer with 6 µl ß-mercaptoethanol and mixed with 600 µl 70% ethanol. Lysate was applied to a column and centrifuged for 30 seconds at 8.000x *g*. The Column was washed with 350 µl RWE and two times with 500 µl PRE buffer. RNA was eluted in 2x 30 µl ddH_2O (RNAse free). RNA samples were stored at -80°C.

RNA Gel electrophoresis

For RNA Gel electrophoresis 3 µg of RNA in 4 µl ddH_2O were mixed with 7.2 µl glyoxal solution and denatured for 45 minutes at 50°C. Samples were separated in a horizontal RNA gel (1.4 g Ambion Agarose-LE in 98 ml ddH_2O and mixed with 2 ml 50xRNA buffer). 1xRNA buffer was used as running buffer and RNA fragments were separated at 10 V/cm for 90 minutes.

Northern Blot

RNA was transferred to nitrocellulose membranes (*Hybond-N, Amersham*) by capillary blot. Transfer was performed with 20xSSC over night. UV cross-link was performed for 1 hour at 80°C (1200x100 µJ/cm^2).

DIG labeled Northern probes

DIG labeled DNA probes were generated for topoisomerase II and α -tubulin as described before (Hiltensperger et al., 2012). Hybridization was carried out at 50°C overnight. DNA probe detection was performed using the chemiluminescence reagent CSPD (Roche).

Table 12. Oligonucleotides for Northern blot analysis

Name	Sequence (5' > 3')
Topoisomerase II upper	gcggaggcacacaagtat
Topoisomerase II lower	acgaggaaaactagaata
α-tubulin upper	cacttctatttatttatc
α-tubulin lower	gtcatcatggaggcgggc

5.2.5 Working with proteins

Protein isolation

Trypanosomes were harvested by centrifugation (1400x *g*, 4°C, 10min), washed once in ice-cold TDB and resuspended in 1x *Lämmli sample buffe*r to a concentration of $2x10^5$ cells/µl. Samples were heated at 98°C for 5 min and stored at -20°C.

Discontinuously SDS electrophoresis

Proteins were separated using a 12.5% separation gel. For Western Blot analysis $2x10^6$ cells (recommended for low abundant genes) were applied per lane. The voltage was set to 100 V until the samples entered the separation gel afterwards the voltage was raised up to 130 V.

Western Blot

After SDS electrophoresis proteins were transferred to a PVDF membrane (55 mA per gel for 1 h). Assemble semidry blotting sandwich from bottom to top: 2 sheets of Whatman paper (Anode buffer), PVDF membrane, SDS gel, 2 sheets of Whatman paper (Cathode buffer). Afterwards the membrane was blocked in 5% (w/v) milk in PBS over night at 4°C. The membrane was incubated with the primary antibody diluted in 0.1% Tween in PBS for 1 hour at room temperature and washed 3x 10 minutes in 0.1% Tween in PBS. Afterwards the membrane was incubated with the secondary antibody diluted in 0.02% SDS/ 0.1% Tween in PBS for 1 hour at room temperature protected from light. Membrane was washed 3x 10 minutes in 0.2% Tween in PBS and dried between Whatman papers. The dried membrane was analysed with the *Odyssey Infrared Scanner*.

5.2.6 Preparing trypanosomes for microscopy

Immobilisation of trypanosomes

For live cell microscopy 10^7 trypanosomes were concentrated in a minimal volume of 20 µl trypanosome dilution buffer (TDB; 5 mM KCl, 80 mM NaCl, 1 mM MgSO4, 20 mM Na2HPO4, 2 mM NaH2PO4, 20 mM glucose [pH 7.4]). 3 µl of cell suspension was mixed with 5 µl of 10% (w/v) type-A gelatin in TDB (from porcine skin; Sigma-Aldrich) and pipetted between two cover slips. The coverslips were mounted in a temperature controlled sample holder (Hartel, 2013). The analyses were done at 20 °C. After data acquisition, stage temperature was adjusted to 37 °C to verify viability. Alternatively cells were mounted on microscope slides and cooled down in the incubation system with an DMI6000 wide-field microscope (Leica Microsystems, Mannheim, Germany, software version LAS 3.1.0)

Chemical fixation of T. brucei

$2x10^7$ cells were harvested by centrifugation (1400x *g*, 4°C, 10min), washed once with ice cold TDB, resuspended in 500 µl TDB and carefully mixed with one volume of formaldehyde. Cells were inverted a few times and after fixation washed once to remove the fixative. Cells were stored in at least 500 µl PBS at 4°C. Fixative and fixation time varied dependent on the structure of interest.

Surface staining

$2x10^7$ cells were harvested by centrifugation (1400x *g*, 4°C, 10min), washed three times with ice cold TDB, resuspended in 100 µl TDB and incubated for 15 minutes with the Sulfo-NHS-Fluorescence dye on ice and protected from light. After incubation cells were washed twice with 1 ml ice cold TDB and fixed.

Table 13. Sulfo-NHS-dyes used for surface staining. EX, Excitation wavelength; EM, Emission wavelength

Sulfo-NHS-dye	Source	Concentration	Fluorescence properties
sulfo-NHS-AMCA	Thermo Fisher	1 mM	Ex: 375 nm / Em: 420 nm
sulfo-NHS-Atto488	Atto-Tec	100 µM	Ex: 488 nm/ Em: 530 nm
sulfo-NHS-Rhodamine	Thermo Fisher	100 µM	Ex: 560nm/ Em: 600nm

Organelle staining with fluorescent dyes

Commercial available dyes were used to visualise trypanosome compartments e.g. mitochondrion, plasma membrane, endosomes or lysosome. The staining procedures are described in the results section; *Vizualisation of* T. brucei *organelle*s.

Table 14. Organelle staining with fluorescent dyes

Fluorescence dye	Source	Concentration	Target
MitoTracker Red CMXRos	Molecular Probes	100 nM	mitochondrion
FM 4-64FX	Molecular Probes	6 mM	lipid membrane
Dextran Alexa546 (10,000 MW)	Molecular Probes	0.1 mg/ml	endosomal compartment

3D Fluorescence microscopy.

Images were recorded with a fully automated wide field fluorescence microscope iMIC (FEI Munich GmbH formerly TILL Photonics GmbH, Germany), controlled by the Live acquisition software (FEI Munich GmbH formerly TILL Photonics GmbH, Germany) and equipped with 100× (NA 1.4) and 60× (1.45 NA) objectives (Olympus). Images were recorded with the sensicam.qe CCD cameras (Sensicam, pixel size 64,5 nm, PCO, Kelheim).

High-Speed Live Cell Microscopy.

Live cell microscopy was performed with an inverted fully automated DMI6000 wide-field microscope (Leica Microsystems, Mannheim, Germany, software version LAS 3.1.0) equipped with an incubation system. For high-speed microscopy the sCMOS pco.edge (PCO) was used at frame-rates of 200 –400 fps (pco.edge, pixel size 65 nm, PCO, Kelheim). For medium speed live cell microscopy the Leica DFC 365 FX (DFC 365 FX, pixel size 64.5 nm, Leica, Wetzlar) was used at frame-rates of 10 to 30 fps.

Fluorescence recovery after photobleaching (FRAP)

FRAP analysis was performed using the iMIC microscope (FEI Munich GmbH formerly TILL Photonics GmbH, Germany), 473 nm and 561 nm laser and a 60x Olympus objective (NA 1.45). Data acquisition was performed using the *Live Acquisition* software (FEI Munich GmbH formerly TILL Photonics GmbH, Germany) and *Offline Analysis* (FEI Munich GmbH formerly TILL Photonics GmbH, Germany). Trypanosomes were surface labelled cells with sulfo-NHS-Atto488 and immobilized with gelatine. The ROI was set to cover the whole cell diameter in the area where the nucleus was located. Data acquisition was performed at 21°C. The procedure for FRAP analysis with immobilised trypanosomes was established by Andreas Hartel (Hartel, 2013).

DAPI staining

For staining of DNA a 5 mg/ml stock solution (in ddH_2O) was used and diluted 1:10.000 directly before microscopy. For live cells DAPI was diluted 1:1.000 and incubated for 15 minutes prior to microscopy.

5.2.7 Immunofluorescence

In the tube

$2x10^7$ cells were harvested by centrifugation, washed once with ice cold TDB, resuspended in 0.5 ml TDB and carefully mixed with one volume of formaldehyde. Formaldehyde concentration and fixation time varied dependent on the antibodies used. Cells were washed in PBS and sediment resuspended in PBS. Washing steps were performed in a picofuge minicentrifuge (Labnet) for 90 seconds. Antibodies were diluted in 0.1% BSA in PBS and washing steps performed with 1% BSA in PBS. After blocking for 30 minutes in 1% BSA in PBS incubation with primary and secondary antibodies varied between 30 and 60 minutes.

On the slide

$4x10^6$ BSF trypanosomes were harvested by centrifugation (1400x *g*, 4°C, 10min), washed once in TDB and fixed in 4% formaldehyde for 30 minutes at room temperature. Afterwards cells were washed in 12 ml PBS and resuspended in 120 µl PBS. A *PAP pen* (Kisker) was used to draw circles on Poly-L-lysine slides (Thermo scientific) and $1x10^6$ cells were applied and allowed to settle for 1 hour. All further incubation steps were performed in a humid chamber. Slides were washed in PBS and 100 mM Tris HCl for 10 minutes. If required permeabilization was performed. Slides were blocked with 1%BSA in PBS for 1 hour. Afterwards the primary antibody (diluted in 0.1% BSA in PBS) was applied for 1 hour. Slides were washed three times in PBS and secondary antibody (diluted in 0.1% BSA in PBS) was applied and incubated for 30 minutes protected from light. After three washed in PBS DAPI was added and incubated for 5-10 minutes. Slides were washed once in PBS and cover slips were mounted with 80% glycerol in PBS.

Table 15. Fixation conditions for immunofluorescence. FA, formaldehyde; RT, room temperature;

Antibody	Fixation	Permeabilization	Immunofluorescence
anti-p67 (mAB280)	2% FA 1h/RT	none	Tube
anti-p67 (mAB280)	1% FA 30 min/RT	0.05% Digitonin 10 min	Slide
anti-Bip	4% FA 1h/RT	0.1% NP-40 10 min	Slide
anti-GAPDH (Do403)	4% FA 10 min/RT	0.2% NP40 5 min	Slide
anti-HXK (Do408)	4% FA 10 min/RT	0.2% NP40 5 min	Slide
anti-ALD (Do423)	4% FA 10 min/RT	0.2% NP40 5 min	Slide

5.2.8 Image processing and analysis.

Measurement of distances in 3D was performed with the Imaris® Pro 7.6.5 Measurement Pro package and the Amira software package (version 5.5.0, Visage Imaging, Berlin, Germany). The image parameters, such as pixel size and z-step size, were changed in the image properties. To measure the length of a structure (e.g. flagellum length), it has to be extracted from the rest of the image by manually tracing the structure with a line (2D) or polygon (3D). To visualise volumes, the image was rendered with the surface tool. Unless otherwise specified all images displayed in the results chapters are maximum intensity projections from digitally deconvolved 3D image data sets. Pseudocoloring and maximum intensity projections were done using ImageJ software (version 1.46 for Mac OS X, National Institutes of Health).

Cell volume modelling

Cells were double stained with both fluorescent dyes and fixed in 2% formaldehyde and 0.05% glutaraldehyde for 1 hour. 3D stacks were generated with 100 slices and 200 nm step size and deconvolved using the Huygens software package with >80 iterations. Deconvolved ics-files were opened with the Imaris software package and flagellum lengths were measured, afterwards volume rendering was performed with the surface tool in the *surpass mode* and a new surface model was generated in the software options. *Load parameters* were set to default and the rhodamine stack was chosen as source channel. The *absolute Intensity* was used as *Threshold parameter* and *Surface area details* were set to 2 µm. Maximum and minimum threshold were set automatically to avoid any bias and surface details like volume and area were extracted from the *Statistics options* of the rendered surface areas.

3D-modelling.

For 3D modelling of fixed cells, xyz-stacks were acquired in 100 nm steps. The cells were fixed in a final concentration of 4% w/v formaldehyde and 0.05% v/v glutaraldehyde in 0.1 M HEPES buffer. Duration and temperature for fixation were chosen dependent on the structure of interest. The stacks were deconvolved using Huygens Essential software (version 3.7.0, SVI, Hilversum, Netherlands). 3D maximum intensity projections were generated from these stacks and false-coloured in ImageJ software (version 1.46 for Mac OS X, National Institutes of Health). Animations of 3D-models and annotated Videos were produced with Amira, ImageJ or Imaris.

Cell fluorescence quantification

For quantification of fluorescence 16-bit undeconvolved raw data tiff stacks were opened with ImageJ. With the *Z-project* tool and the *Sum Slices* option the stacks were reduced to one single slide. First the background was calculated. Therefore three regions that have no fluorescence were selected using a rectangle tool, the cells of interest were selected as well. The *Set measurement* options were set to AREA, INTEGRATED DENSITY and MEAN GREY VALUE. Total cell fluorescence was calculated (RFU = Relative Fluorescence Units; Int. Den. = Integrated Density; BG = background).

$$Cell\ fluorescence\ (RFU) = Int.Den.(cell) - Area\ (cell)\ x\ Mean\ gray\ value\ (BG)$$

6 Abbreviations List

1390 = *MITat 1.2 bloodstream form 13-90*

$1K^{B}1N$ = cell with kinetoplast in bone conformation

$1K^{V}1N$ = cell with kinetoplast in v-shape conformation

ALD = aldolase

AMCA = 7-Amino-4-methylcoumarin-3-acetat

bit = basic unit of information storage – binary digit

blas = blasticidin

bp = base pair

BSA = bovine serum albumin

BSF = bloodstream form

CIAP = calf intestine alkaline phosphatase

CLC = clathrin light chain

CLEM = correlative light electron microscopy

CO_2 = carbon dioxide

D = diffusion coefficient

DAPI = 4,6-Diamidino-2-phenylindole

ddH_2O = bidest water

DMSO = Dimethyl sulfoxide

EA = endosomal apparatus

EDTA = ethylenediaminetetraacetic acid

EdU = 5-ethynyl-2´-deoxyuridine

EE = early endosomes

EP1 = PCF specific surface GPI-anchored glycoprotein

ER = endoplasmic reticulum

ERB = ER branch

ERES = endoplasmic reticulum exit-site

ESB = Expression Site Body

et al. = *et alteri* ; and others

EX = excitation

EM = emission

FAZ = flagellum attachment zone

FCS = fetal calf serum

FP = flagellar pocket

FRAP = fluorescence recovery after photobleaching
FPS = frames per second
g = acceleration due to gravity
g = gram
GAPDH = Glyceraldehyde 3-phosphate dehydrogenase
GFP = green fluorescent protein
GntB = GlcNAc-Transferase
GPI = glycosylphosphatidylinositol
h = hours
HEPES = 4-(2-Hydroxyethyl)-1-piperazineethanesulfonic acid
HMI-9 = culture medium for bloodstream form trypanosomes
HU = hydroxyurea
hyg = hygromycin
HXK = hexokinase
Ig = immunoglobulin
IgG = immunoglobulin G
ims = Imaris file format
J = joule
kDNA = kinetoplast DNA
kb = kilo base pair
l = litre
LE = late endosomes
M = molarity
MF = mobile fraction
mg = milligram
min = minute
MITat = Molteno Institute Trypanozoon antigen type
ml = millilitre
MLS = mitochondrial leader sequence
mRNA = messenger RNA
ms = milliseconds
neo = G-418
nm = nanometre
nt = nucleotide
OD = optical density
PBS = phosphate buffered saline

PCF = procyclic form
PCR = polymerase chain reaction
PDT = population doubling time
PFA = paraformaldehyde
phle = phleomycin
PTS1 = peroxisome targeting signal 1
pur = puromycin
RE = recycling endosomes
RFU = relative fluorescence unit
RNAi = RNA-interference
ROI = region of interest
rpm = rounds per minute
sec = seconds
T7 RNAP = T7 RNA polymerase
TDB = trypanosome dilution buffer
tet = tetracycline
UV = ultra violet
V = volt
VSG = variant surface glycoprotein
wt = wild type
YFP = yellow fluorescent protein
µl = microlitre
µg = microgram
°C = degrees celcius

7 References

Adams, R.L., and Lindsay, J.G. (1967). Hydroxyurea reversal of inhibition and use as a cell-synchronizing agent. J. Biol. Chem. *242*, 1314–1317.

Agrawal, G., and Subramani, S. (2013). Emerging role of the endoplasmic reticulum in peroxisome biogenesis. Front. Physiol. *4*, 286.

Alexander, D.L., Schwartz, K.J., Balber, A.E., and Bangs, J.D. (2002). Developmentally regulated trafficking of the lysosomal membrane protein p67 in *Trypanosoma brucei*. J. Cell. Sci. *115*, 3253–3263.

Allen, C.L., Goulding, D., and Field, M.C. (2003). Clathrin-mediated endocytosis is essential in *Trypanosoma brucei*. Embo J. *22*, 4991–5002.

Angelopoulus (1970). Pellicular Microtubules in the Family Trypanosomatidae. Journal of Protozoology *17*, 39–51.

Appelqvist, H., Wäster, P., Kågedal, K., and Öllinger, K. (2013). The lysosome: from waste bag to potential therapeutic target. J. Mol. Cell. Biol. *5*, 214–226.

Aslett, M., Aurrecoechea, C., Berriman, M., and Al, E. (2010). TriTrypDB: a functional genomic resource for the Trypanosomatidae. Nucleic Acids Res. *38*, D457–D462.

Bakker, B.M., Michels, P.A., Opperdoes, F.R., and Westerhoff, H.V. (1997). Glycolysis in bloodstream form *Trypanosoma brucei* can be understood in terms of the kinetics of the glycolytic enzymes. J. Biol. Chem. *272*, 3207–3215.

Bangs, J.D. (2011). Replication of the ERES:Golgi junction in bloodstream-form African trypanosomes. Mol. Microbiol. *82*, 1433–1443.

Bangs, J.D., Andrews, N.W., Hart, G.W., and Englund, P.T. (1986). Posttranslational modification and intracellular transport of a trypanosome variant surface glycoprotein. J. Cell Biol. *103*, 255–263.

Bangs, J.D., Uyetake, L., Brickman, M.J., Balber, A.E., and Boothroyd, J.C. (1993). Molecular cloning and cellular localization of a BiP homologue in *Trypanosoma brucei*. Divergent ER retention signals in a lower eukaryote. J. Cell. Sci. *105 (Pt 4)*, 1101–1113.

Barford, J.P., and Hall, R.J. (1976). Estimation of the length of cell cycle phases from asynchronous cultures of *Saccharomyces cerevisiae*. Exp. Cell Res. *102*, 276–284.

Barry, J.D., and McCulloch, R. (2001). Antigenic variation in trypanosomes: Enhanced phenotypic variation in a eukaryotic parasite. In Sciencedirect.com, (Elsevier), 1–70.

Batram, C. (2013). Die Kontrolle der monoallelen Expression, antigenen Variation und Entwicklung in *Trypanosoma brucei*. Dissertation. Universität Würzburg.

Best, A., Handoko, L., Schlüter, E., and Göringer, H.U. (2005). *In vitro* synthesized small interfering RNAs elicit RNA interference in african trypanosomes: an *in vitro* and *in vivo* analysis. J. Biol. Chem. *280*, 20573–20579.

Bevis, B.J., Hammond, A.T., Reinke, C.A., and Glick, B.S. (2002). *De novo* formation of transitional ER sites and Golgi structures in *Pichia pastoris*. Nat. Cell Biol. *4*, 750–756.

Blattner, J., Helfert, S., Michels, P., and Clayton, C. (1998). Compartmentation of phosphoglycerate kinase in *Trypanosoma brucei* plays a critical role in parasite energy metabolism. Proc. Natl. Acad. Sci. USA. *95*, 11596–11600.

Blum, M.L., Down, J.A., Gurnett, A.M., Carrington, M., Turner, M.J., and Wiley, D.C. (1993). A structural motif in the variant surface glycoproteins of *Trypanosoma brucei*. Nature *362*, 603–609.

Borst, P., Rudenko, G., Taylor, M.C., Blundell, P.A., Van Leeuwen, F., Bitter, W., Cross, M., and McCulloch, R. (1996). Antigenic variation in trypanosomes. Arch. Med. Res. *27*, 379–388.

Broadhead, R., Dawe, H.R., Farr, H., Griffiths, S., Hart, S.R., Portman, N., Shaw, M.K., Ginger, M.L., Gaskell, S.J., McKean, P.G., et al. (2006). Flagellar motility is required for the viability of the bloodstream trypanosome. Nature *440*, 224–227.

Brun, R. (1980). Hydroxyurea: effect on growth, structure, and [3H]thymidine uptake of *Trypanosoma brucei* procyclic culture forms. Journal of Protozoology *27*, 122–128.

Chanez, A.L., Hehl, A.B., Engstler, M., and Schneider, A. (2006). Ablation of the single dynamin of *T. brucei* blocks mitochondrial fission and endocytosis and leads to a precise cytokinesis arrest. J. Cell. Sci. *119*, 2968–2974.

Chowdhury, A.R., Zhao, Z., and Englund, P.T. (2008). Effect of hydroxyurea on procyclic *Trypanosoma brucei*: an unconventional mechanism for achieving synchronous growth. Eukaryotic Cell *7*, 425–428.

Cross, G.A. (1975). Identification, purification and properties of clone-specific glycoprotein antigens constituting the surface coat of *Trypanosoma brucei*. Parasitology *71*, 393–417.

D'Archivio, S., Medina, M., Cosson, A., Chamond, N., Rotureau, B., Minoprio, P., and Goyard, S. (2011). Genetic Engineering of *Trypanosoma (Dutonella) vivax* and *In Vitro* Differentiation under Axenic Conditions. PLoS Negl. Trop. Dis. *5*, e1461.

Dacks, J.B., Walker, G., and Field, M.C. (2008). Implications of the new eukaryotic systematics for parasitologists. Parasitol. Int. *57*, 97–104.

Das, A., Gale, M., Carter, V., and Parsons, M. (1994). The protein phosphatase inhibitor okadaic acid induces defects in cytokinesis and organellar genome segregation in *Trypanosoma brucei*. J. Cell. Sci. *107 (Pt 12)*, 3477–3483.

dasilva, L.L.P., Snapp, E.L., Denecke, J., Lippincott-Schwartz, J., Hawes, C., and Brandizzi, F. (2004). Endoplasmic reticulum export sites and Golgi bodies behave as single mobile secretory units in plant cells. Plant Cell *16*, 1753–1771.

De Souza, C.P.C., and Osmani, S.A. (2007). Mitosis, not just open or closed. Eukaryotic Cell *6*, 1521–1527.

Diao, J., Liu, R., Rong, Y., Zhao, M., Zhang, J., Lai, Y., Zhou, Q., Wilz, L.M., Li, J., Vivona, S., et al. (2015). ATG14 promotes membrane tethering and fusion of autophagosomes to endolysosomes. Nature *520*, 563–566.

Distel, B., Erdmann, R., Gould, S.J., Blobel, G., Crane, D.I., Cregg, J.M., Dodt, G., Fujiki, Y., Goodman, J.M., Just, W.W., et al. (1996). A unified nomenclature for peroxisome biogenesis factors. J. Cell Biol. *135*, 1–3.

Engstler, M., Pfohl, T., Herminghaus, S., Boshart, M., Wiegertjes, G., Heddergott, N., and Overath, P. (2007). Hydrodynamic Flow-Mediated Protein Sorting on the Cell Surface of Trypanosomes. Cell *131*, 505–515.

Engstler, M., Thilo, L., Weise, F., Grünfelder, C.G., Schwarz, H., Boshart, M., and Overath, P. (2004). Kinetics of endocytosis and recycling of the GPI-anchored variant surface glycoprotein in *Trypanosoma brucei*. J. Cell. Sci. *117*, 1105–1115.

Engstler, M., Weise, F., Bopp, K., Grünfelder, C.G., Günzel, M., Heddergott, N., and Overath, P. (2005). The membrane-bound histidine acid phosphatase *Tb*MBAP1 is essential for endocytosis and membrane recycling in *Trypanosoma brucei*. J. Cell. Sci. *118*, 2105–2118.

Erdmann, R., and Blobel, G. (1995). Giant peroxisomes in oleic acid-induced *Saccharomyces cerevisiae* lacking the peroxisomal membrane protein Pmp27p. J. Cell Biol. *128*, 509–523.

Esson, H.J., Morriswood, B., Yavuz, S., Vidilaseris, K., Dong, G., and Warren, G. (2012). Morphology of the trypanosome bilobe, a novel cytoskeletal structure. Eukaryotic Cell *11*, 761–772.

Farhan, H., Weiss, M., Tani, K., Kaufman, R.J., and Hauri, H.-P. (2008). Adaptation of endoplasmic reticulum exit sites to acute and chronic increases in cargo load. Embo J. *27*, 2043–2054.

Fehrenbacher, K.L., Boldogh, I.R., and Pon, L.A. (2003). Taking the A-train: Actin-based force generators and organelle targeting. Trends Cell Biol. *13*, 472–477.

Fehrenbacher, K.L., Davis, D., Wu, M., Boldogh, I., and Pon, L.A. (2002). Endoplasmic reticulum dynamics, inheritance, and cytoskeletal interactions in budding yeast. Mol. Biol. Cell *13*, 854–865.

Ferguson, M.A., Homans, S.W., Dwek, R.A., and Rademacher, T.W. (1988). Glycosylphosphatidylinositol moiety that anchors *Trypanosoma brucei* variant surface glycoprotein to the membrane. Science *239*, 753–759.

Forsythe, G.R., McCulloch, R., and Hammarton, T.C. (2009). Hydroxyurea-induced synchronisation of bloodstream stage *Trypanosoma brucei*. Mol. Biochem. Parasitol. *164*, 131–136.

Galanti, N., Dvorak, J.A., Grenet, J., and McDaniel, J.P. (1994). Hydroxyurea-induced synchrony of DNA replication in the Kinetoplastida. Exp. Cell Res. *214*, 225–230.

Galland, N., de Walque, S., Voncken, F.G.J., Verlinde, C.L.M.J., and Michels, P.A.M. (2010). An internal sequence targets *Trypanosoma brucei* triosephosphate isomerase to glycosomes. Mol. Biochem. Parasitol. *171*, 45–49.

Geigy, R., and Kauffmann, M. (1973). Sleeping sickness survey in the Serengeti area (Tanzania) 1971. I. Examination of large mammals for trypanosomes. Acta Trop. *30*, 12–23.

Glick, B.S. (2000). Organization of the Golgi apparatus. Curr. Opin. Cell Biol. *12*, 450–456.

Glick, B.S., and Luini, A. (2011). Models for Golgi traffic: a critical assessment. Cold Spring Harbor Perspectives in Biology *3*, a005215.

Glick, B.S., and Malhotra, V. (1998). The curious status of the Golgi apparatus. Cell *95*, 883–889.

Gluenz, E., Povelones, M.L., Englund, P.T., and Gull, K. (2011). The kinetoplast duplication cycle in *Trypanosoma brucei* is orchestrated by cytoskeleton-mediated cell morphogenesis. Mol. Cell. Biol. *31*, 1012–1021.

Gourguechon, S., and Wang, C.C. (2009). CRK9 contributes to regulation of mitosis and cytokinesis in the procyclic form of *Trypanosoma brucei*. BMC Cell Biol. *10*, 68.

Gourguechon, S., Savich, J.M., and Wang, C.C. (2007). The multiple roles of cyclin E1 in controlling cell cycle progression and cellular morphology of *Trypanosoma brucei*. J. Mol. Biol. *368*, 939–950.

Grünfelder, C.G. (2003). Endocytosis of a Glycosylphosphatidylinositol-anchored Protein via Clathrin-coated Vesicles, Sorting by Default in Endosomes, and Exocytosis via RAB11-positive Carriers. Mol. Biol. Cell *14*, 2029–2040.

Grünfelder, C.G., Engstler, M., Weise, F., Schwarz, H., Stierhof, Y.-D., Boshart, M., and Overath, P. (2002). Accumulation of a GPI-anchored protein at the cell surface requires sorting at multiple intracellular levels. Traffic *3*, 547–559.

Günzel, M. (2010). Charakterisierung des Transportweges von GPI-verankerten Proteinen in *T. brucei*. Dissertation. Universität Darmstadt.

Hammarton, T.C. (2007). Cell cycle regulation in *Trypanosoma brucei*. Mol. Biochem. Parasitol. *153*, 1–8.

Hammarton, T.C., Clark, J., Douglas, F., Boshart, M., and Mottram, J.C. (2003). Stage-specific differences in cell cycle control in *Trypanosoma brucei* revealed by RNA interference of a mitotic cyclin. J. Biol. Chem. *278*, 22877–22886.

Hammarton, T.C., Kramer, S., Tetley, L., Boshart, M., and Mottram, J.C. (2007). *Trypanosoma brucei* Polo-like kinase is essential for basal body duplication, kDNA segregation and cytokinesis. Mol. Microbiol. *65*, 1229–1248.

Hart, D.T., Misset, O., Edwards, S.W., and Opperdoes, F.R. (1984). A comparison of the glycosomes (microbodies) isolated from *Trypanosoma brucei* bloodstream form and cultured procyclic trypomastigotes. Mol. Biochem. Parasitol. *12*, 25–35.

Hartel, A. (2013). Die laterale Diffusion des variablen Oberflächenglykoproteins in Trypanosomen und in artifiziellen Membranen. Dissertation. Universität Würzburg.

He, C.Y., Pypaert, M., and Warren, G. (2005). Golgi duplication in *Trypanosoma brucei* requires Centrin2. Science *310*, 1196–1198.

He, C.Y., Ho, H.H., Malsam, J., Chalouni, C., West, C.M., Ullu, E., Toomre, D., and Warren, G. (2004). Golgi duplication in *Trypanosoma brucei*. J. Cell Biol. *165*, 313–321.

Heddergott, N. (2006). Clathrin-mediated endocytosis in *Trypanosoma brucei.* Diplomarbeit. LMU München.

Hemphill, A., Lawson, D., and Seebeck, T. (1991). The cytoskeletal architecture of *Trypanosoma brucei*. J. Parasitol. *77*, 603–612.

Hettema, E.H., and Motley, A.M. (2009). How peroxisomes multiply. J. Cell. Sci. *122*, 2331–2336.

Hiltensperger, G., Jones, N.G., Niedermeier, S., Stich, A., Kaiser, M., Jung, J., Puhl, S., Damme, A., Braunschweig, H., Meinel, L., et al. (2012). Synthesis and structure-activity relationships of new quinolone-type molecules against *Trypanosoma brucei*. Journal of Medicinal Chemistry *55*, 2538–2548.

Hirumi, H., and Hirumi, K. (1991). *In vitro* cultivation of *Trypanosoma congolense* bloodstream forms in the absence of feeder cell layers. Parasitology *102 Pt 2*, 225–236.

Ho, H.H., He, C.Y., de Graffenried, C.L., Murrells, L.J., and Warren, G. (2006). Ordered assembly of the duplicating Golgi in *Trypanosoma brucei*. Proc. Natl. Acad. Sci. USA. *103*, 7676–7681.

Hoepfner, D., van den Berg, M., Philippsen, P., Tabak, H.F., and Hettema, E.H. (2001). A role for Vps1p, actin, and the Myo2p motor in peroxisome abundance and inheritance in *Saccharomyces cerevisiae*. J. Cell Biol. *155*, 979–990.

Hu, L., Hu, H., and Li, Z. (2012). A kinetoplastid-specific kinesin is required for cytokinesis and for maintenance of cell morphology in *Trypanosoma brucei*. Mol. Microbiol. *83*, 565–578.

Hughes, L., Towers, K., Starborg, T., Gull, K., and Vaughan, S. (2013). A cell-body groove housing the new flagellum tip suggests an adaptation of cellular morphogenesis for parasitism in the bloodstream form of *Trypanosoma brucei*. J. Cell. Sci. *126*, 5748–5757.

Igoillo-Esteve, M., Mazet, M., Deumer, G., Wallemacq, P., and Michels, P.A.M. (2011). Glycosomal ABC transporters of *Trypanosoma brucei*: characterisation of their expression, topology and substrate specificity. Int. J. Parasitol. *41*, 429–438.

Imanaka, T., Small, G.M., and Lazarow, P.B. (1987). Translocation of acyl-CoA oxidase into peroxisomes required ATP hydrolysis but not a membrane potential. J. Cell Biol. *105*, 2915–2922.

Jackson, D.G., Owen, M.J., and Voorheis, H.P. (1985). A new method for the rapid purification of both the membrane-bound and released forms of the variant surface glycoprotein from *Trypanosoma brucei*. Biochem. J. *230*, 195–202.

Jones, N.G., Nietlispach, D., Sharma, R., Burke, D.F., Eyres, I., Mues, M., Mott, H.R., and Carrington, M. (2008). Structure of a glycosylphosphatidylinositol-anchored domain from a trypanosome variant surface glycoprotein. J. Biol. Chem. *283*, 3584–3593.

Jung, J. (2009). Digital synchronization of the bloodstream form *Trypanosoma brucei* cell division cycle. Diplomarbeit. Universität Darmstadt.

Karo, O. (2008). Ultrastructure of the *Trypanosoma brucei* endomembrane system. Diplomarbeit. Universität Darmstadt.

Keiser, J., and Burri, C. (2001). Evaluation of quinolone derivatives for antitrypanosomal activity. Trop. Med. Int. Health *6*, 369–389.

Kim, P.K., Mullen, R.T., Schumann, U., and Lippincott-Schwartz, J. (2006). The origin and maintenance of mammalian peroxisomes involves a de novo PEX16-dependent pathway from the ER. J. Cell Biol. *173*, 521–532.

Kohl, L., Robinson, D., and Bastin, P. (2003). Novel roles for the flagellum in cell morphogenesis and cytokinesis of trypanosomes. Embo J. *22*, 5336–5346.

Kohl, L., Sherwin, T., and Gull, K. (1999). Assembly of the paraflagellar rod and the flagellum attachment zone complex during the *Trypanosoma brucei* cell cycle. J. Eukaryot. Microbiol. *46*, 105–109.

Kornmann, B., Currie, E., Collins, S.R., Schuldiner, M., Nunnari, J., Weissman, J.S., and Walter, P. (2009). An ER-mitochondria tethering complex revealed by a synthetic biology screen. Science *325*, 477–481.

Koumandou, V.L., Klute, M.J., Herman, E.K., Nunez-Miguel, R., Dacks, J.B., and Field, M.C. (2011). Evolutionary reconstruction of the retromer complex and its function in *Trypanosoma brucei*. J. Cell. Sci. *124*, 1496–1509.

Lacomble, S., Vaughan, S., Gadelha, C., Morphew, M.K., Shaw, M.K., McIntosh, J.R., and Gull, K. (2010). Basal body movements orchestrate membrane organelle division and cell morphogenesis in *Trypanosoma brucei.* J. Cell. Sci. *123*, 2884–2891.

Landeira, D., Bart, J.-M., Van Tyne, D., and Navarro, M. (2009). Cohesin regulates VSG monoallelic expression in trypanosomes. J. Cell Biol. *186*, 243–254.

Langhans, M., Hawes, C., Hillmer, S., Hummel, E., and Robinson, D.G. (2007). Golgi regeneration after brefeldin A treatment in BY-2 cells entails stack enlargement and cisternal growth followed by division. Plant Physiol. *145*, 527–538.

Lazarow, P.B., and Fujiki, Y. (1985). Biogenesis of peroxisomes. Annu. Rev. Cell Biol. *1*, 489–530.

Lee, S.H., Stephens, J.L., and Englund, P.T. (2007). A fatty-acid synthesis mechanism specialized for parasitism. Nature Reviews Microbiology *5*, 287–297.

Lemaire, S., Hours, M., Gerard-Hirne, C., Trouabal, A., Roche, O., and Jacquot, J.-P. (1999). (Chlorophyta) cells by flow cytometry. European Journal of Phycology *34*, 279–286.

Li, X., and Gould, S.J. (2002). PEX11 promotes peroxisome division independently of peroxisome metabolism. J. Cell Biol. *156*, 643–651.

Lindsay, M.E., Gluenz, E., Gull, K., and Englund, P.T. (2008). A new function of *Trypanosoma brucei* mitochondrial topoisomerase II is to maintain kinetoplast DNA network topology. Mol. Microbiol. *70*, 1465–1476.

Lorenz, P., Maier, A.G., Baumgart, E., Erdmann, R., and Clayton, C. (1998). Elongation and clustering of glycosomes in *Trypanosoma brucei* overexpressing the glycosomal Pex11p. Embo J. *17*, 3542–3555.

Losev, E., Reinke, C.A., Jellen, J., Strongin, D.E., Bevis, B.J., and Glick, B.S. (2006). Golgi maturation visualized in living yeast. Nature *441*, 1002–1006.

Lowe, M., and Barr, F.A. (2007). Inheritance and biogenesis of organelles in the secretory pathway. Nat. Rev. Mol. Cell Biol. *8*, 429–439.

Luginbuehl, E., Ryter, D., Schranz-Zumkehr, J., Oberholzer, M., Kunz, S., and Seebeck, T. (2010). The N terminus of phosphodiesterase TbrPDEB1 of *Trypanosoma brucei* contains the signal for integration into the flagellar skeleton. Eukaryotic Cell *9*, 1466–1475.

Ma, C., Agrawal, G., and Subramani, S. (2011). Peroxisome assembly: matrix and membrane protein biogenesis. J. Cell Biol. *193*, 7–16.

Mogelsvang, S., Marsh, B.J., Ladinsky, M.S., and Howell, K.E. (2004). Predicting function from structure: 3D structure studies of the mammalian Golgi complex. Traffic *5*, 338–345.

Moreira-Leite, F.F., Sherwin, T., Kohl, L., and Gull, K. (2001). A trypanosome structure involved in transmitting cytoplasmic information during cell division. Science *294*, 610–612.

Morga, B., and Bastin, P. (2013). Getting to the heart of intraflagellar transport using Trypanosoma and Chlamydomonas models: the strength is in their differences. Cilia *2*, 16–16.

Morgan, G.W., Denny, P.W., Vaughan, S., Goulding, D., Jeffries, T.R., Smith, D.F., Gull, K., and Field, M.C. (2005). An evolutionarily conserved coiled-coil protein implicated in polycystic kidney disease is involved in basal body duplication and flagellar biogenesis in *Trypanosoma brucei*. Mol. Cell. Biol. *25*, 3774–3783.

Moseley, J.B., Mayeux, A., Paoletti, A., and Nurse, P. (2009). A spatial gradient coordinates cell size and mitotic entry in fission yeast. Nature *459*, 857-860.

Mottram, J.C., and Smith, G. (1995). A family of trypanosome cdc2-related protein kinases. Gene *162*, 147–152.

Muñoz-Jordán, J.L., and Cross, G.A. (2001). Telomere shortening and cell cycle arrest in *Trypanosoma brucei* expressing human telomeric repeat factor TRF1. Mol. Biochem. Parasitol. *114*, 169–181.

Muñoz-Jordán, J.L., Davies, K.P., and Cross, G.A. (1996). Stable expression of mosaic coats of variant surface glycoproteins in *Trypanosoma brucei*. Science *272*, 1795–1797.

Mutomba, M.C., and Wang, C.C. (1996). Effects of aphidicolin and hydroxyurea on the cell cycle and differentiation of *Trypanosoma brucei* bloodstream forms. Mol. Biochem. Parasitol. *80*, 89–102.

Nair, D.M., Purdue, P.E., and Lazarow, P.B. (2004). Pex7p translocates in and out of peroxisomes in *Saccharomyces cerevisiae*. J. Cell Biol. *167*, 599–604.

Navarro, M., and Gull, K. (2001). A pol I transcriptional body associated with VSG mono-allelic expression in *Trypanosoma brucei*. Nature *414*, 759–763.

Nenortas, E., Kulikowicz, T., Burri, C., and Shapiro, T.A. (2003). Antitrypanosomal activities of fluoroquinolones with pyrrolidinyl substitutions. Antimicrob. Agents Chemother. *47*, 3015–3017.

Nigg, E.A. (1995). Cyclin-dependent protein kinases: key regulators of the eukaryotic cell cycle. Bioessays *17*, 471–480.

Opperdoes, F.R., and Borst, P. (1977). Localization of nine glycolytic enzymes in a microbody-like organelle in *Trypanosoma brucei*: the glycosome. FEBS Lett. *80*, 360–364.

Otigbuo, I.N., and Oyerinde, J.P. (1993). A modified medium for the *in vitro* cultivation of trypanosomes. African Journal of Medicine and Medical Sciences *22*, 63–71.

Overath, P., and Engstler, M. (2004). Endocytosis, membrane recycling and sorting of GPI-anchored proteins: *Trypanosoma brucei* as a model system. Mol. Microbiol. *53*, 735–744.

Payne, W.E., Kaiser, C.A., Bevis, B.J., Soderholm, J., Fu, D., Sears, I.B., and Glick, B.S. (2000). Isolation of *Pichia pastoris* genes involved in ER-to-Golgi transport. Yeast *16*, 979–993.

Pelham, H.R. (1989). Control of protein exit from the endoplasmic reticulum. Annu. Rev. Cell Biol. *5*, 1–23.

Pelletier, L., Stern, C.A., Pypaert, M., Sheff, D., Ngô, H.M., Roper, N., He, C.Y., Hu, K., Toomre, D., Coppens, I., et al. (2002). Golgi biogenesis in *Toxoplasma gondii*. Nature *418*, 548–552.

Pfeffer, S.R. (2001). Membrane transport: Retromer to the rescue. Curr. Biol. *11*.

Ploubidou, A., Robinson, D.R., Docherty, R.C., Ogbadoyi, E.O., and Gull, K. (1999). Evidence for novel cell cycle checkpoints in trypanosomes: kinetoplast segregation and cytokinesis in the absence of mitosis. J. Cell. Sci. *112 (Pt 24)*, 4641–4650.

Poteryaev, D., Squirrell, J.M., Campbell, J.M., White, J.G., and Spang, A. (2005). Involvement of the actin cytoskeleton and homotypic membrane fusion in ER dynamics in *Caenorhabditis elegans*. Mol. Biol. Cell *16*, 2139–2153.

Preuss, D., Mulholland, J., Kaiser, C.A., Orlean, P., Albright, C., Rose, M.D., Robbins, P.W., and Botstein, D. (1991). Structure of the yeast endoplasmic reticulum: localization of ER proteins using immunofluorescence and immunoelectron microscopy. Yeast *7*, 891–911.

Purdue, P.E., and Lazarow, P.B. (2001). Peroxisome biogenesis. Annu. Rev. Cell Dev. Biol. *17*, 701–752.

Robinson, D.R., and Gull, K. (1991). Basal body movements as a mechanism for mitochondrial genome segregation in the trypanosome cell cycle. Nature *352*, 731–733.

Robinson, D.R., Sherwin, T., Ploubidou, A., Byard, E.H., and Gull, K. (1995). Microtubule polarity and dynamics in the control of organelle positioning, segregation, and cytokinesis in the trypanosome cell cycle. J. Cell Biol. *128*, 1163–1172.

Rolls, M.M., Hall, D.H., Victor, M., Stelzer, E.H.K., and Rapoport, T.A. (2002). Targeting of rough endoplasmic reticulum membrane proteins and ribosomes in invertebrate neurons. Mol. Biol. Cell *13*, 1778–1791.

Romsdahl, M.M. (1968). Synchronization of human cell lines with colcemid. Exp. Cell Res. *50*, 463–467.

Rooney, D.W., Yen, B.C., and Mikita, D.J. (1971). Synchronization of Chlamydomonas division with intermittent hyperthermia. Exp. Cell Res. *65*, 94–98.

Ross, R., and Thomson, D. (1910). A Case of Sleeping Sickness Studied by Precise Enumerative Methods: Regular Periodical Increase of the Parasites Disclosed. Proceedings of the Royal Society B: Biological Sciences *82*, 411–415.

Rossanese, O.W., Soderholm, J., Bevis, B.J., Sears, I.B., O'Connor, J., Williamson, E.K., and Glick, B.S. (1999). Golgi structure correlates with transitional endoplasmic reticulum organization in *Pichia pastoris* and *Saccharomyces cerevisiae*. J. Cell Biol. *145*, 69–81.

Rotureau, B., Subota, I., and Bastin, P. (2011). Molecular bases of cytoskeleton plasticity during the *Trypanosoma brucei* parasite cycle. Cell. Microbiol. *13*, 705–716.

Sampathkumar, P., Roach, C., Michels, P.A.M., and Hol, W.G.J. (2008). Structural insights into the recognition of peroxisomal targeting signal 1 by *Trypanosoma brucei* peroxin 5. J. Mol. Biol. *381*, 867–880.

Sealey-Cardona, M., Schmidt, K., Demmel, L., Hirschmugl, T., Gesell, T., Dong, G., and Warren, G. (2014). Sec16 Determines the Size and Functioning of the Golgi in the Protist Parasite, *Trypanosoma brucei*. Traffic *15*, 613–629.

Seaman, M.N.J. (2005). Recycle your receptors with retromer. Trends Cell Biol *15*, 68–75.

Settembre, C., Fraldi, A., Medina, D.L., and Ballabio, A. (2013). Signals from the lysosome: a control centre for cellular clearance and energy metabolism. Cell Death Differ *14*, 283–296.

Sheader, K., Vaughan, S., Minchin, J., Hughes, K., Gull, K., and Rudenko, G. (2005). Variant surface glycoprotein RNA interference triggers a precytokinesis cell cycle arrest in African trypanosomes. Proc. Natl. Acad. Sci. USA. *102*, 8716–8721.

Sherwin, T., and Gull, K. (1988). Visualization of detyrosination along single microtubules reveals novel mechanisms of assembly during cytoskeletal duplication in trypanosomes. Cell *57*, 211–221.

Sherwin, T., and Gull, K. (1989). The cell division cycle of *Trypanosoma brucei brucei*: timing of event markers and cytoskeletal modulations. Philos. Trans. R. Soc. Lond., B, Biol. Sci. *323*, 573–588.

Siegel, T.N., Hekstra, D.R., and Cross, G.A.M. (2008). Analysis of the *Trypanosoma brucei* cell cycle by quantitative DAPI imaging. Mol. Biochem. Parasitol. *160*, 171–174.

Soto, M., Quijada, L., Alonso, C., and Requena, J.M. (2000). Histone synthesis in *Leishmania infantum* is tightly linked to DNA replication by a translational control. Biochem. J. *346 Pt 1*, 99–105.

Stanners, C.P., and Till, J.E. (1959). DNA synthesis in individual L-strain mouse cells. Biochim. Biophys. Acta *37*, 406–419.

Stein, K., Schell-Steven, A., Erdmann, R., and Rottensteiner, H. (2002). Interactions of Pex7p and Pex18p/Pex21p with the peroxisomal docking machinery: implications for the first steps in PTS2 protein import. Mol. Cell. Biol. *22*, 6056–6069.

Sunter, J.D., Varga, V., Dean, S., and Gull, K. (2015). A dynamic coordination of flagellum and cytoplasmic cytoskeleton assembly specifies cell morphogenesis in trypanosomes. J. Cell. Sci. *128*, 1580–1594.

Tatsuta, T., Scharwey, M., and Langer, T. (2014). Mitochondrial lipid trafficking. Trends Cell Biol. *24*, 44–52.

Taylor, A.E., and Godfrey, D.G. (1969). A new organelle of bloodstream salivarian trypanosomes. J. Protozool. *16*, 466–470.

Taylor, E.W. (1965). The mechanism of colchicine inhibition of mitosis. J. Cell Biol. *25*, 145–160.

Trager, W. (1975). On the cultivation of *Trypanosoma vivax*: a tale of two visits in Nigeria. J. Parasitol. *61*, 3–11.

Tu, X., Mancuso, J., Cande, W.Z., and Wang, C.C. (2005). Distinct cytoskeletal modulation and regulation of G1-S transition in the two life stages of *Trypanosoma brucei*. J. Cell. Sci. *118*, 4353–4364.

Turner, C.M., and Barry, J.D. (1989). High frequency of antigenic variation in *Trypanosoma brucei rhodesiense* infections. Parasitology *99 Pt 1*, 67–75.

Tyler, K.M., Matthews, K.R., and Gull, K. (2001). Anisomorphic cell division by African trypanosomes. Protist *152*, 367–378.

Van Hellemond, J.J., Neuville, P., Schwarz, R.T., Matthews, K.R., and Mottram, J.C. (2000). Isolation of *Trypanosoma brucei* CYC2 and CYC3 cyclin genes by rescue of a yeast G(1) cyclin mutant. Functional characterization of CYC2. J. Biol. Chem. *275*, 8315–8323.

Vaughan, S., Kohl, L., Ngai, I., Wheeler, R.J., and Gull, K. (2008). A Repetitive Protein Essential for the Flagellum Attachment Zone Filament Structure and Function in *Trypanosoma brucei*. Protist *159*, 127–136.

Vickerman, K. (1969). On the surface coat and flagellar adhesion in trypanosomes. J. Cell. Sci. *5*, 163–193.

Wang, Z., and Englund, P.T. (2001). RNA interference of a trypanosome topoisomerase II causes progressive loss of mitochondrial DNA. Embo J. *20*, 4674–4683.

Warren, G., and Wickner, W. (1996). Organelle inheritance. Cell *84*, 395–400.

West, M., Zurek, N., Hoenger, A., and Voeltz, G.K. (2011). A 3D analysis of yeast ER structure reveals how ER domains are organized by membrane curvature. J. Cell Biol. *193*, 333–346.

Wheeler, R.J., Gluenz, E., and Gull, K. (2011). The cell cycle of Leishmania: morphogenetic events and their implications for parasite biology. Mol. Microbiol. *79*, 647–662.

Wickstead, B., Ersfeld, K., and Gull, K. (2002). Targeting of a tetracycline-inducible expression system to the transcriptionally silent minichromosomes of *Trypanosoma brucei*. Mol. Biochem. Parasitol. *125*, 211–216.

Wirtz, E., Leal, S., Ochatt, C., and Cross, G.A. (1999). A tightly regulated inducible expression system for conditional gene knock-outs and dominant-negative genetics in *Trypanosoma brucei*. Mol. Biochem. Parasitol. *99*, 89–101.

Wolf, W., Kilic, A., Schrul, B., Lorenz, H., Schwappach, B., and Seedorf, M. (2012). Yeast Ist2 recruits the endoplasmic reticulum to the plasma membrane and creates a ribosome-free membrane microcompartment. PLoS ONE *7*.

Woodward, R., and Gull, K. (1990). Timing of nuclear and kinetoplast DNA replication and early morphological events in the cell cycle of *Trypanosoma brucei*. J. Cell. Sci. *95 (Pt 1)*, 49–57.

Yelinek, J.T., He, C.Y., and Warren, G. (2009). Ultrastructural study of Golgi duplication in *Trypanosoma brucei*. Traffic *10*, 300–306.

Zacharogianni, M., Kondylis, V., Tang, Y., Farhan, H., Xanthakis, D., Fuchs, F., Boutros, M., and Rabouille, C. (2011). ERK7 is a negative regulator of protein secretion in response to amino-acid starvation by modulating Sec16 membrane association. Embo J. *30*, 3684–3700.

Zick, A., Onn, I., Bezalel, R., Margalit, H., and Shlomai, J. (2005). Assigning functions to genes: identification of S-phase expressed genes in *Leishmania major* based on post-transcriptional control elements. Nucleic Acids Res *33*, 4235–4242.

Zeuthen, E. (1971). Synchronization of the *Tetrahymena* cell cycle. Adv. Cell Biol. 2, 111-152.

8 Appendix

8.1 Eidesstattliche Erklärung

Die vorliegende Arbeit wurde am Lehrstuhl für Zell- und Entwicklungsbiologie der Universität Würzburg in der Arbeitsgruppe von Prof. Dr. Markus Engstler von Oktober 2009 bis Mai 2015 angefertigt.

Gemäß §4, Abs. 3, Nr. 3, 5 und 8 der Promotionsordnung der Fakultät für Biologie der Bayerischen Julius-Maximilians-Universität Würzburg erkläre ich hiermit ehrenwörtlich, dass ich die vorliegende Dissertation selbständig angefertigt und keine anderen als die angegebenen Quellen und Hilfsmittel verwendet habe.

Ich erkläre weiterhin, dass die vorliegende Dissertation weder in gleicher noch in ähnlicher Form bereits in einem anderen Prüfungsverfahren vorgelegen hat.

Weiterhin erkläre ich, dass ich außer den mit dem Zulassungsantrag urkundlich vorgelegten Graden keine weiteren akademischen Grade erworben habe oder zu erwerben versucht habe.

Bei der Verwendung von Abbildungen aus anderen Publikationen ist das Einverständnis des Verlages eingeholt worden. Diese wurden über das Copyright Clearance Center "Rightslink"-Portal erhalten.

Würzburg, Mai 2015

Jamin Jung

8.2 Publikationsliste

Teile dieser Arbeit sind in folgenden Publikationen enthalten:

Bargul, J. L.*, **Jung, J.***, McOdimba, F. A., Omogo, C. O., Adung'a, V. O., Krüger, T., Masiga, D. K., Engstler, M. *Motility and morphology of bloodstream form African trypanosomes show species-specific adaptions to the variable physical environment of the mammalian host.* (Manuskript eingereicht bei PLOS Pathogens). * The authors contributed equally to this work.

Jung, J., Günzel, M., Jones, N., Engstler, M., *Separation of organelle formation and cell growth guarantees surface coat homeostasis in African trypanosomes*. (Manuskript in Vorbereitung. Geplante Einreichung bei Journal of Cell Biology, Juli 2015).

Hiltensperger, G., Jones, N. G., Niedermeier, S., Stich, A., Kaiser, M., **Jung, J.**, Puhl, S., Damme, A., Braunschweig, H., Meinel, L., Engstler, M., Holzgrabe, U., *Synthesis and structure-activity relationships of new quinolone-type molecules against* Trypanosoma brucei. Journal of Medicinal Chemistry, 55(6), 2538–2548. 2012

8.4 Danksagung

Besonders bedanken möchte ich mich an dieser Stelle bei

Markus, für eine spannende und interessante Herausforderung und das Vertrauen und die Unterstützung während der gesamten Zeit.

Prof. Dr. Thomas Dandekar, für die bereitwillige Übernahme des Zweitgutachtens.

Ines, für tolle Zusammenarbeit und Hilfe in jeder Lebenslage auch wenn wir die MLS wohl nie entschlüsseln werden.

Nicola, für tolle Zusammenarbeit und die lange gemeinsame Zeit im Labor, beginnend in Darmstadt während meiner Diplomarbeit.

Tim, für Deine Expertise in der Mikroskopie und die tolle Zusammenarbeit im Afrikaprojekt.

Susanne, Janne, Manfred und Brooke für hilfreiche Diskussionen und Anregungen

Mark Günzel, von dem ich sehr viel gelernt habe.

Joel, Francis, Dan, Kabi und Shem für die tolle Zeit in Kenia, ich habe dort viel erlebt, erfahren und gelernt.

Kathrin, Reinhild, Mona, Elina, Beate, Lidia, Elisabeth, Silke und Barbara für eure technische Kompetenz. Ihr sorgt dafür, dass der Laboralltag läuft.

Uli, für all die Hilfe und Unterstützung während der letzten Jahre. Das Denkmahl steht.

Christopher, Barti, Henriette, Jasmin, Sarah, Andi und Niko. Wir saßen gemeinsam im selben Boot und das hat immer Spaß gemacht.

Dem gesamten Lehrstuhl Zoo I und den anderen Arbeitsgruppen um Janne, Susanne, Ricardo, Christian und Manfred für eine super Atmosphäre.

Julia, Timo und Christin und allen anderen Bios für eine schöne gemeinsame Zeit.

Meinen Freunden, dia auch nach langer Zeit noch meine Freunde sind.

Meiner Familie, die mir die Freiheit gegeben hat selbst zu entscheiden welchen Weg ich gehen möchte.